

THE EFFECTS OF RADIOPROTECTANT AMIFOSTINE ON IRRADIATED
RAT BRAIN AND LIVER TISSUES

A THESIS SUBMITTED TO
THE GRADUATE SCHOOL OF NATURAL AND APPLIED SCIENCES
OF
MIDDLE EAST TECHNICAL UNIVERSITY

BY

GÜLGÜN ÇAKMAK

IN PARTIAL FULFILLMENT OF THE REQUIREMENTS
FOR
THE DEGREE OF DOCTOR OF PHILOSOPHY
IN
BIOLOGY

SEPTEMBER 2010

Approval of the thesis:

**THE EFFECTS OF RADIOPROTECTANT AMIFOSTINE ON
IRRADIATED RAT BRAIN AND LIVER TISSUES**

submitted by **GÜLGÜN ÇAKMAK** in partial fulfillment of the requirements for the
degree of **Doctor of Philosophy in Biology Department, Middle East Technical
University** by,

Prof. Dr. Canan Özgen
Dean, Graduate School of **Natural and Applied Sciences**

Prof. Dr. Musa Doğan
Head of Department, **Biological Sciences**

Prof. Dr. Feride SEVERCAN
Supervisor, **Biological Sciences Dept., METU**

Examining Committee Members:

Prof. Dr. İnci Togan
Biological Sciences Dept., METU

Prof. Dr. Feride Severcan
Biological Sciences Dept., METU

Prof. Dr. Faruk Zorlu
Faculty of Medicine, Hacettepe University

Assoc. Prof. Dr. Neslihan Toyran Al-Otaibi
Faculty of Medicine, Baskent University

Assist. Prof. Dr. Sreeparna Banerjee
Biological Sciences Dept., METU

Date:

17.09.2010

I hereby declare that all information in this document has been obtained and presented in accordance with academic rules and ethical conduct. I also declare that, as required by these rules and conduct, I have fully cited and referenced all material and results that are not original to this work.

Name, Last Name : GÜLGÜN ÇAKMAK

Signature :

ABSTRACT

THE EFFECTS OF RADIOPROTECTANT AMIFOSTINE ON IRRADIATED RAT BRAIN AND LIVER TISSUES

Çakmak, Gülgün

Ph.D., Department of Biology

Supervisor: Prof. Dr. Feride Severcan

September 2010, 156 pages

Amifostine is the only approved radioprotective agent by the Food and Drug Administration for reducing the damaging effects of radiation on healthy tissues. In this study, the effects of ionizing radiation on rat liver microsomal membrane and brain tissue and the protecting effects of amifostine on these systems were investigated at molecular level. Sprague-Dawley rats, which were administered amifostine or not, were whole-body irradiated and different regions of the brain and liver microsomal membranes of these rats were analyzed using FTIR spectroscopy, FTIR microspectroscopy and synchrotron FTIR microspectroscopy.

The first part of this study revealed that ionizing radiation caused a decrease in the total lipid content and CH₂ groups of lipids, an increase in the carbonyl esters, olefinic=CH and CH₃ groups of lipids in the white matter and grey matter regions of the brain, which could be interpreted as a result of lipid peroxidation. In addition,

radiation altered the protein structure of the brain. Amifostine caused significant protective effect against all the radiation induced damages in the brain.

In the second part of the study, FTIR results showed that radiation induced a decrease in the lipid/protein ratio and a degradation of lipids into smaller fragments that contain less CH_2 and more carbonyl esters, olefinic=CH and CH_3 groups in microsomal membranes. In addition, radiation caused an alteration in the secondary structure of proteins, an increase in lipid order and a decrease in the membrane dynamics. Amifostine prevented all the radiation induced compositional, structural and functional damages in the liver microsomal membranes.

Keywords: Amifostine, Ionizing Radiation, FTIR Spectroscopy, Brain, Microsomal membrane.

ÖZ

RADYOPROTEKTANT OLARAK KULLANILAN AMİFOSTİNİN İRRADIYE SIÇAN BEYİN VE KARACİĞER DOKULARINDAKİ ETKİLERİ

Çakmak, Gülgün

Doktora, Biyoloji Bölümü

Tez Yöneticisi: Prof. Dr. Feride Severcan

Eylül 2010, 156 sayfa

Amifostin, radyasyonun sağlıklı dokular üzerindeki zararlı etkilerini azaltmak için Gıda ve İlaç Dairesi tarafından kabul edilmiş olan tek radyoprotektant ajandır. Bu çalışmada, iyonize radyasyonun sıçan karaciğer mikrosomal membranı ve beyin dokusu üzerindeki etkileri ve amifostinin bu sistemler üzerindeki koruyucu etkisi moleküler düzeyde araştırılmıştır. Amifostin enjekte edilmiş veya edilmemiş Sprague-Dawley sıçanlarına tüm vücut ışınlama yapılmış ve bu sıçanların beyin dokularının farklı bölümleri ve karaciğer mikrosomal membranları FTIR spektroskopisi, FTIR mikrospektroskopisi ve sinkrotron FTIR mikrospektroskopisi kullanılarak incelenmiştir.

Çalışmanın ilk bölümü, iyonize radyasyonun beynin ak madde ve boz madde bölgelerindeki toplam lipid ve lipidlerin CH₂ gruplarının miktarında bir azalmaya, lipidlerin karbonil ester, olefinik=CH ve CH₃ gruplarının miktarında ise bir artışa sebep olduğunu ortaya çıkarmıştır. Bütün bunlar lipid peroksidasyonunun bir sonucu

olarak yorumlanabilir. Ek olarak, radyasyon beyindeki proteinlerin yapısını da deęiřtirmiřtir. Amifostin radyasyonun beyinde meydana getirdięi bütn zararlı etkilere karřı koruyucu etki saęlamıřtır.

Çalıřmanın ikinci bölümündeki FTIR sonuçları, radyasyonun mikrosomal membranlardaki lipid/protein oranında bir azalmaya ve lipidlerin daha az CH₂ ve daha fazla karbonil ester, olefinik=CH ve CH₃ grubu içeren küçük fragmentlere parçalanmasına sebep olduęunu göstermiřtir. Bunlara ek olarak, radyasyon proteinlerin ikincil yapılarında bir deęiřikliğe, lipid düzeninde önemli bir artışa ve lipid dinamięinde önemli bir azalmaya sebep olmuřtur. Amifostin radyasyonun karacięer mikrosomal membranlarında meydana getirdięi bütn kompozisyonel, yapısal ve fonksiyonel zararları önlemiřtir.

Anahtar Kelimeler: Amifostine, İyonize Radyasyon, FTIR Spektroskopisi, Beyin, Mikrosomal membran.

To My Mother, Emir Ayşe ÇAKMAK

ACKNOWLEDGMENTS

I would like to express my deepest gratitude to my supervisor Prof. Dr. Feride Severcan for her valuable support, guidance, encouragement and supervision during this thesis study.

I also would like to convey many thanks to Prof. Dr. Faruk Zorlu for this project and his valuable support during my study.

I am thankful to Dr. Lisa M. Miller for her valuable suggestions and support in National Brookhaven Laboratory (USA) where I had a chance to carry out some of my experiments in a unique laboratory and in a friendly environment.

I would like to extend my thanks to the members of my thesis follow-up committee, Prof. Dr. İnci Togan and Associate Proffesor Dr. Neslihan Toyran Al-Otaibi for their constructive contributions during this study.

This work was supported by The Scientific and Technical Research Council of Turkey (TUBITAK), SBAG-2939 research fund, and by the METU-research fund, BAP-2006-07-02-0001. The author was a recipient of a grant within the National Ph.D. Scholarship Programme of the Scientific and Technical Research Council of Turkey (TÜBİTAK).

I feel so lucky, since I have my parents and brothers. My greatest thanks go to my Mommy, Dady and my brothers. You are always there and you always encouraged me.

I also express my special thanks to Yakup ARSLAN to his precious help and lovely attitude in the course of writing this thesis.

My special thanks go to my labmates: Şebnem, Nihal, Özlem, Sevgi, Banu and Ceren. Thank you for being all together for many years sharing all challenges and all good times. I also thank our new members in Lab 146: Seza, Damla, İlke and Ebru.

TABLE OF CONTENTS

ABSTRACT	iv
ÖZ	vi
ACKNOWLEDGMENTS	ix
TABLE OF CONTENTS	xi
LIST OF TABLES	xiv
LIST OF FIGURES	xvi
CHAPTERS	
1. INTRODUCTION.....	1
1.1 Radiation	1
1.1.1 Types of Radiation	2
1.1.2 Dose Units.....	3
1.1.3 Biological Effects of Ionizing Radiation.....	4
1.1.3.1 Effects of Ionizing Radiation on DNA	6
1.1.3.2 Lipid Peroxidation.....	7
1.1.3.3 Effects of Ionizing Radiation on Biological Membranes.....	11
1.1.3.4 Effects of Ionizing Radiation on Other Cellular Macromolecules.	11

1.1.3.5 Tissue Radiosensitivity	12
1.2 Radiotherapy	13
1.3 Radioprotectors	14
1.4 Amifostine.....	17
1.4.1 Chemistry of Amifostine.....	18
1.4.2 Mechanism of Action.....	19
1.4.3 Pharmacokinetics	22
1.5 Brain.....	23
1.6 Biological Membranes	24
1.6.1 Liver Microsomal Membrane	26
1.7 Spectroscopy	27
1.7.1 Infrared Spectroscopy	30
1.7.1.1 Fourier Transform Infrared Spectroscopy.....	33
1.7.1.1.1 The Advantages of FTIR Spectroscopy	35
1.7.1.1.2 FTIR Spectroscopy in Biological Studies.....	36
1.7.1.2 Fourier Transform Infrared Microspectroscopy.....	37
1.7.1.2.1 The Advantages of FTIR Microspectroscopy	38
1.7.1.2.2 FTIR Microspectroscopy in Biological Studies.....	39
1.7.1.3 Synchrotron Fourier Transform Infrared Microspectroscopy.....	40

1.7.1.3.1 The Advantages of Synchrotron-FTIR Microspectroscopy	42
1.7.1.3.2 SR-FTIR Microspectroscopy in Biological Studies.....	43
1.8 Aim of the Study	44
2. MATERIALS AND METHODS	48
2.1 Reagents	48
2.2 Animals	48
2.3 Brain Tissue Studies.....	49
2.3.1 Tissue Preparation:.....	49
2.3.2 Conventional FTIR Microspectroscopic Studies	49
2.3.3 Synchrotron Infrared Microspectroscopic Studies.....	50
2.3.4 Data Analysis:	50
2.3.5 Statistical Study.....	52
2.4 Liver Microsomal Membrane Studies.....	52
2.4.1 Isolation of Rat Liver Microsomal Membranes	52
2.4.2 FTIR Spectroscopic Study	53
2.4.3 Data Analysis	54
2.4.4 Statistical Study.....	56
3. RESULTS	57
3.1 The Effects of Ionizing Radiation and Amifostine on Rat Brain Tissue	57

3.1.1 Band Assignment of the Rat Brain Tissue	57
3.1.2 Comparison of FTIR Spectra of White and Grey Matter in Rat Brain Tissue	64
3.1.3 The Effects of Ionizing Radiation and Amifostine on the Composition and Structure of Rat Brain White Matter and Grey Matter.....	68
3.2 The Effects of Ionizing Radiation and Amifostine on Rat Liver Microsomal Membranes	88
3.2.1 Band Assignment of the Liver Microsomal Membrane.....	88
3.2.2 General Comparison of the Control and Treated Spectra in 3025-2820 cm^{-1} and 1800-1000 cm^{-1} Regions	91
3.2.3 Detailed Spectral Analysis	95
3.2.3.1 The Effects of Ionizing Radiation and Amifostine on the Composition and Structure of Rat Liver Microsomal Membranes	95
3.2.3.2 The Effects of Ionizing Radiation and Amifostine on Rat Liver Microsomal Membrane Dynamics	106
4. DISCUSSION	110
4.1 The Effects of Ionizing Radiation and Amifostine on Rat Brain Tissue ..	110
4.2 The Effects of Ionizing Radiation and Amifostine on Rat Liver Microsomal Membranes	118
5. CONCLUSION	124
REFERENCES.....	127
CURRICULUM VITAE	146

LIST OF TABLES

TABLES

Table 1.1 List of tissues and organs from most radiosensitive to least radiosensitive. ...	13
Table 1.2 Different radioprotectors and their mechanism of action	16
Table 1.3 Three subregions of infrared region.....	31
Table 2.1 The spectral regions and baseline points used for particular infrared bands ...	51
Table 3.1 General band assignment for the FTIR spectra of rat brain tissue.....	59
Table 3.2 FTIR band ratios and their assignments.....	71
Table 3.3 Changes in the band area ratios of various functional groups of control, irradiated, amifostine treated and amifostine treated + irradiated groups in white matter and grey matter. The values are shown as ‘mean ± standard deviation’ for each group. The degree of significance was denoted as: *p < 0.05, **p<0.01 and obtained by comparing each treated group with the control group.....	72
Table 3.4 FTIR spectral band assignments of rat liver microsomal membrane in the region of 3050-1000 cm ⁻¹	90
Table 3.5 Changes in the band area ratios of various functional groups in control, irradiated, amifostine treated and amifostine treated + irradiated liver microsomal membranes. The values are shown as “mean ± standard deviation” for each group. The degree of significance was denoted as: *p < 0.05.....	93
Table 3.6 Changes in the A) wavenumber and B) bandwidth values of various functional groups in control, irradiated, amifostine treated and amifostine treated + irradiated liver	

microsomal membranes. The values are shown as 'mean \pm standard deviation' for each group. The degree of significance was denoted as: * $p < 0.05$ 94

LIST OF FIGURES

FIGURES

Figure 1.1 Types of radiation in the electromagnetic spectrum.....	2
Figure 1.2 The process and products of ROS damage	6
Figure 1.3 Schematic proceed of lipid peroxidation.	8
Figure 1.4 Pathways of lipid peroxidation	10
Figure 1.5 Chemical structure of amifostine.....	18
Figure 1.6 Metabolism of amifostine	20
Figure 1.7 The section of human brain	24
Figure 1.8 The parts of a phospholipid molecule.....	25
Figure 1.9 Electromagnetic radiation and the scales used.	27
Figure 1.10 An electromagnetic wave	28
Figure 1.11 A typical energy-level diagram illustrating the ground and first excited electronic energy levels and their vibrational levels	30
Figure 1.12 The schematic representation of some molecular vibrations in linear triatomic molecules (A) and non-linear triatomic molecules (B). (+) and (–) symbols represent atomic displacement out of page plane	33
Figure 1.13 The components of an FTIR spectrometer	34
Figure 1.14 Perkin Elmer Spectrum/One Spotlight 400 FTIR microspectroscopy ...	38

Figure 1.15 Diagram of National Synchrotron Light Source (A: electron source, B: linear accelerator, C: booster accelerator ring, VUV: Vacuum ultraviolet storage ring with associated beamlines. Electrons are accelerated from with a linear accelerator and produce an energy of 75 million electron milivolts (meV), and enter a booster ring, and are accelerated more and enter vacuum ultraviolet (VUV) storage ring .	41
Figure 2.1 The infrared spectrum of air	54
Figure 2.2 FTIR spectra of control rat liver microsomal membranes before (A) and after (B) buffer subtraction in the region between 3050 – 1000 cm ⁻¹	55
Figure 3.1 A typical FTIR spectrum of rat brain tissue in the 4000-800 cm ⁻¹	58
Figure 3.2 The average absorbance (A), deconvolved (B) and second derivative (C) FTIR spectra of control rat brain white matter in the 1800-1350 cm ⁻¹ region	62
Figure 3.3 The average absorbance (A), deconvolved (B) and second derivative (C) FTIR spectra of control rat brain grey matter in the 1800-1350 cm ⁻¹ region	63
Figure 3.4 A) A light microscope image of control rat brain section. B) Lipid/protein image (25 µm X 25 µm pixel size) of the same section. C) A high resolution (6.25 µm X 6.25 µm pixel size) lipid/protein image of the rectangular area indicated in (A) and (B). D) Lipid/protein image of the rectangular area indicated in (C) obtained using synchrotron source	65
Figure 3.5 FTIR spectra of white and grey matter in control rat brain. Arrow indicates the lipid absorbtion bands at 2922 cm ⁻¹ , 1740 cm ⁻¹ , 1467 cm ⁻¹ , 1239 and 1075 cm ⁻¹ , which are very strong in the WM spectrum	67
Figure 3.6 Functional group maps for one control sample obtained from the ratios of A) lipid to protein B) CH ₂ to CH ₃ C) CH ₂ to lipid D) Amide I/Amide II E) CH ₃ to lipid F) carbonyl ester to lipid G) olefinic=CH to lipid	70

Figure 3.7 Lipid/protein ratio images of control, irradiated, amifostine treated and amifostine treated + irradiated groups	74
Figure 3.8 The numerical comparisons of the lipid/protein ratios of control, irradiated, amifostine treated and amifostine treated + irradiated groups in white matter (A) and grey matter (B).....	74
Figure 3.9 CH ₂ /CH ₃ ratio images of control, irradiated, amifostine treated and amifostine treated + irradiated groups	75
Figure 3.10 The numerical comparisons of the CH ₂ /CH ₃ ratios of control, irradiated, amifostine treated and amifostine treated + irradiated groups in white matter (A) and grey matter (B).	76
Figure 3.11 CH ₂ /lipid ratio images of control, irradiated, amifostine treated and amifostine treated + irradiated groups	77
Figure 3.12 The numerical comparisons of the CH ₂ /lipid ratios of control, irradiated, amifostine treated and amifostine treated + irradiated groups in white matter (A) and grey matter (B).	77
Figure 3.13 CH ₃ /lipid ratio images of control, irradiated, amifostine treated and amifostine treated + irradiated groups.	78
Figure 3.14 The numerical comparisons of the CH ₃ /lipid ratios of control, irradiated, amifostine treated and amifostine treated + irradiated groups in white matter (A) and grey matter (B).	79
Figure 3.15 Carbonyl ester/lipid ratio images of control, irradiated, amifostine treated and amifostine treated + irradiated groups	80
Figure 3.16 The numerical comparisons of the carbonyl ester/lipid ratios of control, irradiated, amifostine treated and amifostine treated + irradiated groups in white matter (A) and grey matter (B).....	80

Figure 3.17 Olefinic=CH/lipid ratio images of control, irradiated, amifostine treated and amifostine treated + irradiated groups	81
Figure 3.18 The numerical comparisons of the olefinic=CH/lipid ratios of control, irradiated, amifostine treated and amifostine treated + irradiated groups in white matter (A) and grey matter (B)	82
Figure 3.19 Amide I/amide II ratio images of control, irradiated, amifostine treated and amifostine treated + irradiated groups.....	83
Figure 3.20 The numerical comparisons of the amide I/amide II ratios of control, irradiated, amifostine treated and amifostine treated + irradiated groups in white matter (A) and grey matter (B).....	83
Figure 3.21 The second derivative spectra of control, irradiated, amifostine treated and amifostine treated + irradiated rat brain WM and GM in the 1700-1600 cm^{-1} region.....	85
Figure 3.22 The numerical comparisons of the intensities of the main protein secondary structures for control, irradiated, amifostine treated and amifostine treated + irradiated rat brain WM.	86
Figure 3.23 The numerical comparisons of the intensities of the main protein secondary structures for control, irradiated, amifostine treated and amifostine treated + irradiated rat brain GM.	87
Figure 3.24 An FTIR spectrum of control rat liver microsomal membrane in 3050-1000 cm^{-1} region.....	89
Figure 3.25 The average baseline corrected infrared spectra of control, irradiated, amifostine treated and amifostine treated + irradiated rat liver microsomal membranes A) in the 3025-2820 cm^{-1} region B) in the 1800-1000 cm^{-1} region. The spectra were normalized with respect to the amide I band (A) and to the CH_2 asymmetric stretching band (B).	92

Figure 3.26 The numerical comparisons of the lipid/protein ratios of control, irradiated, amifostine treated and amifostine treated + irradiated rat liver microsomal membranes	96
Figure 3.27 The numerical comparisons of the CH ₂ /lipid ratios of control, irradiated, amifostine treated and amifostine treated + irradiated rat liver microsomal membranes.	97
Figure 3.28 The numerical comparisons of the carbonyl ester/total lipid (A), the CH ₃ asym. stretc./total lipid (B), unsaturation/saturation (C) ratios of control, irradiated, amifostine treated and amifostine treated + irradiated rat liver microsomal membranes.	99
Figure 3.29 The numerical comparisons of the Amide I/AmideI I ratios of control, irradiated, amifostine treated and amifostine treated + irradiated rat liver microsomal membranes.	100
Figure 3.30 The numerical comparisons of the Amide I average bandwidth (A) and band frequency (B) values of control, irradiated, amifostine treated and amifostine treated + irradiated rat liver microsomal membranes.	102
Figure 3.31 The average A) absorbance infrared spectra, B) second derivative spectra of control, irradiated, amifostine treated and amifostine treated + irradiated rat liver microsomal membranes in the 1700-1600 cm ⁻¹ region.....	104
Figure 3.32 The numerical comparisons of the intensities of the main protein secondary structures for control, irradiated, amifostine treated and amifostine treated + irradiated rat liver microsomal membranes.	105
Figure 3.33 The numerical comparisons of the CH ₂ asymmetric average band frequency (A) and bandwidth (B) values of control, irradiated, amifostine treated and amifostine treated + irradiated rat liver microsomal membranes.....	107

Figure 3.34 The numerical comparisons of the CH₃ asymmetric (A) and PO₂⁻ asym. (B) average band frequency values of control, irradiated, amifostine treated and amifostine treated + irradiated rat liver microsomal membranes..... 109

CHAPTER 1

INTRODUCTION

1.1 Radiation

Radiation is the energy that travels as waves or in the form of particles. The existence of radiation is perhaps as old as the universe itself. In our galaxy, radiation emanating from the Sun formed the basis for the evolution of life on Earth nearly 4.5 billion years ago. Although humans evolved much later on Earth, they developed ways to control radiation. Humans have utilized it for a variety of purposes, often turning it from a friend to an enemy (Arora, 2008).

Humans are exposed to different sources of radiation in the environment. The sources of radiation exposure include radon in houses, contamination from weapon testing sites, nuclear accidents and radiotherapy of cancer. In addition, radiation exposure is common during medical diagnostic procedures, space or air travel, cosmic radiation and use of certain electronic devices (Jagetia *et al.*, 2005). “The steadily increasing use of radiation technologies in medicine, industry, agriculture and scientific research has been paralleled by increasing potential risk for over exposure” (Abou Seif *et al.*, 2003). Thus, protecting living systems from the damaging impacts of radiation is very vital in radiation biology. Radiation protection has specific importance in nuclear warfare, nuclear accidents, and nuclear terrorism. It is also very important in the radiotherapy of cancer patients where normal tissues need to be protected while patients are exposed to ionizing radiation (Gandhi *et al.*, 2004).

1.1.1 Types of Radiation

Depending on its ability to ionize matter, radiation is divided into two distinct types: non-ionizing radiation and ionizing radiation. Figure 1.1 shows the types of radiation in electromagnetic spectrum.

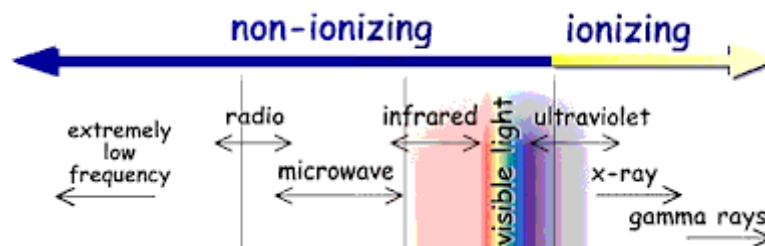


Figure 1.1 Types of radiation in the electromagnetic spectrum

Radiation that does not have enough energy to remove electrons from their orbits is known as "non-ionizing radiation". Radio frequencies, microwaves, infrared radiation, visible light and ultraviolet light are the kinds of non-ionizing radiation.

Ionizing radiation is known as radiation which possesses sufficient energy to take out electrons from their orbits, consequently inducing ionization. Ionization results in the production of negatively charged free electrons and positively charged ionized atoms. "Ionizing radiation can be classified into two groups: photons (includes x-radiation and gamma radiation) and particles (includes alpha and beta particles and neutrons)" (Casarett, 1968). These energetic particles and photons are able to pass through to biological tissue and bring about the transfer of radiation energy to the living cells (Jagetia *et al.*, 2005).

Ionizing radiation is differentiated on the basis of their LET (linear energy transfer) which is described as the amount of energy lost per unit distance as an ionizing particle travels through material. High LET radiation, such as alpha particles, causes more localized, dense ionization in biological tissue than does low LET radiation (Shikazona *et al.*, 2003)

1.1.2 Dose Units

Since the energy absorbed causes chemical changes in a material, dose usually represents absorbed dose. Therefore, dose is defined as the amount of energy absorbed per unit mass of the irradiated material (Mozumder, 1999).

Three different units are used in the measurement of radiation:

1. Rad (Radiation Absorbed Dose)

The rad, a unit of absorbed dose, is regarding to the amount of energy absorbed per gram of material. It is used for any type of radiation and any material. One rad is defined as the absorption of 100 ergs per gram of material.

“The SI unit of absorbed dose is the gray (Gy) which represents the amount of radiation required to deposit 1 Joule of energy in 1 kilogram of any kind of matter (Dunne-Daly, 1999)”.

$$1 \text{ Gy} = 1 \text{ J/kg}$$

The unit also can be referred to as centigray (cGy), which is interchangeable with the rad.

$$1 \text{ cGy} = 1 \text{ rad}$$

2. R (Roentgen)

Roentgen is a unit describing the amount of energy, in the form of gamma or X-rays, in the air (Casarett, 1968).

3. Rem (Roentgen Equivalent Man)

Rem is a unit which measures the biological damage of radiation. To determine rem, absorbed dose (rad) is multiplied by a quality factor (Q) which is unique to the type of incident radiation (Casarett, 1968).

1.1.3 Biological Effects of Ionizing Radiation

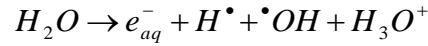
“Ionizing radiation interacts with living tissues inducing a series of biochemical responses that are dependent on radiation LET, dose, dose rate, and cell type” (Meade *et al.*, 2010). “Radiation can exert a number of adverse toxicological effects on many tissues in the body by ionizing and subsequently altering the DNA in the nucleus and other macromolecules of the irradiated cell and possibly even the cytoplasm itself” (Jagetia *et al.*, 2005).

The damaging effects of ionizing radiation may be occurred directly or indirectly:

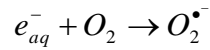
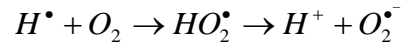
Direct Effects of Ionizing Radiation: Direct damage of ionizing radiation occurs when the energy is transferred to electrons on a molecule. The electrons that are provided sufficient energy to overwhelm the attractive forces of the nucleus escape from the biological molecules and leave them as charged ions. Thus a direct interaction occurs when ionizing radiation hits and ionizes an atom or molecule. As a result of direct interaction of ionizing radiation with a molecule, two chemically reactive pieces are produced at the point of impact. High LET radiation primarily causes direct damage (Arora, 2008).

Indirect Effects of Ionizing Radiation: The indirect effects of ionizing happen by means of the ionization of target molecules. “The absorbed energy of ionizing radiation can cause ionization of different atoms and molecules, including water and different biologically important macromolecules, such as nucleic acids, membrane lipids and proteins” (Jagetia *et al.*, 2005).

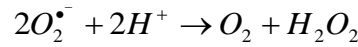
The large amount of radiation damage to biological molecules in a hydrous media is caused by the formation of reactive oxygen species (ROS). When oxygenated hydrous media subjected to ionizing radiation, reactive species, such as e_{aq}^- , HO^\bullet , H^\bullet , H_2 and H_2O_2 are produced according to the following reactions (Abou-Seif *et al.*, 2003; Riley 1994).



The energy-rich radicals, e^- and H^\bullet , yield superoxide ($O_2^{\bullet -}$) radicals in the presence of oxygen according to the following reaction:



Superoxide generates H_2O_2 as a secondary product as follow:



“Formation of free radicals may cause a wide variety of events and many different products could be formed as a result of reactions with cellular macromolecules” (Abou-Seif *et al.*, 2003). “Free radicals can attack almost any cellular molecule, such as DNA, cell membranes or proteins” (Zwart *et al.*, 1999). “The free radical-mediated indirect effect is known to account for approximately 75% of the subsequent damage to cells exposed to ionizing radiation” (Murley *et al.*, 2006). The products originating from reactive oxygen species (ROS) attack to different macromolecules were represented in Figure 1.2 (Zwart *et al.*, 1999).

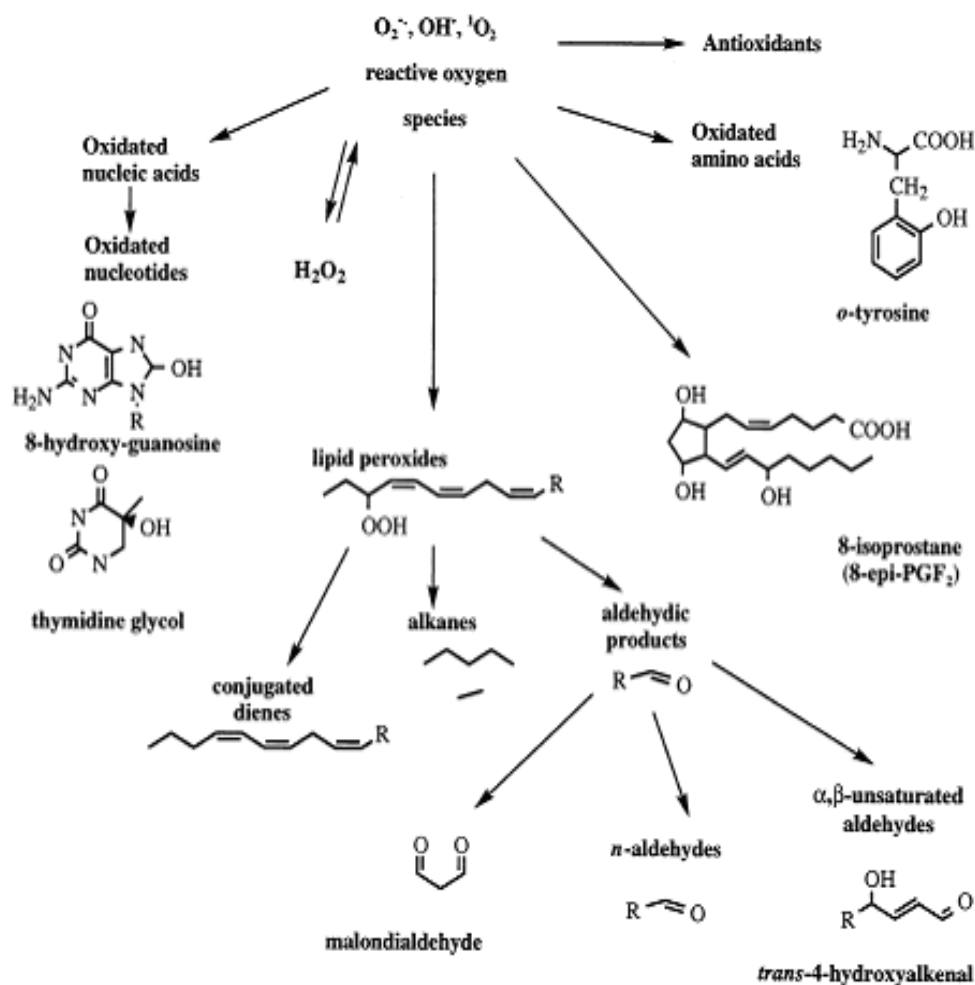


Figure 1.2 The process and products of ROS damage (Zwart *et al.*, 1999).

1.1.3.1 Effects of Ionizing Radiation on DNA

“Direct interaction of ionizing radiation produces a range of lesions in cellular DNA, including over 20 types of base damage, single-strand breaks, double-strand breaks, and DNA–DNA and DNA–protein crosslinks” (Prise *et al.*, 2003). In addition, a large diversity of biological results of radiation harm appears because of ROS attack. “OH is known as the most harmful free radical of all ROS generated in biological

tissues. The most significant DNA damages induced by $\cdot\text{OH}$ are oxidized bases, DNA-DNA intrastrand adducts, DNA strand breaks, and DNA-protein cross-links” (Cadet *et al.*, 1999). These damages take place mainly by reaction of ROS with DNA bases and sugars. It has been reported that guanine is the most susceptible DNA base for free radical damage (Cadet *et al.*, 1999).

Since the single-strand breaks which are produced by the interaction of ROS with DNA sugars can be easily repaired in biological tissues, double strand breaks are thought to cause more important effects and the main injury in cellular death (Elia *et al.*, 1991).

“It is estimated that 1 Gy of radiation produces 10^5 ionizations per cell, which cause about 2000 single-strand and 40 double-strand in addition to other types of DNA damage” (Lewanski and Gullick, 2001).

1.1.3.2 Lipid Peroxidation

Lipids are essential molecules which participate in a numerous biological procedures. “In a lipid-rich environment, as in the biological membranes, both phospholipid acyl chains and phospholipid backbone as well as cholesterol are subject to radiation damage” (Karbownik and Reiter, 2000). The high amount of membrane lipids at sites where ROS are produced make them easily accessible targets. “Especially the group of polyunsaturated fatty acids (PUFAs) is highly susceptible to reactions with free radicals. Peroxidation of lipids in fatty acids may lead to a radical chain reaction” (Zwart *et al.*, 1999).

A general scheme for the steps of lipid peroxidation induced by a free radical was presented in Figure 1.3 (Zwart *et al.*, 1999).

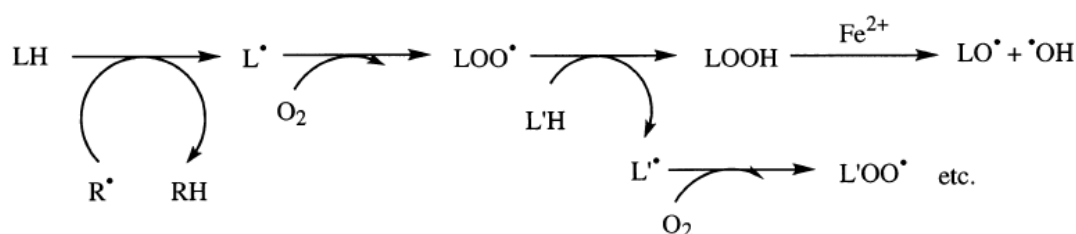


Figure 1.3 Schematic proceed of lipid peroxidation (Zwart et al., 1999).

Because of these chain reactions, one substrate radical (R^\bullet) may result in the formation of many equivalents of lipid peroxides ($LOOH$). These degenerative propagation reactions in lipid membranes are usually accompanied by the formation of a wide variety of products, including alkanes and carbonyl compounds. Because some of these products, especially hydroxyalkenals, are toxic by themselves, they may serve as second messengers for radical damage (Zwart *et al.*, 1999).

The PUFAs of the membrane are oxidised by a free radical in a lipid peroxidation process which consists of three distinct steps: initiation, propagation and termination. The initiation step represents the formation of a lipid radical from a lipid molecule. The free radicals, in particular, the hydroxyl radical (HO^\bullet), abstracts allylic hydrogen from PUFA to initiate lipid peroxidation (1).



In propagation, the carbon-centered lipid radical (L^\bullet) reacts rapidly with O_2 to form peroxy radical (LOO^\bullet) (2).



In a subsequent slower reaction, LOO^\bullet attacks another lipid molecule (LH), forming non-radical hydroperoxides ($LOOH$) while generating a new lipid radical (L^\bullet) (3). The latter can be converted to LOO^\bullet on encountering O_2 , completing the self-

propagating cycle (2). Thus, once initiated, lipid peroxidation proceeds to establish a chain reaction with a low energy requirement.



In termination, two free radicals combine to yield a non-radical product to end the chain reaction (4-6) (Choudhary *et al.*, 1998).

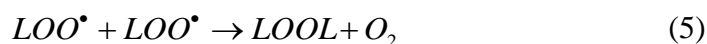


Figure 1.4 shows the overall mechanism of a PUFA oxidation.

The free radicals abstract hydrogen atoms from the methylene groups which are highly reactive to oxidizing agents (1). The carbon-centered radicals react with O₂ to form peroxy radicals. The fate of the peroxy radical depends on its position in the carbon chain. If the peroxy radical exists at one of the two ends of the double bond system (2), it is reduced to a hydroperoxide and a conjugated diene hydroperoxides was produced such as 4 which is the simplest product of lipid peroxidation. If the peroxy radical is at an internal position in the fatty acid chain (3), cyclization to an adjacent double bond will compete with reduction to hydroperoxide. The cyclization product (5) is a cyclic peroxide adjacent to a carbon-centered radical. This carbon-centered radical has two fates. The radical can couple with O₂ to form a peroxy radical which is reduced to a hydroperoxide (6) as described above. Alternatively, carbon-centered radical 5 can undergo a second cyclization to form a bicyclic peroxide which after coupling to O₂ and reduction yields a molecule (7). Compound **7** serves as a common intermediate for the production of isoprostanes and malondialdehyde (MDA) through chemical conversion of the bicyclic peroxide group. MDA has been used for many years as a convenient biomarker for lipid peroxidation because of its facile reaction with thiobarbituric acid to form an intensely colored chromogen (Marnett, 1999).

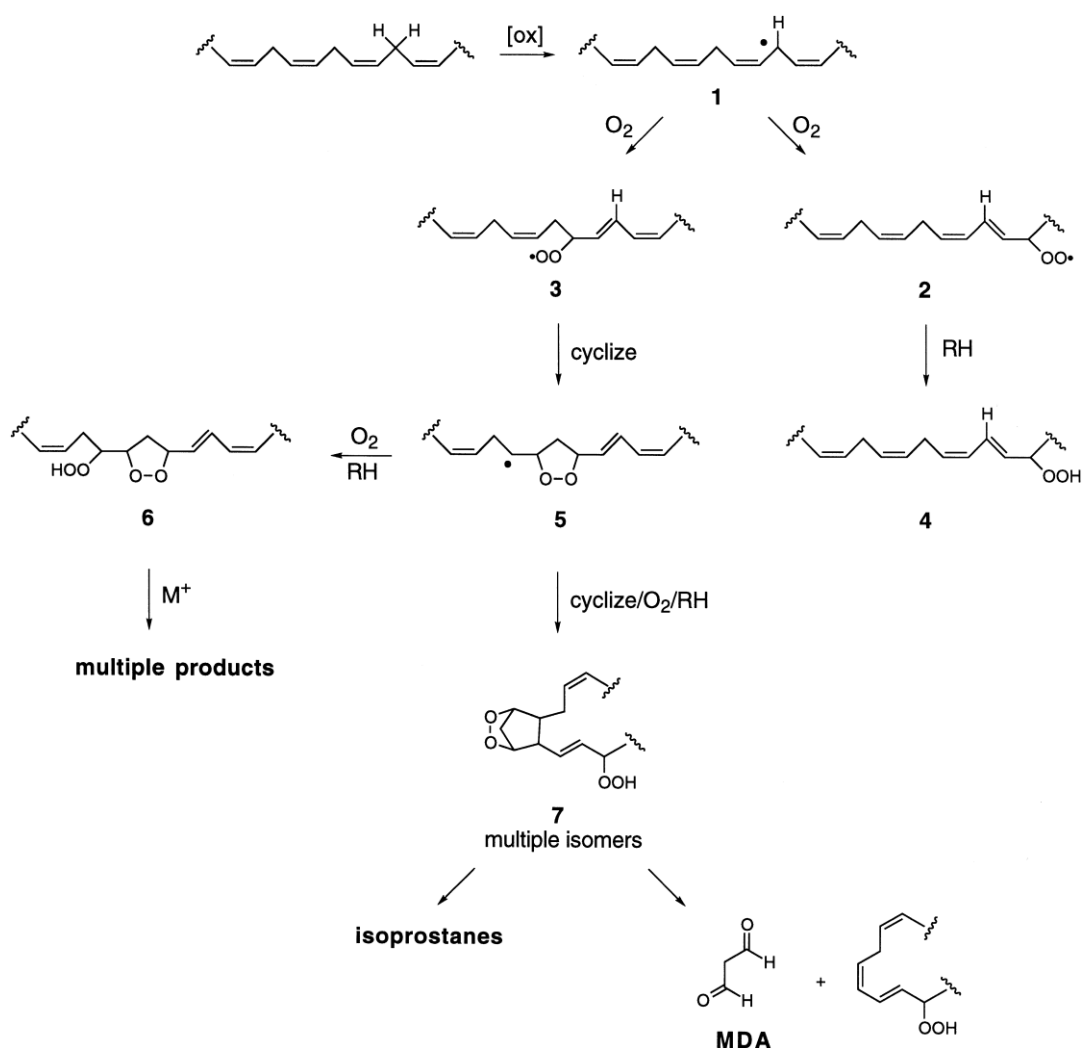


Figure 1.4 Pathways of lipid peroxidation (Marnett, 1999).

The biochemical techniques (TBARS test and HPLC) are commonly used to examine the lipid peroxidation in biological systems. In this study, similar to our previous studies we used FTIR spectroscopy, FTIR microspectroscopy and synchrotron-FTIRM as non-destructive, easy, rapid and sensitive tools to monitor ionizing radiation induced-lipid peroxidation in different parts of the rat brain and liver microsomal membrane (Severcan *et al.*, 2005; Ozek *et al.*, 2009).

1.1.3.3 Effects of Ionizing Radiation on Biological Membranes

As argued above, lipid peroxidation is a key impact of ionizing radiation on membranes. Peroxidation of membrane lipids induces changes in permeability, fluidity and structure of membrane, inactivates membrane-bound enzymes and protein receptors (Choudhary, 1998). “These changes cause swelling and alterations of respiratory functions and loss of –SH groups from proteins, mediate DNA damage, and alters the RNA transport from nucleus to cytoplasm” (Choudhary, 1998). The chain reactions of lipid peroxidation process cause the production of various degradation products in membranes. These end products cause some alterations in the membrane composition and structure which are increased by the accumulation of free radical mutilated proteins. After the degradation products are transferred into the cell, they can react with nucleic acids and proteins, thus they contribute to DNA damage and mutagenesis. The dramatic alterations in composition, structure and function of biological membranes cause cell death through apoptosis (Karbownik and Reiter, 2000).

1.1.3.4 Effects of Ionizing Radiation on Other Cellular Macromolecules

Besides DNA and membranes, a large number of biological molecules may be harmfully influenced by radiation exposure. The damaging effect of radiation could be occurred directly or indirectly. The final results of the radiation damage can be conformational changes, crosslinkages and broken chemical bonds. The alterations in a molecule can affect its biological function. For instance, conformational changes in a protein or an enzyme can affect its essential function in a metabolic pathway and thus terminates certain functions of the cell. Proteins and their smaller constituents, polypeptides, peptides and amino acids, are also sensitive to radiation damage. The exposure of the radiation to these molecules may cause cross-linking with other proteins or DNA, disulfide bridges and breakage of hydrogen bonds.

Protein oxidation products and carbonyl derivatives of proteins may result from oxidative modifications of amino acid side chains, reactive oxygen-mediated peptide

cleavage and from reactions with lipid and carbohydrate oxidation products. It is now becoming clear that the presence of carbonyl groups in proteins may indicate that the proteins have been subjected to oxidative free radical damage (Labieniec and Gabryelak, 2004).

All of these effects may cause changes in the conformation and function of molecules. It has been reported that radiation brings about the breakage of glycosidic bonds in glycogen and in other biological molecules and the depolymerization of glycogen. Gluconeogenesis and glycogenesis pathways in cell may be activated by radiation. Also, it has been found that blood glucose and insulin levels were increased after radiation exposure.

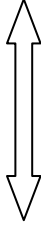
1.1.3.5 Tissue Radiosensitivity

Radiosensitivity is described as the relative sensitivity of tissues to the harmful effect of radiation. Not all the tissues in the body have equal radiosensitivity.

“In general, the radiation sensitivity of a tissue is directly proportional to the rate of proliferation of its cells and inversely proportional to the degree of cell differentiation” (Rubin and Casarett, 1968). In other words the actively dividing cells or the cells not fully mature are the most sensitive cells to damage induced by radiation.

For example in Table 1.1 tissues and organs are listed from the most radiosensitive to the least radiosensitive (Rubin and Casarett, 1968).

Table 1.1 List of tissues and organs from most radiosensitive to least radiosensitive.

<div>Most Radiosensitive</div> <div></div> <div>Least Radiosensitive</div>	Blood forming organs
	Reproductive organs
	Skin
	Bone and teeth
	Muscle
	Nervous system

1.2 Radiotherapy

Radiotherapy is the medical use of ionizing radiation to control malignant tumors (Dunne-Daly, 1999). “The first clinical use of radiation for the treatment of tumours was recorded in 1897. Today, it is an important and the most common therapeutic option for a number of malignancies” (Prise *et al.*, 2005). 80% of cancer patients need radiotherapy at some time, either for curative or palliative purpose (Nair *et al.*, 2001). “The goal of radiotherapy is to maximize tumor kill while minimizing damage to normal tissues in the body” (McCumber, 2004).

Basically, there are two types of radiation treatment:

1. External Beam Radiation Therapy (EBRT) or Teletherapy:

EBRT is the most common form of the radiation therapy which use the radiation produced by external treatment machine. The source of radiation used in EBRT may come from X-rays or gamma rays. X-rays are created by machines called linear accelerators. Compared with other types of radiation, X-rays can deliver radiation to a relatively large area. Gamma rays are produced when isotopes of certain elements (such as iridium and cobalt-60) release radiation energy as they break down. Gamma

rays produced by the breakdown of cobalt-60 are used in the treatment called the “gamma knife”

“In EBRT, treatment is usually in a fractionated pattern. For example, a typical course of therapy would consist of 30 treatments each of 2 Gy, over a 6-week period, to give a total dose of 60 Gy to the tissue” (Little, 2001).

2. Brachytherapy or Internal Therapy:

This form of radiation therapy involves treatment through radioactive sources implanted directly into the tissue or inserted into body cavities from which the tissue can be reached. The Caesium and Iridium are commonly used radioactive materials used in brachytherapy (Little, 2001).

1.3 Radioprotectors

When cancer patients undergo radiotherapy, there is a dose-response relationship between the dose given to the patients and the response of tumor cells. Unfortunately, radiotherapy is toxic both to tumor cells and healthy tissues (Grdina *et al.*, 2002a). Since there is an even steeper increase in normal tissue damage with increasing radiation dose, the healthy cell reactions can cause important side effects in cancer patients and they limit the total dose that can be exposed to the patients (Andreassen *et al.*, 2003). For this reason, inactivation of tumor cells while maintaining the integrity of normal tissues has been an important subject in radiation therapy for many years. Today, in order to reduce radiotherapy-induced damage to normal tissue, several attempts have been made. One of such approaches is to use radioprotective agents (radioprotectors) in order to preserve healthy tissue. “Radioprotectors are agents that provide protection of normal tissue during radiotherapy. The purpose of these compounds is to increase the number of tumor cells killed without a proportional increase in normal tissue damage” (Dunne-Daly, 1999).

“Since exposure to radiation in radiotherapy, or accidental exposure to radiation, can produce significant unwanted side effects, it is very important to ameliorate such effects by the use of radioprotective agents” (Hosseinimehr, 2007). An ideal radioprotective agent has to have following properties (Andreassan *et al.*, 2003; Hosseinimehr, 2007; Herscher *et al.*, 1999):

- It must provide meaningful protection against the effects of radiation.
- It should not cause tumor protection (It should protect normal tissues selectively).
- It must have a general protective effect on the majority of organs.
- It must have to exhibit acceptable toxicity profile.
- It should be easy to handle in daily radiotherapy logistics.
- It must have an acceptable route of administration (preferably oral, or alternatively intramuscular)

A wide range of agents have shown various degrees of protective properties. A list of various categories of radioprotectors and their mechanism of action were given in Table 1.2 (Nair, 2007; Zabbavora and Kanai, 2008).

Table 1.2 Different radioprotectors and their mechanism of action

Radioprotectors	Mechanism of action
A. Sulfhydryl compounds Cysteine, Cysteamine, Glutathione, AET, WR 2127 and other WR-compounds	Free radical scavenging, donation of H atom
B. Antioxidants Tempace, Vitamin A, E & C, TMG, Melatonin, <i>etc.</i>	Free radical scavenging
C. ACE inhibitors Captopril, Elanopril, Pencillamine, Pentoxifylline, L-158, 809, <i>etc.</i>	Protease inhibition (through renin-angiotensin system), anti-oxidation collagen synthesis inhibition.
D. Metalloelements Manganese chloride, Cadmium salts, Bismuth Subnitrate, <i>etc.</i>	Metallothionine induction
E. Immunomodulators Gamma-interferon, Polysaccharides AM5, AM218, Heat killed <i>Lactobacillus</i> cells, Broncho-Vaxom, Trehalose dicorynomycolate, AS101	Immune stimulation, increased production of cytokines
F. Lipopolysaccharides and Prostaglandins	Prostaglandin synthesis, elevated levels of cyclic AMP, DNA repair
G. Plant extracts and isolated compounds Curcmin, Orientin, Vicinin	Free-radical scavenging, anti-oxidation
H. DNA binding ligands Hoechst 33342	Electron transfer, free radical scavenging
I. Other Compounds Carnosin Tempace, Tempol	Free-radical scavenging Antioxidant, free-radical scavenging
J. NOS inhibitors AMT, L-NAME, 7-nitroindazole	Prevent overproduction of <i>NO</i> and ONO_2^-
K. Anti-inflammatory agents Resveratrol, Palifermin, Benzydamine and others	Anti-inflammatory properties, regulate intrinsic cytoprotective mechanisms, stimulate or inhibit cellular proliferation and differentiation

The vast majority of the radioprotectant agents developed to date are either too weak in terms of radioprotection, too toxic or without any apparent mechanisms to ensure selective normal tissue protection. Therefore, only a very limited number of substances are presently of clinical relevance (Andreassan *et al.*, 2003). The sulfhydryl compound amifostine is the only radioprotective agent that has been approved by the Food and Drug Administration (FDA) to protect normal tissues against the toxic effects of radiotherapy (Cassatt *et al.*, 2002).

1.4 Amifostine

Amifostine, formerly known as WR-2721, was originally developed as a radioprotective agent during the Cold War in the 1950s by Walter Reed Army Institute which is a part of the Anti-radiation Drug Development Programme of the United States Army. The aim of this programme was to develop compounds which are capable of protecting the military and civil persons from the harmful effects of radiation in the event of a nuclear attack. More than 4400 sulphhydryl-containing substances with radioprotective properties were tested and only amifostine was found to exhibit the effective radioprotection and acceptable toxicity. Subsequently, it was investigated for its potential use in radiotherapy and chemotherapy as a cytoprotectant agent. During the 1980s some clinical phase I-II studies provided evidence that amifostine might protect normal tissues from irradiation and chemotherapy (Grochava and Smordova, 2007).

In 1996, FDA approved amifostine as a cytoprotective agent with cisplatin-based chemotherapy against ovarian cancer. In 1999, based on a phase III study which has provided strong evidence that amifostine prevents xerostomia in patients treated with radiotherapy for head and neck cancer, the FDA approval was extended to postoperative radiotherapy for head and neck cancer as well (Andreassan *et al.*, 2003).

“Today, amifostine is considered as a broad-spectrum radio- and chemoprotective drug and it has been clinically used as a reducer of the toxic side effects induced by

ionizing radiation and a number of chemotherapeutic agents” (Grochava and Smordova, 2007). Amifostine is generally well-tolerated and it has some temporary side effects including hypotension, nausea, vomiting, sneezing, sleepiness and occasional allergic reactions (Hensley *et al.* 1999; Andreassan *et al.*, 2003; Grochava and Smordova, 2007).

Amifostine has been largely investigated in some clinical studies and has shown different protective effects. For instance, it can ameliorate or prevent radiation-induced xerostomia (Brizel *et al.*, 2000), cisplatin-induced nephrotoxicity (Anand and Bashey, 1993), anthracycline-induced cardiotoxicity (Dorr, 1996), chemotherapy-related thrombocytopenia (Budd, 1996). However, the molecular effect of amifostine on the structural and functional properties of tissues and cell membranes are unknown, yet.

1.4.1 Chemistry of Amifostine

Amifostine (Ethyol; Ethiophos) is an organic thiophosphate prodrug known chemically as S-2-(3-aminopropylamino)-ethylphosphorothioic acid (Foster-Nora and Siden, 1997). The chemical structure of amifostine was shown in Figure 1.5.

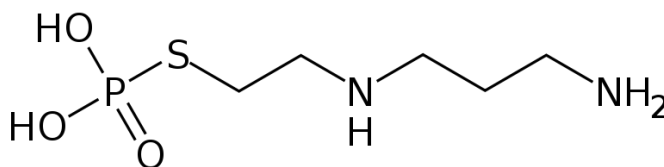


Figure 1.5 Chemical structure of amifostine.

Amifostine has a molecular weight of 214.224 g/mol. It is highly water soluble molecule, with the solubility of the trihydrate being more than 9 g per 100 ml at room temperature. The compound has four ionizable groups, two of which are associated with the phosphate group and two with the amino group. At physiological pH, amifostine exists as a double zwitterions with an isoelectric point of about 6.6. It is also very polar, with an octanol/water partition coefficient smaller than 0.01. Its free active thiol (WR-1065) has an octanol/water partition coefficient of 0.037 (Felckenstein *et al.*, 1988). It has a pKa of 9.2 (Merck index).

1.4.2 Mechanism of Action

Amifostine can not readily cross cell membranes since it is very hydrophilic (Yuhás, 1982). “It only becomes active when it combines with alkaline phosphatase, an enzyme found on the cell membranes of epithelial tissues. The alkaline phosphatase removes the phosphorus group from amifostine, converting it into the active thiol compound WR-1065” (McCumber 2004). After dephosphorylation process, amifostine becomes less hydrophilic and can easily cross the cell membrane (Yuhás *et al.*, 1982). “WR-1065 is further metabolized to the disulfide, WR-33278, that may also cause radioprotection, although to a much lesser extent” (Andreassan *et al.*, 2003). Figure 1.6 shows the metabolism of amifostine (Grochova and Smardova, 2007).

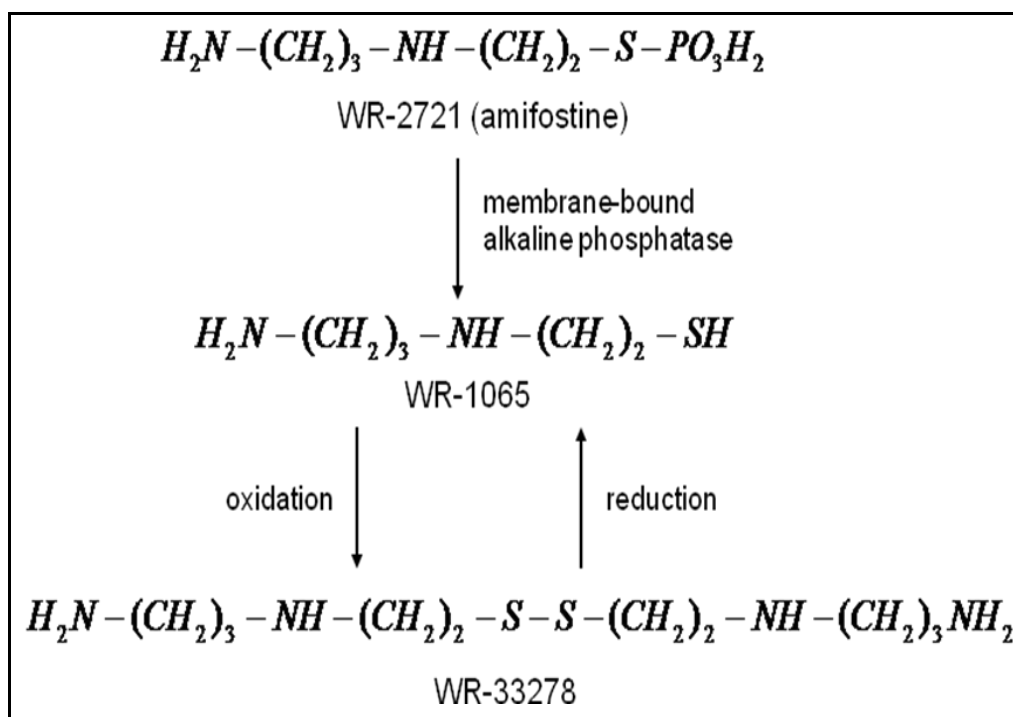


Figure 1.6 Metabolism of amifostine (Grochova and Smardova, 2007)

The active thiol, WR-1065, can provide protection by various mechanisms in the cell. They include the following:

- “It can act as a potent scavenger of oxygen free radicals, those derived from ionizing radiation” (Capizzi, 1999).
- “It may also react directly with oxygen and thus protect the cell by creating local hypoxia at the target” (Andreassan *et al.*, 2003).
- “It can bind to DNA molecules, changing their shape into a compact form that is less vulnerable to damage by cytotoxic agents such as free radicals” (McCumber *et al.*, 2004). “Because WR-1065 has a net charge of +2, it will be attracted to DNA (which is negatively charged) and is therefore more

likely to exert a protective effect against radiation induced damage than a compound with a net charge of 0 or a negative net charge” (Grdina *et al.*, 2002a).

- “It may facilitate chemical repair processes by donation of hydrogen” (Andreassan *et al.*, 2003).
- “It may exerts cytoprotective effects by a catalytic inhibition of the enzyme DNA topoisomerase II alpha, leading to prolong the cell cycle, hence providing more time for DNA repair” (Snyder and Grdina, 2000).
- Besides the protective effects of WR-1065, the other metabolite of amifostine, WR-33278, have cytoprotective properties. “WR-33278 exhibits structural similarities to naturally occurring polyamines and may affect processes related to DNA synthesis, DNA repair, gene expression, and cell cycle progression” (Andreassan *et al.*, 2003).

It has been demonstrated that amifostine has a unique ability to protect normal tissues without protecting tumor cells from radiation induced cellular injury. The selective protection derives from several mechanisms as follows: first the concentration of alkaline phosphatase, which is the amifostine-activating enzyme, is higher (275-fold) in normal cells than in tumor cells; second, the lower blood supply in tumor cells in comparison to normal cells may result lower delivery of the drug to tumors; third the neutral pH of normal tissue results in a higher uptake of the drug than tumor tissue which has an acidic environment; fourth the drug is absorbed by active transport in normal tissues but by passive diffusion in tumors. All these mechanisms bring higher (about 50-100 fold) active-drug concentrations in normal cells than in tumor cells (Santini and Giles, 1999).

1.4.3 Pharmacokinetics

Amifostine is not orally active and thus needs to be administered systemically (Bonner and Shaw, 2002). “It is suitable for intravenous infusion to humans or intraperitoneal administration to rats at 200 to 400 mg/kg body weight” (Atalay *et al.*, 2006). Alternatively, subcutaneous administration of amifostine has been described by some authors (Hosseinimehr, 2007).

“After intravenous administration, amifostine is rapidly dephosphorylated to its active metabolite WR-1065 by alkaline phosphatase with a pH optimum at 8 to 9” (Andreassan *et al.*, 2003). Dephosphorylation occurs prevalently in peripheral tissues, whereas it is unremarkable in blood circulation.

Amifostine has an extremely short half-life, with a $T_{1/2\alpha}$ of 0.8 min and $T_{1/2\beta}$ of 8.8 min, which means that 90% of the drug disappears from the plasma in 6 min (Castiglione *et al.*, 2000). The rapid clearance of amifostine from plasma may be attributed to its rapid conversion into WR-1065 in normal tissues (Santini and Giles 1999). WR-1065 half-life is longer (7.3 hr) and disulfides half-life is 8-13 hr (Castiglione *et al.*, 2000).

Uptake of WR-1065 varies considerably between different tissues. It appears to be greatest in the kidney, salivary glands, intestinal mucosa, liver and lung and lowest brain and skeletal muscle (Capizzi, 1999).

“The elimination rate of WR-1065 varies considerably between different tissues. In lung and skin, tissue concentrations decline rapidly during the first 30 minutes, whereas concentrations remain high in salivary glands for up to 3 hours” (Andreassen *et al.*, 2003). It has been shown that liver eliminates amifostine more extensively than kidneys, lungs and the gastrointestinal tract. Approximately, 90% of the drug is extracted by the liver (i.e converted to WR-1065) (Levi *et al.*, 2002).

“Quantitatively, there is great variability in the radioprotection achieved by amifostine in different normal tissues: protection factors range from 3 in the

haematopoietic system and salivary gland to near 1 in lung, kidney, and bladder” (Andreassen *et al.*, 2003). “It has been reported that injection of amifostine protects against both early and late irradiation-induced injuries in a number of animal models. Maximum radioprotection results when amifostine is administered 30 to 60 minutes before irradiation” (Spencer and Goa, 1995).

1.5 Brain

The brain, which is the main part of central nervous system (CNS), is a complex organ with both structural and biochemical heterogeneity. If a coronal section is taken from the brain, some areas appear white (white matter) and others appear grey (grey matter) (Figure 1.7). The white matter is made up of axons. An axon is a part of neuron that carries electrical signals away from neuronal cell body. Since it contains myelin sheaths which have very high lipid content, it appears white.

Myelin is rich in lipid content because of its multilamellar structure and a greater lipid-to-protein ratio than most cellular membranes. Although all lipids present in myelin can also be found in other cellular membranes, there are some lipids that are much abundant in myelin than in other cellular membranes. These lipids include the galactolipids, cerebroside and sulfatide. Other lipids, like cholesterol, are also present in high concentrations in myelin but are also represented strongly in other membranes. The grey matter consists of the neuronal cell body so it appears grey (Levine and Wetzel, 1993).

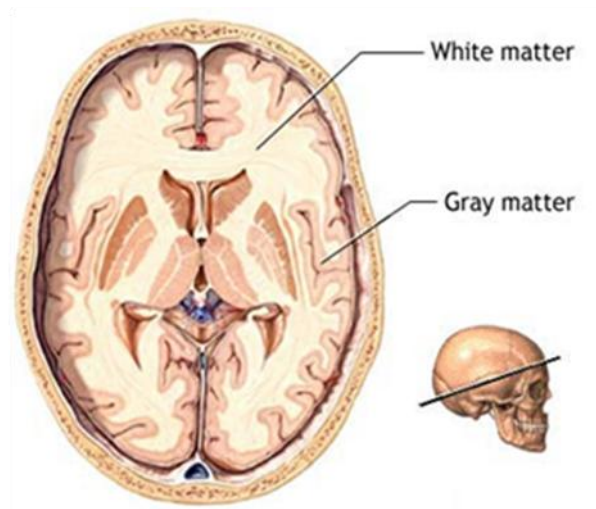


Figure 1.7 The section of human brain

The CNS is a major dose-limiting organ for the radiotherapy of various cancers, particularly for those arising within the CNS and the severity of ionizing radiation's side effects and its harmful effects on normal brain tissues makes this treatment difficult (Yoneoka *et al.*, 1999). The brain is particularly vulnerable to free radical damage since it has limited antioxidant enzymes (eg. catalase, GSH peroxidase) and consumes approximately 20% of oxygen in the body (Atalay *et al.*, 2006). In addition, the high concentration of PUFAs and metals (eg. iron) makes brain very vulnerable to free radical damage (Floyd and Carney 1993; Zwart *et al.*, 1999).

1.6 Biological Membranes

An essential feature of every cell is the presence of membrane which defines the boundaries of the cell and serves as the interface between the machinery in the interior of the cell and extracellular matrix (Becker *et al.*, 2002).

All biological membranes contain polar lipids, which make up from 20 to 80 percent of membrane mass, depending on the type of membrane; the remainder is mostly protein (Lehninger, 1982). The most abundant lipids found in membranes are the phospholipids which have a polar head group and two hydrocarbon tails. In Figure 1.8, a phosphatidylcholine molecule represented schematically (A), in formula (B), as a space-filling model (C), and as a symbol (D).

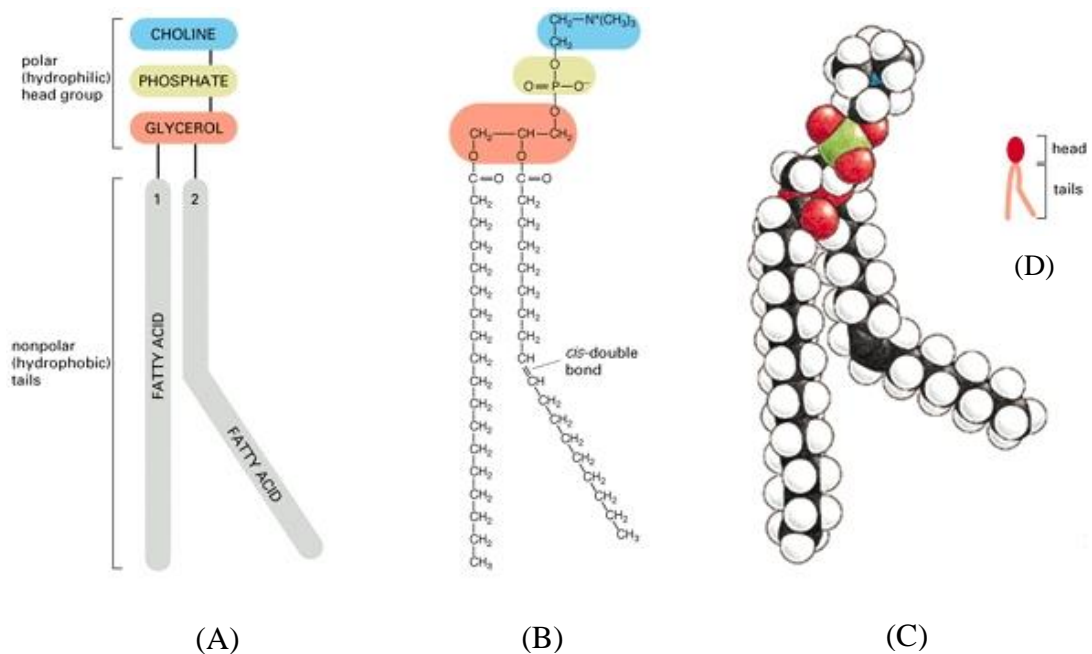


Figure 1.8 The parts of a phospholipid molecule

The tails of a phospholipid molecule are composed of fatty acids which can differ in length and saturation. The difference in length and saturation of fatty acids influence

the fluidity of membrane. The other factor affects the fluidity is the amount of cholesterol present in the membrane (Alberts *et al.*, 2002).

“The capacity of the plasma membrane to control interface, signal transfer and subsequent metabolic pathways involves the integrity of the spatial and intermolecular arrangements of its components” (Berroud *et al.*, 1996). Since the lipid dynamics of the biological membranes controls many of cell functions including signal transduction, solute transport and activity of enzymes associated with the membrane, it is very essential to preserve the membrane fluidity at optimum level (Van Blitterswijk, 1985; Garcia *et al.*, 2001). In addition, today it is known that differences in lipid order, lipid dynamics, protein secondary structure in membranes together with the changes in the content of macromolecules disturb the kinetics and functions of ion channels and also lead to many diseases (Awayda *et al.*, 2004). The variations in the ratios of biomolecules such as unsaturated to saturated lipids, lipid to protein are related to lipid structure such as membrane thickness, lipid order, which are also related with membrane permeability (Szalontai *et al.*, 2000; Awayda *et al.*, 2004).

1.6.1 Liver Microsomal Membrane

The liver is a central organ for alcohol and drug metabolism and the main site of biosynthesis of unsaturated lipids (Foucher *et al.*, 1997; Nakajima *et al.*, 2002). In liver, the most vulnerable site for lipid peroxidation is the endoplasmic reticulum which is a continuous network of flattened sacs, tubules and associated vesicles stretching throughout the eukaryotic cell's cytoplasm. When a tissue is homogenized for subcellular fractionation, the endoplasmic reticulum membranes break into smaller fragments that spontaneously close to form sealed vesicles known as microsomes (Becker, 2002). Microsomal fractions, which have rough and smooth endoplasmic reticulum vesicles in roughly 2:1 ratio, contain enzymes involved in reduction and oxidation reactions, drug metabolism, cholesterol synthesis and fatty acid metabolism (Garg *et al.*, 1985).

Liver microsomes contain great variety of phospholipids in a high concentration, in washed membranes the protein to phospholipid ratio is around 2. Microsomes contain the following species of phospholipids: phosphatidylcholine, phosphatidylethanolamine, phosphatidylserine, phosphatidylinositol, sphingomyelin. Microsomal membranes also contain cholesterol. The fatty acid composition of the bulk lipids of rat liver microsomes is so highly unsaturated that they are very fluid at physiological temperatures (Catala, 1993).

The endoplasmic reticulum is the most abundant membrane in metabolically active cells. Thus, microsomes are an ideal preparation in which to study the relationships between enzyme structures, the functional properties of membrane bound enzymes, lipid-protein and protein-protein interactions, and (Heinemann and Ozols, 1998).

1.7 Spectroscopy

Spectroscopy is defined as the use of electromagnetic radiation to study a matter qualitatively and quantitatively. In spectroscopic techniques, a sample is irradiated with some form of electromagnetic radiation and the emission, absorption or scattering are measured in terms of some parameters. The interpretation of these parameters gives useful information about the sample. Figure 1.9 sums up many of the important regions of the electromagnetic spectrum.

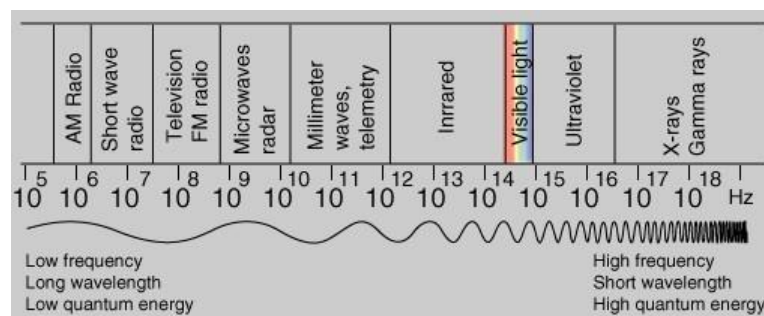


Figure 1.9 Electromagnetic radiation and the scales used

An electromagnetic wave is composed of two mutually perpendicular magnetic and electric fields which oscillate in single planes at right angles to each other. These fields are in phase and are propagated as a sine wave as shown in Figure 1.10, where E is the direction of the electric field while B is the direction of the magnetic field (Stuart, 1997).

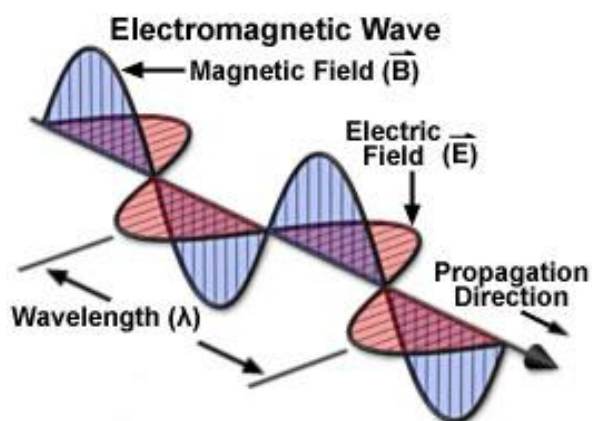


Figure 1.10 An electromagnetic wave

λ symbolizes wavelength, which is the distance between two peaks. The product of wavelength λ and frequency ν (Hz), which is the number of cycles per second, will give the velocity of propagation of a wave. It follows that:

$$c = \lambda \nu \quad \text{where } c \text{ is the velocity of light in vacuum } (c = 3.0 \times 10^8 \text{ ms}^{-1}).$$

Electromagnetic radiation covers a wide range of wavelengths and therefore, frequencies. However, in some cases, such as in infrared spectroscopy, the unit

wavenumber $\bar{\nu}$ is used for practical reasons. Wavenumber (cm^{-1}) is the number of waves in a length of one centimeter and thus is given by:

$$\bar{\nu} = \frac{1}{\lambda}$$

The energy (J.mol^{-1}) of a wave is given by the Bohr equation:

$$E = h\nu = hc \bar{\nu}$$

where h is Planck's constant ($h = 6.626 \times 10^{-34} \text{ J.s}$).

From these equations, it is clear that both wavenumber and frequency are directly proportional to energy (Volland; 1999).

Any molecule has a number of stacks of energy levels, with each stack corresponding to a particular process, such as electronic, vibrational or rotational change. For most purposes it is convenient to treat a molecule as if it possesses several distinct reservoirs of energy. The total energy is given by the following equation (Campbell and Dwek, 1984).

$$E_{\text{total}} = E_{\text{nuclear spin orientation}} + E_{\text{translation}} + E_{\text{electron spin orientation}} \\ + E_{\text{rotation}} + E_{\text{vibration}} + E_{\text{electronic}}$$

The contributions of $E_{\text{nuclear spin orientation}}$, $E_{\text{translation}}$ and $E_{\text{electron spin orientation}}$ are negligible since the separations between respective energy levels are very small. The separations between the neighboring energy levels corresponding to E_{rotation} , $E_{\text{vibration}}$ and $E_{\text{electronic}}$ are associated with the microwave, infrared and uv-visible regions of the electromagnetic spectrum, respectively (Campbell and Dwek, 1984).

The interaction between electromagnetic radiation and matter can cause redirection of the radiation between energy levels of the atoms or molecules. In this phenomenon, the energy excites a molecule to a higher energy level. The type of excitation depends on the wavelength of the light. For example, the transition is from

one vibrational energy level to another, the radiation will be from the infrared portion of the electromagnetic spectrum (Freifelder, 1982).

A typical energy-level diagram describing these energy levels is presented in Figure 1.11. In this figure, vibrational energy levels are shown as thin horizontal lines. The long arrows show a possible electronic transition from the ground state to the first excited state while the short arrow represents a vibrational transition within the ground electronic state (Freifelder, 1982).

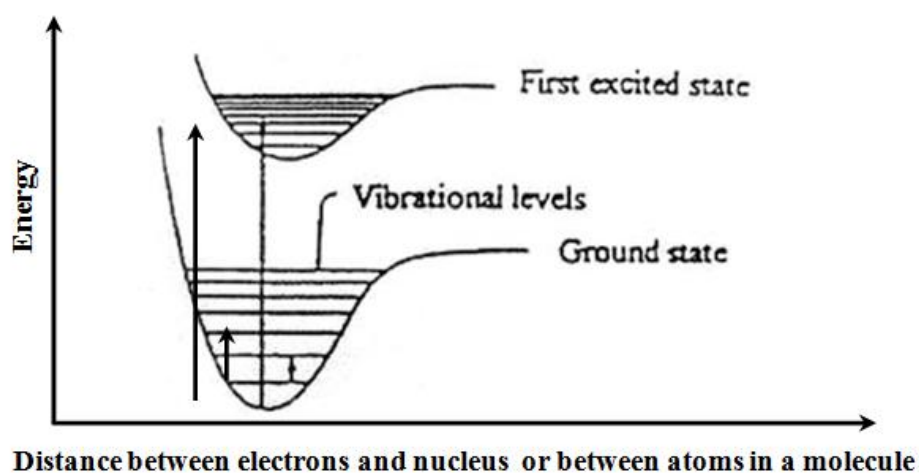


Figure 1.11 A typical energy-level diagram illustrating the ground and first excited electronic energy levels and their vibrational levels (Freifelder, 1982)

1.7.1 Infrared Spectroscopy

Infrared spectroscopy, which is used in a number of branches of science as a quantitative and qualitative tool, is one of the most important analytical techniques available to today's scientists.

The infrared region includes the range of the electromagnetic spectrum at wavenumbers between 4 and 14000 (cm^{-1}). It is divided into three sub regions (Table 1.3) (Smith, 1999). The mid-infrared region is employed in most IR applications, but the far and near IR regions also give information about certain materials.

Table 1.3 Three subregions of infrared region

Region	Wavenumber range (cm^{-1})
Near	14000-4000
Middle	4000-400
Far	400-4

Infrared spectroscopy is based on the transitions between vibration energy levels of the atoms of a molecule. “Spectrum is obtained by passing radiation through a sample and determining what fraction of the incident radiation is absorbed at a particular energy” (Stuart, 1996). The energy of most vibrational transitions corresponds to the infrared region of the electromagnetic radiation spectrum. Hence, the interaction of infrared radiation with matter is associated with molecular vibrations. An infrared spectrum is usually the plot of absorption as a function of wavenumber ($\bar{\nu}$) and consists of absorption bands with wavenumber maxima expressed in terms of cm^{-1} . There are no two compounds which have exact same infrared spectrum since each material has a unique pattern of atoms. Thus, an infrared spectrum can be used to identify different types of materials.

Matter is composed of atoms that are in a continuous motion with respect to each other. These atoms are held together by valence forces and they can vibrate because of their thermal energy. When infrared radiation interacts with matter, it can be absorbed, causing the chemical bonds in the material to vibrate. The presence of chemical bonds in a material is a necessary condition for infrared absorbance to occur. Functional groups tend to absorb infrared radiation in the same wavenumber range. This means that there is correlation between the wavenumbers at which molecule absorbs infrared radiation and its structure. This correlation allows the structure of an unknown molecule to be determined from its infrared spectrum and allows spectra of different samples to be compared to each other to see if they are the same (Stuart, 1997).

The various modes of vibration, which are presented schematically in Figure 1.12, involve a change in either bond angle or bond length (Arrondo *et al*, 1993). The change in bond angle is termed bending vibration, whereas a change in bond length is called stretching vibration, which can either be symmetric or asymmetric depending on the phase of the stretching mode (Stuart, 1997). Consequently, infrared spectra are generated by the characteristic motions of a variety of functional groups (e.g. olefinic=CH, carbonyl, methyl, amide etc.). The sensitivity of these modes of vibration to any alteration in the conformation, structure and environment presents the value of infrared spectroscopy.

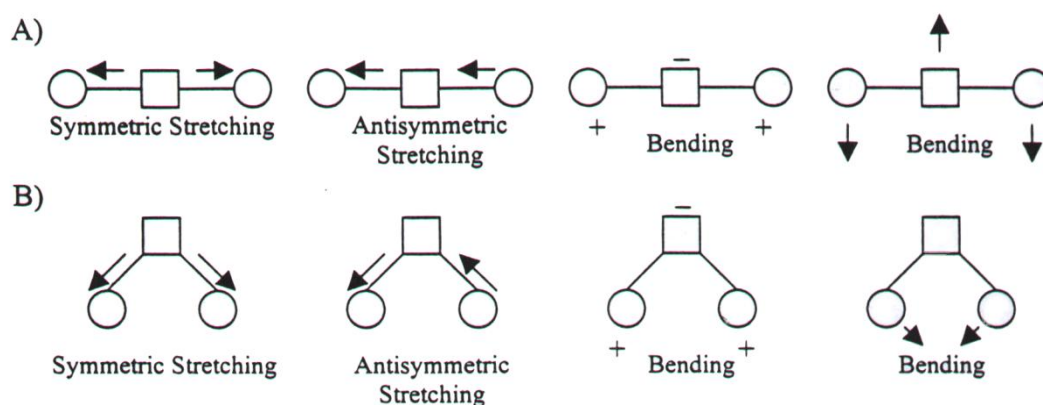


Figure 1.12 The schematic representation of some molecular vibrations in linear triatomic molecules (A) and non-linear triatomic molecules (B). (+) and (-) symbols represent atomic displacement out of page plane (Arrondo *et al.*, 1993)

To have absorption of infrared radiation for a vibration, firstly the molecule should have a frequency of vibration similar to electromagnetic wave, and secondly a change in dipole moment should occur.

1.7.1.1 Fourier Transform Infrared Spectroscopy

“The basic principle of Fourier transform infrared (FTIR) spectroscopy is the interference of radiation between two beams to yield an interferogram. Interferogram is a signal produced as a function of the change of pathlength between the two beams” (Stuart, 2004).

The most important feature of an interferogram is that every individual data point of this signal contains information over the entire infrared region. This process is carried by an interferometer, which is commonly a Michelson Interferometer. This device encodes the initial frequencies into a special form, which the detector can observe. For rapid-scanning interferometers liquid nitrogen cooled mercury cadmium

telluride (MCT) detectors are used. For slower scanning types of interferometer, pyroelectric detectors (e.g. a deuterated triglycine sulfate (DTGS) detector element) can be used. In essence, the detector is always observing all frequencies at the same time (Griffiths and De Haseth, 1986).

“The two domains of distance and frequency are interconvertible by the mathematical method of Fourier transformation” (Stuart, 2004). Therefore, Fourier transformation is simply a mathematical means of sorting out the individual frequencies for the final representation of an infrared spectrum.

Figure 1.13. schematically visualize the basic components of an FTIR spectrometer (Stuart, 1997)

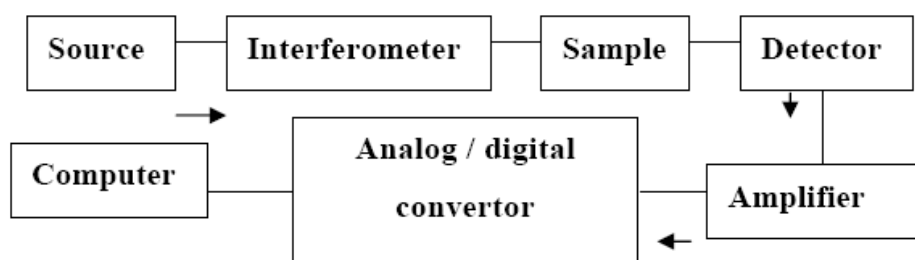


Figure 1.13 The components of an FTIR spectrometer (Stuart, 1997)

The radiation emerging from the source is passed through an interferometer to the sample before reaching a detector. Upon amplification of the signal, in which, high frequency contributions have been eliminated by a filter, the data are converted to a digital form by an analog-to-digital converter and then transferred to the computer

for Fourier transformation to be carried out. The computer can deconvolute (Fourier Transform) all the individual cosine waves that contribute to the interferogram, and so give a plot of absorbance against wavenumber (cm^{-1}) (Stuart, 1996).

1.7.1.1.1 The Advantages of FTIR Spectroscopy

The main advantages of FTIR spectroscopy as follows:

- The system can be applied to the analysis of any type of sample. Materials may be examined in a variety of physical states, such as solids, films, aqueous suspensions and this fact allows the performance of temperature dependent studies because conformational transitions does not present a limitation. (Mendelsohn and Mantsch, 1986; Colthup *et al.*, 1975).
- It gives valuable information about the biological samples by identifying alterations in the functional groups, simultaneously (Kneipp *et al.*, 2000; Bozkurt *et al.*, 2007; Garip *et al.*, 2007).
- It offers an exact measurement method, i.e., it does not require an external calibration (Rigas *et al.*, 1990, Manoharan *et al.*, 1993, Ci *et al.*, 1999).
- Digital subtraction (that is, point-by-point subtraction of the separate spectra by a computer) can be used to produce good difference spectra. This method has great advantages in obtaining infrared spectra in aqueous solutions (Campbell and Dwek, 1984).
- FTIR spectrometry is able to increase the signal-to-noise ratio by signal averaging (Stuart, 1997).
- It is is a non-disturbing method that presents structural and functional data about the sample (Liu *et al.*, 1996; Toyran *et al.*, 2004; Dogan *et al.*, 2007a).
- Small sample quantities are sufficient to analyse and in vivo studies are possible (Mendelsohn and Mantsch, 1986).

- The instruments are relatively easy to use and data processing is simple with the computer softwares. Moreover, system permits permanent data storage, manipulation of data and quantitative calculations (Yano *et al.*, 1996, Ci *et al.*, 1999).
- Since a computer is already used to obtain the Fourier transform, it is easy to perform many scans to improve the signal-to-noise ratio (noise adds up as the square root of the number of scans, whereas signal adds linearly). It has dramatically improved signal to noise ratio by the averaging of numbers of scans per sample (Beaten *et al.*, 1998).
- The method monitors the changes in the molecular vibrations and therefore it gives informations about the microenvironment of molecules.

1.7.1.1.2 FTIR Spectroscopy in Biological Studies

FTIR spectroscopy is a powerful technique because of its ability to detect the alterations in the functional groups of the membrane and the tissue components, such as proteins, lipids, nucleic acids and carbohydrates (Fabian *et al.*, 1995; Kneipp *et al.*, 2000; Lewis *et al.*, 1989; Moore *et al.*, 1995; Toyran *et al.*, 2004; Toyran *et al.*, 2005; Severcan *et al.*, 2005; Akkas *et al.*, 2007). Thus, it can provide a total simultaneous biochemical analysis. It has a number of advantages for the investigation of biological samples since it doesn't require either the performance of chemical reactions prior to the determination of the reaction products or the use of probe molecules (Lewis *et al.*, 1989; Severcan *et al.*, 2005).

The observed spectral features are related to chemical bond vibrations of specific molecular moieties of individual constituents (Lewis *et al.*, 1989). The shift in peak position, bandwidth and peak area/intensity give valuable information about the biological samples such as tissues, membranes, cells and biofluids. All these spectral parameters are sensitive to pathological and other conditions-induced alterations in the macromolecules of the biological system (Toyran *et al.*, 2004; Chen *et al.*,

2008;). Therefore more recently it is widely applied for diagnosis of several diseases (Yano *et al.*, 1996; Liu *et al.*, 1996; Schultz *et al.*, 1998; Ci *et al.*, 1999; Dicko *et al.*, 1999; Severcan *et al.*, 2000; Toyran *et al.*, 2004; Petibois *et al.*, 2006; Dogan *et al.*, 2007b; Bozkurt *et al.*, 2007; Akkas *et al.*, 2007; Severcan *et al.*, 2010). and aquatic toxicological states (Cakmak *et al.*, 2003; Cakmak *et al.*, 2006). It was also employed to determine radiation-induced changes in different tissues such as food (Dogan *et al.*, 2007a) and rat brain (Toyran *et al.*, 2005).

1.7.1.2 Fourier Transform Infrared Microspectroscopy

FTIR microspectroscopy and imaging became powerful technique to study the molecular chemistry of biological materials by allowing connection to morphology. FTIR microspectroscopy is the combination of infrared spectroscopy with light microscopy. It allows locating the area to be analyzed and thus molecular information is obtained with great spatial resolution and microscopic scale (Levin ang Bhargawa, 2005). It is widely used to identify and determine the molecular chemistry of various samples involving forensic materials, animal and plant tissues, minerals, polymer films and pharmaceuticals.

Using FTIR microspectroscopy the whole tissue area can be mapped point-by-point. It can be achieved by recording the infrared spectrum of the sample at one point, moving the sample to another point and recording the spectrum at that point and so on. In this way, a chemical map of the sample can be obtained. This typically involves. In this manner, Figure 1.14 shows a conventional FTIR microspectroscopy.

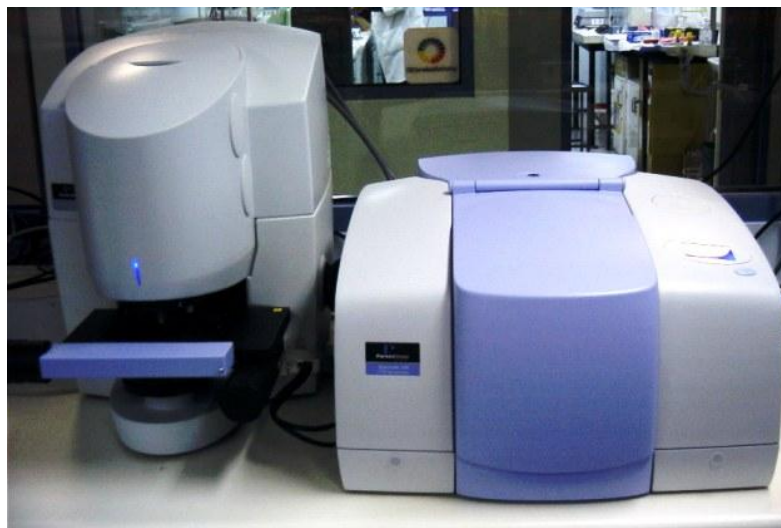


Figure 1.14 Perkin Elmer Spectrum/One Spotlight 400 FTIR microspectroscopy

1.7.1.2.1 The Advantages of FTIR Microspectroscopy

- “Unlike more traditional techniques, FTIR microspectroscopy can provide information about the in situ chemical features from microscopic regions of a tissue section” (Levine and Wetzel 1998).
- It allows the analysis of very small samples. The practical advantage of this sensitivity is that it allows the analysis of trace deposits of biological materials in situ, without extraction (Jackson *et al.*, 1998).
- In traditional techniques, sample preparation includes several steps such as fixation of the tissue, embedding in a matrix and microtoming. Histochemical information is obtained with the application of specific stains that selectively bind to different components and from these specimens it is very difficult to generate quantitative information. No preprocessing, no dying, no labeling

are required for this technique, so FTIR microspectroscopy is a non-destructive technique (Wetzel, 1995; Kretlow *et al.*, 2008).

- FTIR microspectroscopy equipped with computer controlled stages allow the distribution materials within tissue sections to be mapped with a high spatial resolution. This approach termed functional group mapping, can provide a valuable aid for understanding spectral data as the distribution of a number of chromophores within tissues can be analyzed. It may be expected that functional groups arising from the same molecule will show a similar distribution within a tissue, and therefore; a comparison of the distribution of assigned and unassigned absorptions can be used to aid assignments (Jackson *et al.*, 1998).
- It is very fast tool (Kretlow *et al.*, 2008).

1.7.1.2.2 FTIR Microspectroscopy in Biological Studies

An infrared spectrum of a tissue has characteristic frequencies, intensities and bandwidths because the molecular parameters such as composition, structure and the molecular interactions in a tissue are unique. So, FTIR microspectroscopy provides fingerprint-like information and allows the determination of functional groups of macromolecules and consequently it enables the description of conformationally different tissue constructions (Kneipp *et al.*, 2000; Kretlow *et al.*, 2006). During the past years, the power of FTIR spectroscopy has been shown for many kinds of biological tissues, mainly with the aim of improving professional diagnostic methods to be able to detect the pathologies in tissues such as the cervix (Romeo *et al.*, 2002; Chiriboga *et al.*, 1998), brain (Choo *et al.*, 1996; Kneipp *et al.*, 2000), colon (Lasch *et al.*, 2004; Lasch and Naumann, 1998), breast (Zhang *et al.*, 2003), heart (Wang *et al.*, 2005a; Toyran *et al.*, 2006; Toyran *et al.*, 2007) and also of individual normal and cancerous cells (Diem *et al.*, 2002).

1.7.1.3 Synchrotron Fourier Transform Infrared Microspectroscopy

In recent years, synchrotron-based imaging techniques became very popular for identifying the biochemical changes in biological tissues (Miller *et al.*, 2006a). Synchrotron FTIR (SR-FTIR) microspectroscopy, i.e., the combination of FT-IR spectroscopy, microscope and utilizes synchrotron infrared radiation as light source, is a valuable technique that provides ultraspatially resolved spectroscopic information and a higher signal-to-noise ratio on minute quantities of microscopic structures within a given sample. The aim of synchrotron infrared spectroscopy is to bring together the chemical sensitivity of IR spectroscopy and the brightness of synchrotron light and to have valuable information about the biological materials. “SR-FTIR microspectroscopy provides chemical information on tissue components such as proteins, lipids, nucleic acids and carbohydrates at a diffraction-limited spatial resolution of 2–10 μm in the mid-infrared region” (Miller *et al.*, 2006a).

“Synchrotrons are accelerator facilities that provide extremely high-flux and high-brightness electromagnetic radiation, at energies ranging from the infrared through the ultraviolet to the X-ray regions, for investigating the structure of matter” (Dumas *et al.*, 2006).

Synchrotron radiation is an infrared source of radiation generated by electrons travelling at relativistic velocities, either inside a curved path through a constant magnetic field (bending magnet radiation) or on their trajectories inside a variable magnetic field, for example, at the edges of bending magnets (edge radiation). The latter type of emission has a lot in common with the transition radiation. Infrared photons are emitted in narrow angles (Dumas *et al.*, 2006).

In the synchrotron, electrons from an electron source were accelerated with a linear accelerator. It produces an energy of 75 million electron milivolts (meV), these electrons enter a booster ring, here they are accelerated more, and enters a vacuum ultraviolet (VUV) storage ring (Figure 1.15). The VUV storage ring has eight bending magnets, and 176 radiation ports. When electron accelerates, they radiate

energy in the form of electromagnetic waves. Synchrotron light consists of a continuous spectrum of electromagnetic radiation ranging from x-ray to infrared. Infrared beam from the beam line port is extracted and directed to microspectrometer (Wetzel *et al.*, 2003).

Figure 1.15 shows the synchrotron diagram at the National Synchrotron Light Source at Brookhaven National Laboratory in New York, in the USA.

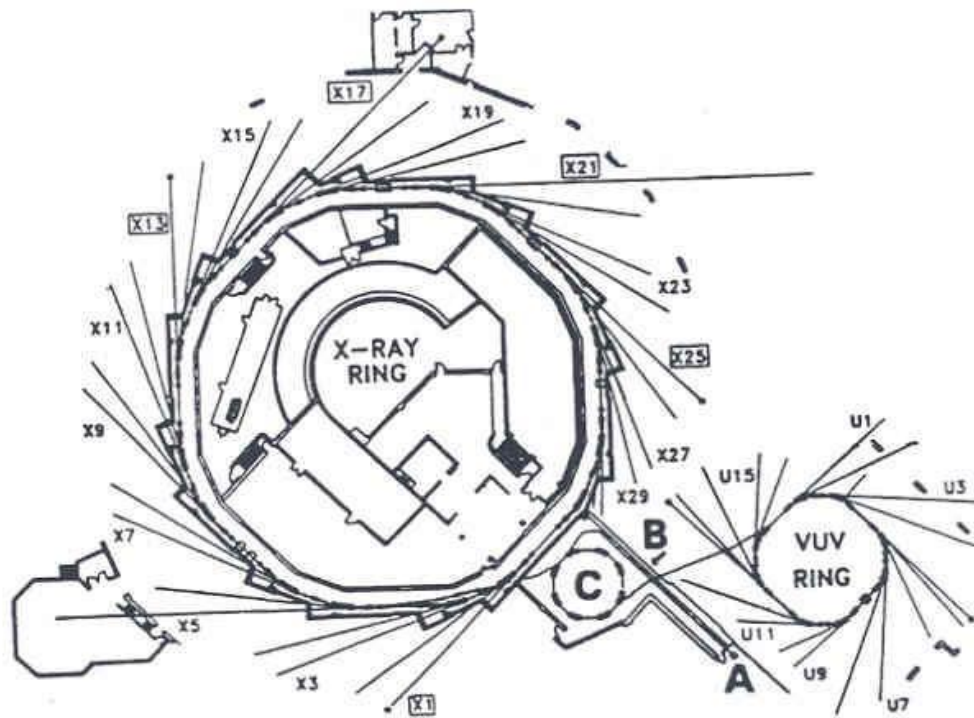


Figure 1.15 Diagram of National Synchrotron Light Source (A: electron source, B: linear accelerator, C: booster accelerator ring, VUV: Vacuum ultraviolet storage ring with associated beamlines. Electrons are accelerated from with a linear accelerator and produce an energy of 75 million electron milivolts (meV), and enter a booster ring, and are accelerated more and enter vacuum ultraviolet (VUV) storage ring

1.7.1.3.1 The Advantages of Synchrotron-FTIR Microspectroscopy

- A synchrotron infrared source is 100–1000 times brighter than a conventional thermal (e.g., globalar) source. A globalar emits light like a light bulb in all directions. In contrast, synchrotron infrared light is highly collimated like a laser, making it much more efficient to focus onto a small spot. But unlike a laser, it emits a wide range of infrared wavelengths, making FTIR spectroscopy possible. Therefore with synchrotron infrared light, we can study samples that are smaller and/or more dilute in concentration. Also, the 1000-fold increase in brightness translates to data collection times that are ~30 times faster with the synchrotron source compared to the globalar source (Miller and Dumas, 2006).
- A single cell has been mapped with 3 μm resolution by means of the high spatial resolution of the synchrotron source. So, SR-FTIR microspectroscopy using the small effective source size and the advantage of synchrotron light brightness enables us to explore the changes in the microstructures with very high signal to noise ratios at high spatial resolutions.
- This technique can cover a wide spectral range. Using this unique property, detailed information about the structure and composition of a tissue can be obtained. It may be employed to detect information of ultrastructural chemistry by imaging or mapping without destruction of the intrinsic microstructures.
- SR-FTIR microspectroscopy enables the successive monitoring of biochemical changes in individual cells non-destructively without having to treat cells with exogenous dyes, fluorescent labels, or stains, or to resort to destructive techniques. The non-invasive and non-destructive nature of the technique allows each cell in a population to be studied sequentially over a period extending to hours or even days. By monitoring individual cells over time it will be possible to detect the onset of disease and other cellular

changes and to probe the heterogeneity of responses to various treatments or insults within a population of living cells (Holman *et al.*, 2003).

- Synchrotron IR light has a pulsed time structure and a high degree of polarization (when a bending magnet is used for producing the IR photons). The pulsed nature of the light comes from the intrinsic characteristics of synchrotron radiation, where the specific pulse structure (10 s to 100 s of picoseconds) is determined by the electron bunch structure in the storage ring (Miller and Dumas, 2006).
- Infrared synchrotron radiation is also in principle more stable, because no thermal fluctuations occur in this type of source (Dumas and Miller, 2003).
- Since the synchrotron source's signal to noise ratio is more than 1000 times better than the thermal source for spatial resolutions, this technique is ideal for the study of small and/or heterogeneous samples, for example; individual living cells, microorganisms, and larger biological systems in which local biochemistry may have significant spatial variations (Holman *et al.*, 2003).

1.7.1.3.2 SR-FTIR Microspectroscopy in Biological Studies

“Variations in nucleic acid, protein and lipid content or structure of a tissue can provide important details about the chemistry of diseased states. With the high spatial resolution of the synchrotron, individual cells within a tissue can be probed with sub-cellular resolution” (Miller and Dumas; 2006). For example, using SR-FTIRM, the misfolded protein aggregates has been identified in the Alzheimer's patients brain (Choo *et al.*, 1996; Miller *et al.*, 2006b; Gallant *et al.*, 2006) and infectious prion proteins have been characterized in scrapie (Kneipp *et al.*, 2000; Kneipp *et al.*, 2003; Kneipp *et al.*, 2004; Wang *et al.*, 2005b). Alterations in bone structure and composition have been revealed in osteoporosis (Huang *et al.*, 2002; Huang *et al.*, 2003), osteopetrosis (Miller *et al.*, 2001), and osteoarthritis (Miller *et al.*, 2004). Changes in lipid and collagen structure and content in myocardium in heart diseases

have been observed (Wang *et al.*, 2005a). For the first time, the subcellular chemical mapping of a single living cell was obtained with the high spatial resolution of a synchrotron source. Single mouse hybridoma B cell has been investigated during the apoptosis (Jamin *et al.*, 2003), during necrosis and mitosis (Jamin *et al.*, 1998). Alterations in nucleic acid content and packing have been shown during the cell cycle of lung epithelial cells (Holman *et al.*, 2000a).

A significant amount of investigation has been performed on the biochemical structure and composition of human hair. The synchrotron infrared source enables to probe the medulla (~10 μm width), cuticle (~5 μm width) and cortex (~40–80 μm width) substructures of hair separately (Dumas *et al.*, 2003; Chan *et al.*, 2005).

1.8 Aim of the Study

Radiation protection is very important in the radiotherapy of cancer patients where normal tissues need to be protected while patients are exposed to ionizing radiation. The utilization of chemical radioprotectors is an important approach to protect normal tissues during radiotherapy. Although a great number of compounds synthesized for this purpose showed good radioprotection in in-vitro studies, most of them failed in-vivo because of their side effects to the mammalian system. The most effective radioprotective drug developed to date is amifostine (WR-2721), which is the only cytoprotective agent specifically approved by the Food and Drug Administration (FDA) as a radioprotector.

In the past, amifostine has been largely investigated in some clinical studies and has shown different protective activities. Despite the fact that a growing number of reports strongly support amifostine's clinical efficacy, the molecular effects of amifostine on the structural and functional properties of normal and irradiated tissues and membranes are largely unknown. It has been demonstrated that amifostine uptake is the lowest in the brain and the highest in the liver in the body (Santini and Giles, 1999). Taking this into consideration, we have selected brain tissues and liver microsomal membranes to investigate the effects of ionizing radiation and amifostine

on living systems at molecular level. Consequently, a major aim of the current thesis was to determine the effects of ionizing radiation on brain tissue and liver microsomal membrane and to test the possible protective effects of amifostine on these systems at molecular level.

Within this context, in the first part of the study the chemical effects of ionizing radiation on the white matter (WM) and grey matter (GM) regions of the brain and the protective effects of amifostine on these regions of the brain were investigated using Fourier transform infrared microspectroscopy (FTIRM) and Synchrotron-Fourier transform infrared microspectroscopy (SR-FTIRM) without perturbing tissue morphology. The brain, with its high concentrations of PUFAs and high oxygen consumption is highly vulnerable to free radical attack (Reiter, 1995). Since brain is a heterogeneous organ, different anatomical regions in this organ may have different susceptibility to ionizing radiation. There are many structural and chemical differences between WM and GM in the brain. It is known that lipid rich environments are more susceptible to free radical damage (Reiter, 1995). Since oxidation products would be expected to be highly localized in the white matter of the brain, data from traditional techniques cannot easily reflect the chemical changes that occur at different parts of the brain. Unlike the traditional techniques, FTIRM can provide information about the in situ chemical features from microscopic regions of a tissue section without disrupting the tissue. Using FTIRM, the structure and composition can be examined precisely in the unstained, unfixed and untreated tissue, thus it reduces the artifacts (Levin and Bhargava 2005; Krafft *et al.*, 2007; Heraud *et al.*, 2010). Moreover, SR-FTIRM, taking advantage of synchrotron light brightness and small effective source size enables to explore the changes in the microstructures of biological tissues at high spatial resolutions with high signal-to-noise ratios (Miller *et al.*, 2000). In the current study, the high signal-to-noise ratio of SR-FTIRM allowed us to monitor small alterations in the lipids and the changes in the protein secondary structures of brain tissue.

In the second part of the thesis, ionizing radiation-induced changes on rat liver microsomal membrane in terms of macromolecular composition, structure and lipid dynamics and the protective effects of amifostine on these structural and functional variations were investigated using FTIR spectroscopy. Today it is known that differences in lipid order, lipid dynamics, protein secondary structure in tissues and membranes together with the changes in the content of macromolecules disturb the kinetics and functions of ion channels and also lead to many diseases. The variations in the ratios of biomolecules such as unsaturated to saturated lipids, lipid to protein are related to lipid structure such as membrane thickness, lipid order, which are also related with membrane permeability (Szalontai *et al.*, 2000; Awayda *et al.*, 2004). Liver is a central organ for drug metabolism and the main site of biosynthesis of lipids. Microsomes are subcellular particles derived from the endoplasmic reticulum after homogenization of the tissue. Microsomal fractions contain enzymes involved in reduction and oxidation reactions, drug metabolism, cholesterol synthesis and fatty acid metabolism (Garg *et al.*, 1985). Therefore, the liver microsomal membrane system is one of the best models for monitoring the damage induced by ionizing radiation and the protecting capability of amifostine in biological membranes.

Monitoring the overall changes appearing in biological membrane upon exposure to ionizing radiation is a complex task. So far, various spectroscopic techniques, such as ESR (Gwozdinski 1991; Bartosz *et al.* 1992) and fluorescence (Kolling *et al.* 1994, Bonnefont-Rousselot *et al.* 1995) and some biochemical methods (Pribrish *et al.*, 1994) have been used for the investigation of radiation-induced damage in membranes. The biochemical techniques such as TBARS test and HPLC, which provide information only about the content and concentration of biomolecules, are destructive and time consuming. The spectroscopic techniques such as ESR and fluorescence spectroscopy require the insertion of either a spin label or bulky fluorophore into the membrane and report changes in the localized environment surrounding the probe molecule (Lewis *et al.*, 1989). These techniques were used as compatible to each other since they give information at different time scale. Among these techniques, FTIR spectroscopy recently has emerged as a valuable technique to

probe the structure, conformation and function of biomolecules, simultaneously, in biologic membranes without introducing foreign perturbing probes into the system (Lewis *et al.*, 1989; Moore *et al.*, 1995; Toyran *et al.*, 2004; Toyran *et al.*, 2005; Severcan *et al.*, 2005; Akkas *et al.*, 2007).

To the best of our knowledge, this will be the first study reporting the effects of ionizing radiation and amifostine on different parts of the brain and liver microsomal membrane at molecular level.

CHAPTER 2

MATERIALS AND METHODS

2.1 Reagents

Amifostine (WR-2721), Trizma Base, KH_2PO_4 (potassium phosphate), PMSF (phenyl methyl sulphonyl fluoride), EDTA (ethylenediamine tetra acetic acid), DTT (dithiothreitol), glycerol and KCl (potassium chloride) were obtained from Sigma (Sigma Chemical Company, Saint Louis, Missouri, USA). All chemicals were obtained from commercial sources at the highest grade of purity available.

2.2 Animals

All animal experimental procedures used in the present study were approved by the Ethics Committee of Hacettepe University, Faculty of Medicine. Approximately 7 week-old male Sprague-Dawley rats (Animal Care Facility, Faculty of Medicine, Hacettepe University), ranging from 180 to 220 g body weight were selected randomly. They were divided into four groups: Group 1: Control group, without any treatment; Group 2: Irradiated group; Group 3: amifostine treated group; Group 4: Irradiated + amifostine treated group. All animals were housed in a room with a 10:14 light/dark cycle and with free access to food and water.

Group 1 was used as an age-matched control group without any treatment. In group 2, rats were irradiated with 800 cGy of single whole body irradiation using a Cobalt-60 irradiator. In group 3, amifostine was dissolved in isotonic saline and the rats were intraperitoneously inoculated with single dose of amifostine (300 mg/kg body

weight). In group 4, the rats were intraperitoneously inoculated with single dose of amifostine (300 mg/kg body weight) 1 hour prior to irradiation with the same protocol as the group 2 rats. Because amifostine was dissolved in isotonic saline, the animals in groups 1 and 2 were similarly injected with equal volumes of isotonic saline intraperitoneously. It should be noted that amifostine is suitable only for intraperitoneal (IP) administration in rats and intravenous infusion in humans. The dose used in this study was in the range of the (therapeutic) doses used in previous studies (200 to 400 mg/kg body weight) (Jirtle *et al.*, 1985). 24 h after radiation exposure the rats were euthanized, their brain and liver tissues were removed, and kept at -80 °C until use.

2.3 Brain Tissue Studies

2.3.1 Tissue Preparation

Frozen brains were embedded in OCT (optimal cutting tool) and coronal sections of 12 µm thickness were taken from the cerebrum using a cryotome set to -20 °C and were thaw-mounted on IR-transparent 1 mm thick X 13 mm diameter BaF₂ slides. The BaF₂ slides were stored at room temperature (25 °C) in a dessicator until use.

2.3.2 Conventional FTIR Microspectroscopic Studies

Infrared images were recorded on a Perkin Elmer Spectrum One/Spotlight 300 Fourier Transform IR Microspectrometer (Perkin Elmer Corp., Sheldon, Connecticut) using image mode of the instrument. For each tissue section, an IR image was obtained with a pixel resolution of 25 x 25 µm using a liquid nitrogen cooled, mercury-cadmium-telluride detector. In addition, smaller regions of the WM and GM were imaged at a higher pixel resolution (6.25 µm X 6.25 µm). IR spectra were collected in transmission mode from 4000-800 cm⁻¹ with a spectral resolution of 8 cm⁻¹ and 4 scans co-added. A spectrum of an area containing no tissue was recorded as a background spectrum. A visible image was also recorded for each tissue section.

2.3.3 Synchrotron Infrared Microspectroscopic Studies

The SR-FTIR Microspectroscopy experiments were performed at beamline U10B of the National Synchrotron Light Source, Brookhaven National Laboratory (Upton, NY). A Thermo Nicolet Magna 860 FTIR spectrometer equipped with a Continuum infrared microscope (ThermoNicolet, Madison, WI), was used with synchrotron light as the infrared source. The microscope was equipped with 32X Schwarzschild objectives, a motorized x-y mapping stage, an adjustable rectangular aperture, and a mercury cadmium telluride (MCT-A) detector. An absorbance spectrum was collected in transmission mode at each point. The spectra were recorded in 4000-800 cm^{-1} at a spectral resolution of 8 cm^{-1} . 32 scans were co-added and an aperture size was set as 10 μm X 10 μm . Again, a spectrum of the BaF_2 window containing no tissue was used as a background.

2.3.4 Data Analysis

Perkin Elmer Spotlight software was used to analyze the conventional FTIR microspectroscopic data and the Thermo Nicolet's software Omnic 7.3 was used to analyze the SR-FTIR microspectroscopic data. A MATLAB routine was then used to mark the region for analysis.

For numerical comparison between control and treated samples, the integrated area ratios for different infrared bands have been calculated. Spectral analyses were performed using the ratios of different functional groups to eliminate the artifacts due to the variations in section thickness.

Functional group images were obtained by calculating the ratios of the baseline corrected areas under some peaks. The integrated spectral regions and baseline points for the infrared bands used in this study are presented in Table 2. 1. The lipid/protein ratio at each pixel was obtained by taking the ratio of the area under the C-H stretching region to the area under the amide II band. The C-H stretching region, which contains vibrations of the fatty acyl chains of membrane lipids, is a sensitive

indicator for lipid content (Kneipp *et al.*, 2002; Wang *et al.*, 2005a). The amide II band gives information about protein concentration (Mendelsohn *et al.*, 2003; Leskovjan *et al.*, 2009). To obtain information about protein concentration and structure, the Amide I/Amide II ratio was calculated. Then to estimate the molecular changes in the structure of tissue lipids, the integrated area under the some specific lipid bands (CH₂ asymmetric band, CH₃ asymmetric band, olefinic=CH band or carbonyl ester band) were divided by the area under the entire C-H stretching region which is sensitive to monitor the total lipid content of a system.

Table 2.1 The spectral regions and baseline points used for particular infrared bands

Infrared Band	Integrated spectral range (cm⁻¹)	Baseline points (cm⁻¹)
Amide II	1555-1535	1780-1345
CH ₂ asymmetric stretching	2915-2930	3100-2750
CH ₃ asymmetric stretching	2950-2960	3100-2750
Carbonyl (C=O) stretching	1745-1731	1780-1345
Olefinic=CH	3000-3027	3000-3027
C-H stretching	2994-2800	3100-2750

For the determination of the variations in the protein secondary structure, the synchrotron data were used. For this purpose the second derivative of amide I band was vector normalized at 1700-1600 cm^{-1} region using OPUS NT data collection software package (Bruker Optics, Reinstetten, Germany). Firstly, the second derivative spectra were obtained by applying a Savitzky–Golay algorithm with nine smoothing points and these derivatives vector normalized at 1700-1600 cm^{-1} and then the peak intensities were calculated. The peak minima of the second derivative signals were used, since they correspond to the peak positions of the original absorption spectra (Toyran *et al.*, 2006; Ozek *et al.*, 2009).

2.3.5 Statistical Study

The ratio values of functional groups were generated for every pixel in every FTIRM image. Regions were divided into grey vs. white matter for the control, irradiated, amifostine treated and amifostine treated + irradiated groups. For each group, a mean and standard deviation were generated for each animal. Then the individual animal values were averaged for each group. Mann Whitney-U test was performed on all data to test for significant differences ($p < 0.05$) between control and treated groups.

2.4 Liver Microsomal Membrane Studies

2.4.1 Isolation of Rat Liver Microsomal Membranes

Microsomal membranes were isolated according to a method described by Severcan *et al.*, (2005). Livers were washed with washing buffer (50 mM Tris, 1 mM EDTA, pH 7.4) to get rid of blood, dried on a filter paper and chopped to little pieces and weighed. Homogenization solution containing 25 mM KH_2PO_4 , 1.15 % KCl, 5 mM EDTA, 0.2 mM PMSF, 2mM DTT (pH 7.4), was added with a ratio of 1:4 g/mL (wet weight). All steps were carried at 0-4 °C.

The tissue was homogenized using Potter-Elvehjem glass homogenizer packed in crush ice, coupled motor-driven (Black & Decker, V850, multispeed drill) teflon pestle at 2400 rpm for 3x20 sec. The homogenate was first centrifuged at 16 000 *g* using SS-34 rotor for 20 min and the resulting mitochondrial pellet was discarded. Then the supernatant was further centrifuged at 125 000 *g* using Beckman Coulter Optima L-100 XP Ultracentrifuge for 60 min. The resulting pellet was suspended in washing buffer and recentrifuged at 125 000 *g* for 55 min. After discarding the supernatant, the microsomal membrane rich-pellet was suspended with 25 mM phosphate buffer (pH 7.4) containing 25% glycerol (v/v), 1.15 KCl (w/v) at a volume of 0.25 mL for each gram of primal liver tissue. The resuspended microsomes was homogenized manually using the teflon-glass homogenizer and stored at -80 °C for spectroscopic studies.

2.4.2 FTIR Spectroscopic Study

To remove the excessive amount of suspension buffer, the microsomal membrane fraction was centrifuged at 14000 rpm for 10 min at 4 °C just before the spectroscopic analysis as previously reported by Severcan *et al.*, 2010. The concentrated pellet containing the liver microsomal membranes was used in the FTIR studies. Infrared spectra were obtained using Perkin-Elmer Spectrum 100 FTIR spectrometer (Perkin-Elmer Inc., Norwalk, CT, USA) equipped with a MIR TGS detector. The sample compartment was continuously purged with dry air to minimize atmospheric water vapor absorbance, which overlaps in the spectral region of interest, and carbon dioxide interference. To overcome this problem, the spectrum of air was recorded as background and subtracted automatically by using appropriate software. Figure 2.1 shows the infrared spectrum of air used as a background in this study. 20 µl of sample was put between CaF₂ windows using a 12 µm path length. Each spectrum of membrane samples were collected in the 1000-4000 cm⁻¹ region at 2 cm⁻¹ resolution. Interferograms were co-added for 100 scans. Each sample was scanned three times and their averages were used for visual and quantitative comparison.

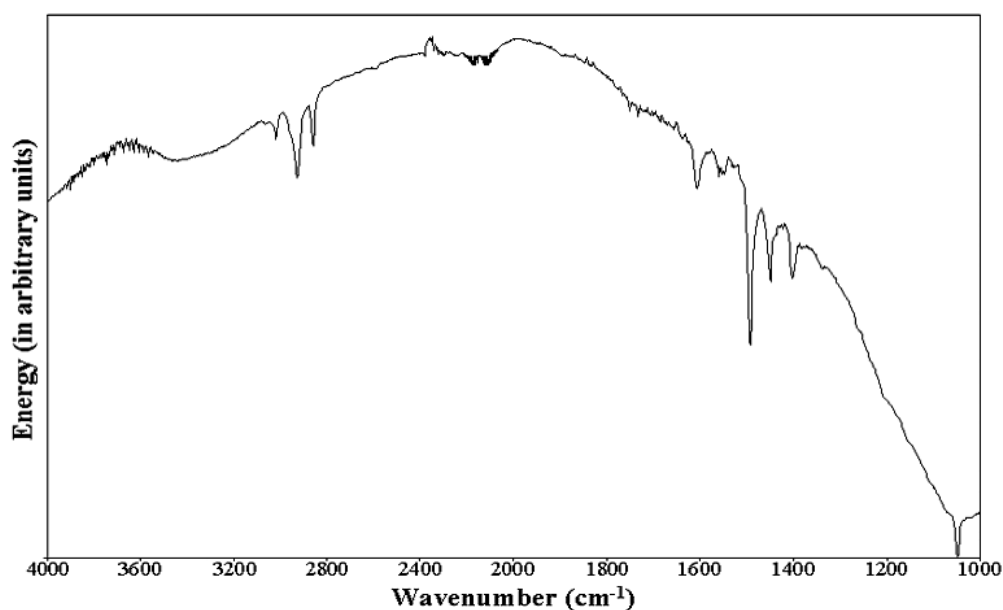


Figure 2.1 The infrared spectrum of air

2.4.3 Data Analysis

Water is the most frequently used environment for biological systems, which is a strong infrared absorber, in the FTIR studies (Mantsch, 1984). It gives strong bands around at $3050\text{--}2800\text{cm}^{-1}$ and $1700\text{--}1500\text{cm}^{-1}$, which interferes with the bands of interest arising from functional groups belonging to proteins and lipids. As the infrared absorption of water masks several lipid bands, it is often required to subtract the water bands from the sample spectra by using the appropriate software. So to remove water absorption bands, the spectrum of suspension buffer were subtracted from the spectra of liver microsomal membranes. In the subtraction process the water

band located around 2125 cm^{-1} was flattened. Figure 2.2 shows the FTIR spectra of control rat liver microsomal membranes before and after the subtraction process.

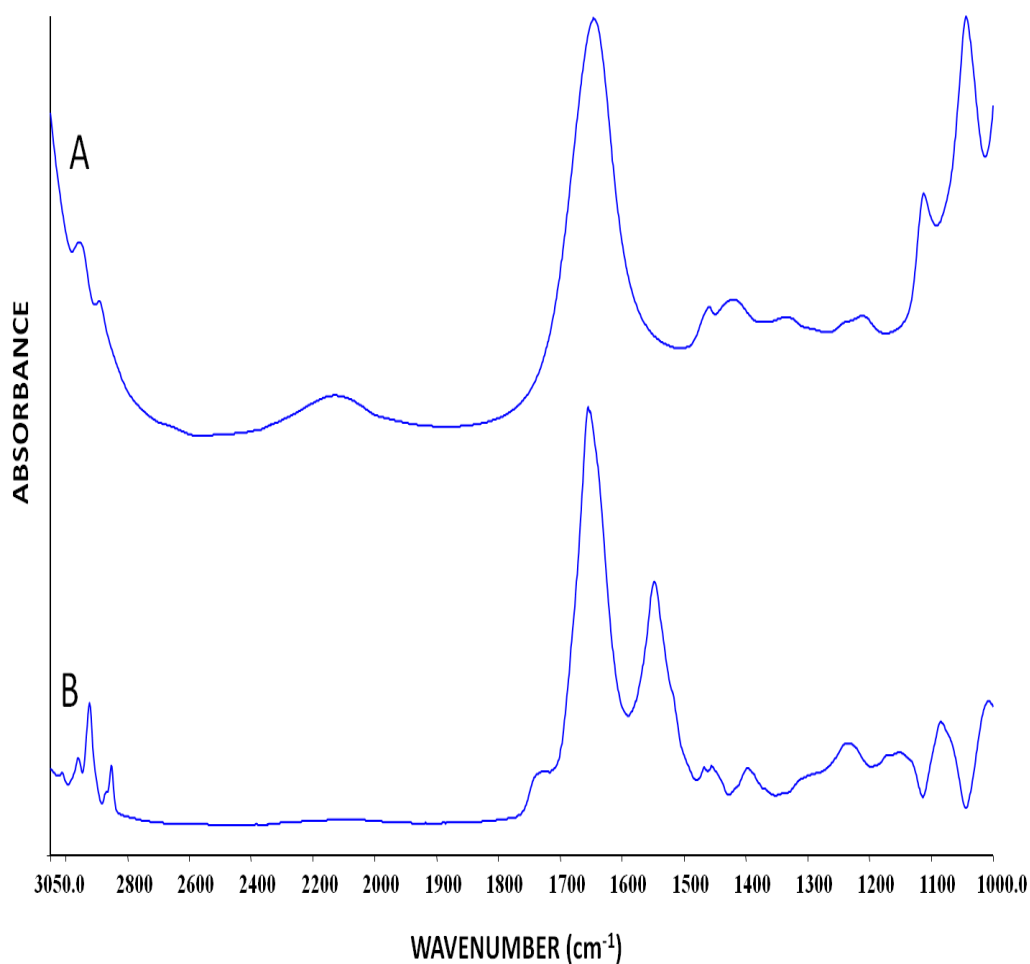


Figure 2.2 FTIR spectra of control rat liver microsomal membranes before (A) and after (B) buffer subtraction in the region between $3050 - 1000\text{ cm}^{-1}$

Spectrum 100 software (Perkin-Elmer) was used for the subtraction procedure. Averages of the spectra belonging to the same experimental groups, baseline

correction, normalization, and the band areas were obtained by using the same software. The normalization process was applied only for visual representation of the differences. For the accurate determination of the mean values for the band areas, band positions and the bandwidth values, the original average spectrum (from three replicates) belonging to each individual of the groups was taken into consideration. The spectra were first smoothed with 9-point Savitsky-Golay smooth function to remove the noise. The deconvolution process was applied to C-H stretching region to increase the resolution of intrinsically overlapped bands. Deconvolution was performed by setting the gamma factor as 0.7 for each of the spectra. The band areas were calculated from smoothed and baseline-corrected spectra using Spectrum software. The band positions were measured according to center of weight. The bandwidth values of Amide I and CH₂ asymmetric stretching bands were calculated at 0.75 X height of the absorption signal in terms of cm⁻¹ from raw spectra.

OPUS NT data collection software package (Bruker Optics, Reinstetten, Germany) was used for vector normalization process to determine the changes in the protein secondary structure as previously described for brain tissue studies.

2.4.4 Statistical Study

The results were expressed as “mean ± standard deviation”. Mann Whitney-U test was performed on the groups to test the significance of the differences between control and treated groups. The p value of less than 0.05 was considered statistically significant. The degree of significance was denoted as *p<0.05.

CHAPTER 3

RESULTS

3.1 The Effects of Ionizing Radiation and Amifostine on Rat Brain Tissue

This part of the study is precisely addressed to investigate the effects of ionizing radiation on the WM and GM regions of the brain and to test the protective effects of amifostine on these regions of the brain without perturbing tissue morphology using FTIR microspectroscopy and SR-FTIR microspectroscopy.

3.1.1 Band Assignment of the Rat Brain Tissue

A brain infrared spectrum is quite complex consisting of several infrared bands belonging to various functional groups in tissue components such as proteins, nucleic acids, carbohydrates and lipids. A representative FT-IR spectrum of control rat brain in the 3600-800 cm^{-1} region was shown in Figure 3.1. The main infrared bands were labeled in this figure and the detailed spectral band assignments were presented in Table 3.1.

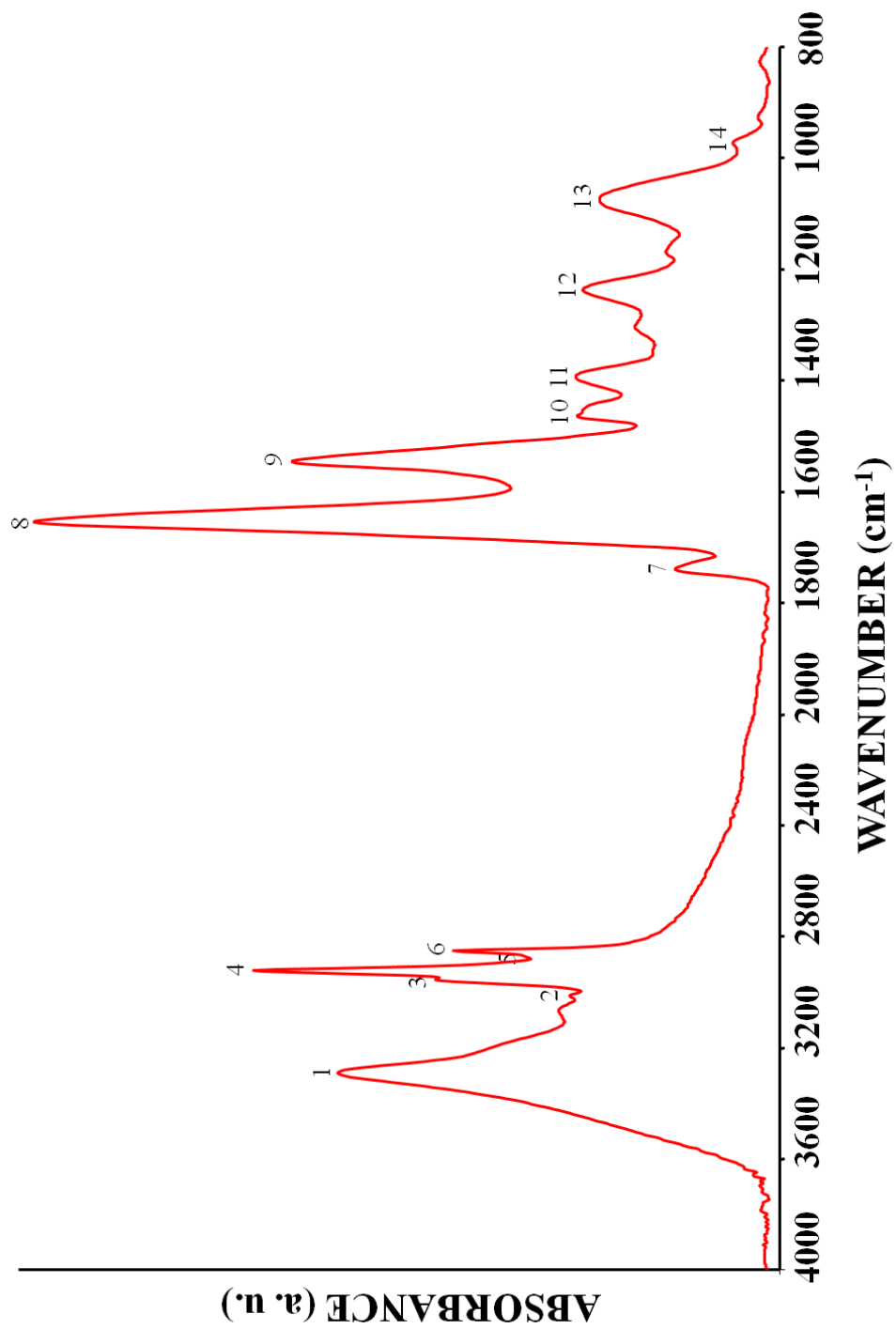


Figure 3.1 A typical FTIR spectrum of rat brain tissue in the 4000-800 cm⁻¹

Table 3.1 General band assignment for the FTIR spectra of rat brain tissue

PEAK #	WAVENUMBER (cm ⁻¹)	DEFINITION
1	3290	N-H and O-H stretching: Mainly N-H stretching (Amide A) of proteins with the little contribution from O-H stretching polysaccharides and intermolecular H bonding (Cakmak <i>et al.</i> , 2003)
2	3012	Olefinic=CH stretching: Unsaturated lipids (Liu <i>et al.</i> , 2002; Severcan <i>et al.</i> 2005)
3	2955	CH₃ asymmetric stretching: Lipids, protein side chains (Holman <i>et al.</i> , 2000b; Szalontai 2009, Severcan <i>et al.</i> , 2010)
4	2922	CH₂ asymmetric stretching: Mainly lipids (Cakmak <i>et al.</i> 2003)
5	2872	CH₃ symmetric stretching: Mainly proteins (Ozek <i>et al.</i> , 2009)
6	2852	CH₂ symmetric stretching: Mainly lipids (Cakmak <i>et al.</i> , 2006)
7	1740	Carbonyl (C=O) stretching: Ester functional groups in lipids (Kneipp <i>et al.</i> , 2000; Mendelsohn <i>et al.</i> , 2003)
8	1653	Amide I: Protein C=O stretching (Haris and Severcan 1999; Krafft <i>et al.</i> , 2004)
9	1545	Amide II: Protein N-H bending, C-N stretching (Kneipp <i>et al.</i> , 2000; Krafft <i>et al.</i> , 2004)
10	1467	CH₂ scissoring: Mainly lipids (Toyran <i>et al.</i> , 2006)
11	1391	COO⁻ symmetric stretching: Fatty acids and amino acids (Cakmak <i>et al.</i> , 2006; Jackson <i>et al.</i> , 1998)
12	1239	PO₂⁻ asymmetric stretching: Phospholipids and nucleic acids (Kneipp <i>et al.</i> , 2000; Akkas <i>et al.</i> , 2007)
13	1075	PO₂⁻ symmetric stretching: Phospholipids and nucleic acids (Kneipp <i>et al.</i> , 2000; Akkas <i>et al.</i> , 2007)
14	971	C-N⁺-C stretching: Nucleic acids (Cakmak <i>et al.</i> , 2003)

The band at $\sim 3290\text{ cm}^{-1}$ contains strong absorptions arising mainly from the N-H stretching (amide A) mode of the proteins with the contribution of the O-H stretching mode of polysaccharides (Cakmak *et al.*, 2003). A weak band at around 3012 cm^{-1} arises from the C-H stretching vibrations of the olefinic=C-H groups in unsaturated fatty acids (Liu *et al.*, 2002; Severcan *et al.*, 2005). This band could be used as a measure of the unsaturation levels of the system (Liu *et al.*, 2002; Severcan *et al.*, 2005). The peaks between 3000 and 2800 cm^{-1} are assigned to C-H stretching modes. The C-H stretching region is sensitive to monitor the lipid content of a system (Wang *et al.*, 2005a). This region contains the asymmetric C-H stretching vibrations of CH_3 and CH_2 functional groups occurring at 2955 cm^{-1} and 2922 cm^{-1} respectively, and the symmetric modes of the same groups at 2872 cm^{-1} and 2852 cm^{-1} , respectively. While CH_2 asymmetric and symmetric bands arise from mainly lipids, the CH_3 asymmetric band has equal contribution from lipids and protein side chains and the CH_3 symmetric band arises from mainly proteins with some contribution from lipids. However, in this study, the bands at 1456 and 1396 cm^{-1} which are due to asymmetric and symmetric CH_3 bending modes of the methyl groups of protein side chains were not observed in the absorbance, deconvolved and second derivative spectra of WM and GM. (Figures 3.2 and 3.3) (Jagadeesan *et al.*, 2005). In addition, the other dominant protein side chain bands at 1375 cm^{-1} , 1400 cm^{-1} , 1600 cm^{-1} and 1617 cm^{-1} were not observed in the WM and GM spectra (Figures 3.2 and 3.3) (Rigas *et al.*, 1990; Barth *et al.*, 2000; Cakmak *et al.*, 2003). Thus, in our study, the main contribution to the asymmetric and symmetric stretching bands at 2955 cm^{-1} and at 2872 cm^{-1} was considered to be from the methyl groups of fatty acyl chains and the C-H region was used to evaluate the total lipid content of the system.

The $1800\text{-}1500\text{ cm}^{-1}$ region is shaped by the C=O stretching band of ester carbonyl groups in lipids (1740 cm^{-1}) and the amide bands of proteins. The amide I band which arise from mainly amide C=O stretching frequencies of the protein backbone is observed at $\sim 1653\text{ cm}^{-1}$. The frequency of this band is conformation-sensitive and it can be used to analyze protein secondary structure (Miller *et al.*, 2000). The amide II band at 1545 cm^{-1} is due to N-H bending and C-N stretching vibrations of the

peptide backbone (Kneipp *et al.*, 2000, Miller *et al.*, 2000). Another CH₂ band which is observed at 1467 cm⁻¹ is due to the scissoring vibration of CH₂ groups in the lipids (Cakmak *et al.*, 2006). The band at 1391 cm⁻¹ arises from the COO⁻ symmetric stretching vibrations in fatty acids and aminoacid side chains (Jakson *et al.*, 1998). However, in our case, the dominant mode for protein side chains around 1600 cm⁻¹ was not observed in the absorbance, deconvolved and second derivative spectra of WM and GM (Figures 3.2 and 3.3). Thus, the main contribution to the 1391 cm⁻¹ band may come from the COO⁻ symmetric stretching of fatty acids (Cakmak *et al.*, 2003). The bands at around 1240 cm⁻¹ and 1080 cm⁻¹ is assigned to asymmetric and symmetric phosphate stretching modes of phosphodiester groups in phospholipids and nucleic acids, respectively (Kneipp *et al.*, 2000, Miller *et al.*, 2000). The band at 971 cm⁻¹ is due to C-N-C stretching vibration of nucleic acids (Cakmak *et al.*, 2003).

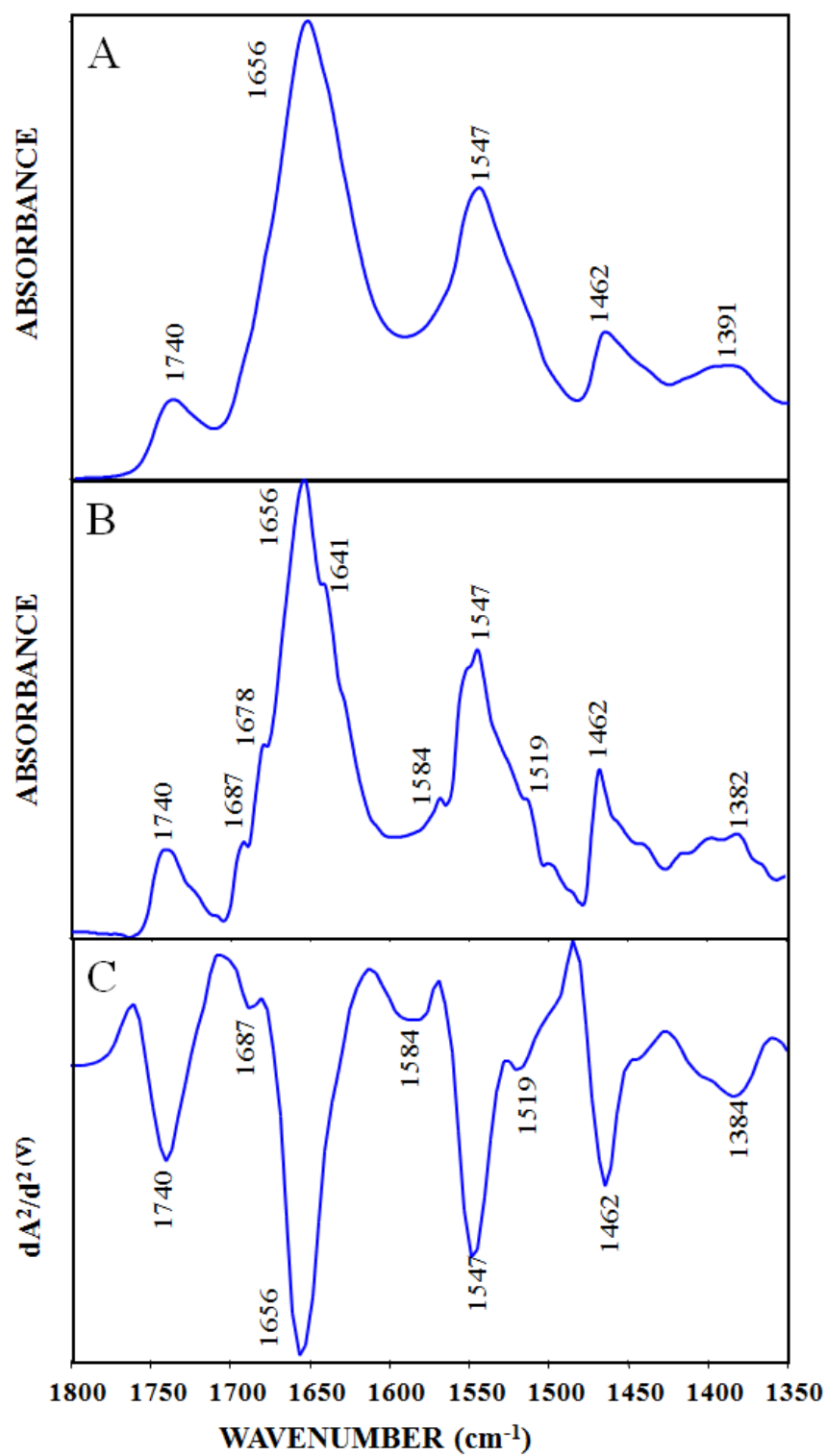


Figure 3.2 The average absorbance (A), deconvoluted (B) and second derivative (C) FTIR spectra of control rat brain white matter in the 1800-1350 cm^{-1} region

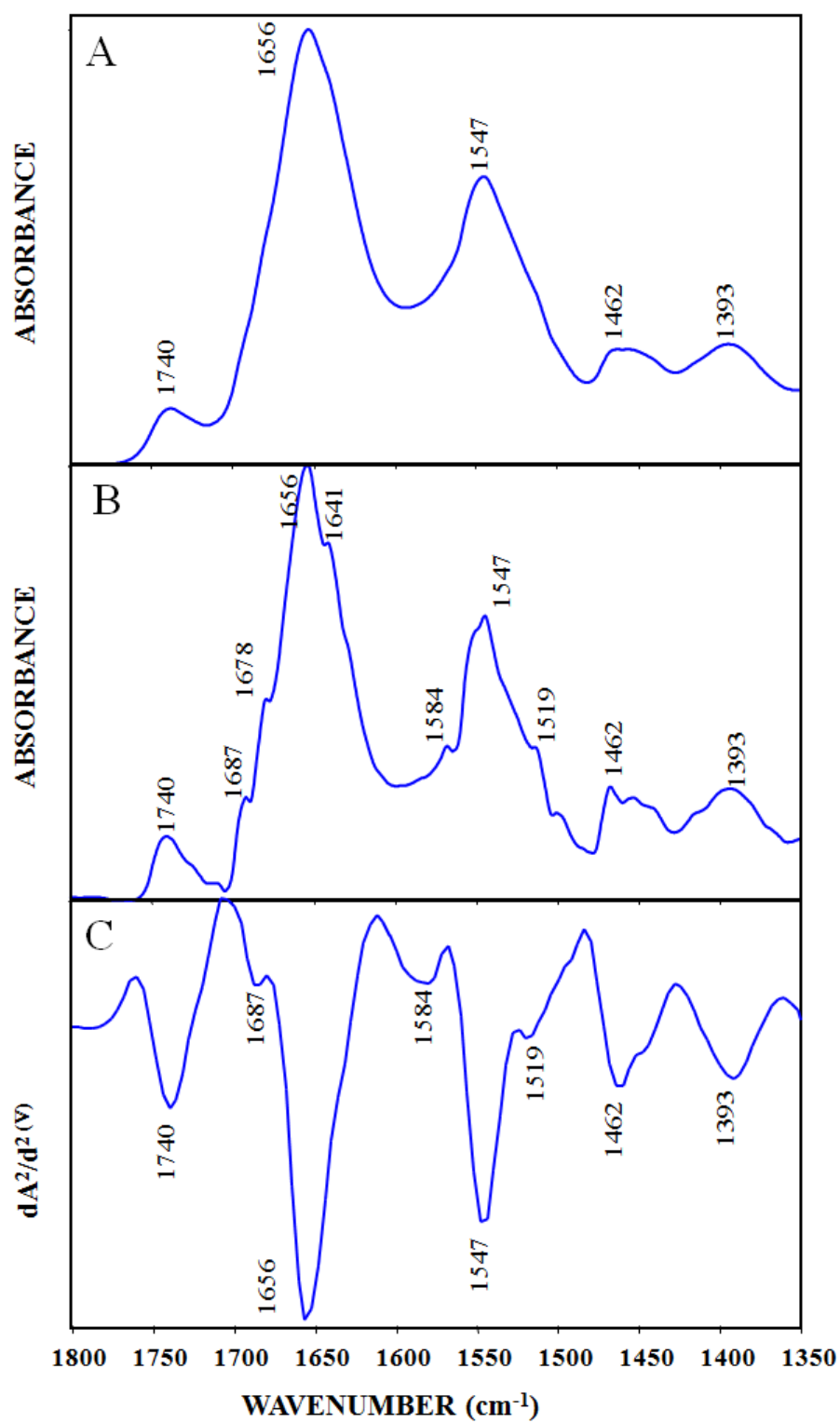


Figure 3.3 The average absorbance (A), deconvoluted (B) and second derivative (C) FTIR spectra of control rat brain grey matter in the 1800-1350 cm^{-1} region

3.1.2 Comparison of FTIR Spectra of White and Grey Matter in Rat Brain Tissue

Using FTIR microspectroscopic data, the distribution of various macromolecules such as lipids and proteins can be exhibited as functional group images based on the variations in the infrared spectra and the spatial heterogeneity of the biological constituents (Lester *et al.* 1998; Liu *et al.*, 2006). These FTIR images give information about the concentration of molecules in the tissue. Because each tissue structure possesses a distinct chemical composition, IR spectral images match with the histological structure of the tissue (Kneipp *et al.*, 2002). Figure 3.4 shows the representative images for a control brain. A light microscope image was shown in Figure 3.4A. The lipid/protein FTIR images of the same section obtained using low resolution (25 μm X 25 μm pixel size), high resolution (6.25 μm X 6.25 μm pixel size) and synchrotron light source were shown in Figure 3.4B, C and D, respectively. As can be seen from these figures, FTIR imaging easily discriminated the WM region from GM region based on the lipid and protein content. After obtaining the low resolution map (Figure 3.4B), the area for mapping was chosen and data from those small part was obtained using high resolution pixel size (Figure 3.4C) and the synchrotron light source (Figure 3.4D).

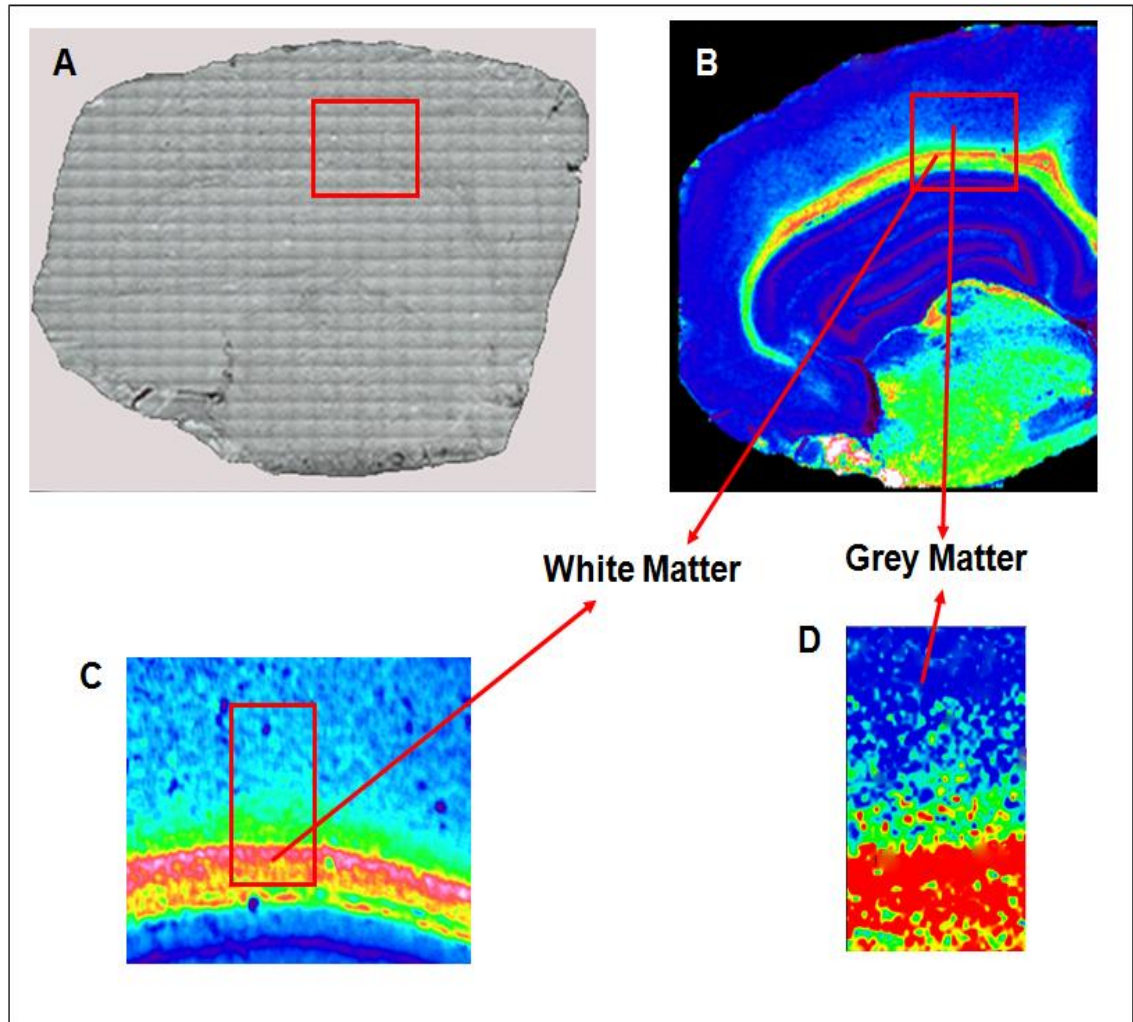


Figure 3.4 **A)** A light microscope image of control rat brain section. **B)** Lipid/protein image (25 μm X 25 μm pixel size) of the same section. **C)** A high resolution (6.25 μm X 6.25 μm pixel size) lipid/protein image of the rectangular area indicated in (A) and (B). **D)** Lipid/protein image of the rectangular area indicated in (C) obtained using synchrotron source

To reveal the differences between WM and GM, the spectra acquired from those regions of brain were compared. This comparison was displayed in Figure 3.5. As seen from this Figure, the absorption bands which are attributed mainly to lipids, especially CH₂ absorptions at 2922 cm⁻¹ and 1467 cm⁻¹, carbonyl absorption at 1740 cm⁻¹, phosphate absorptions at 1239 and 1075 cm⁻¹ are very prominent in WM region.

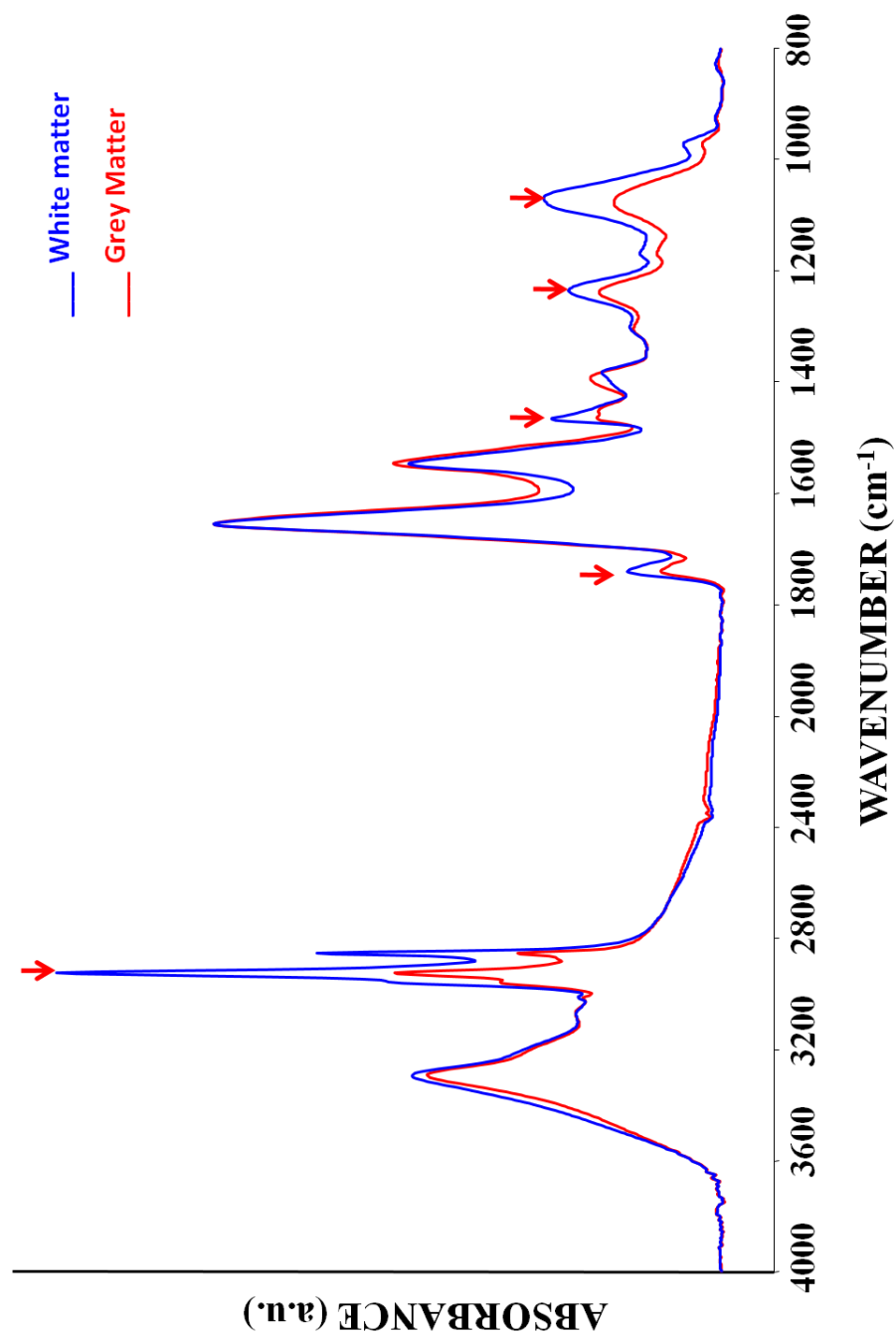


Figure 3.5 FTIR spectra of white and grey matter in control rat brain. Arrow indicates the lipid absorption bands at 2922 cm^{-1} , 1740 cm^{-1} , 1467 cm^{-1} , 1239 and 1075 cm^{-1} , which are very strong in the WM spectrum

3.1.3 The Effects of Ionizing Radiation and Amifostine on the Composition and Structure of Rat Brain White Matter and Grey Matter

FTIR microspectroscopy yielded spatially resolved information on unstained thin sections of rat brain samples that allowed the generation of IR images with high image contrast. Staining is generally useful in identifying the different parts of a tissue but the chemical information obtained from it is relatively non-specific. Unlike staining techniques, the differences in IR spectroscopic images are originated from alterations in the infrared spectra and the special heterogeneity of the biological molecules. Therefore, an FTIR image contains a multiplicity of contrast yielding mechanisms that derive from variations in the chemical composition, without the addition of extrinsic markers or stains (Lester *et al.*, 1998). In this study, brain tissues were mapped to obtain functional group images of the main biological molecules of interest. The various IR images of the selected functional groups obtained using low resolution (25 μm X 25 μm pixel size) were shown for one control sample in Figure 3.6. The comparison of the IR images [(obtained using high resolution (6.25 μm X 6.25 μm pixel size)] of control, irradiated, amifostine treated and amifostine treated + irradiated groups will be shown in the following parts where the numerical comparisons will be discussed.

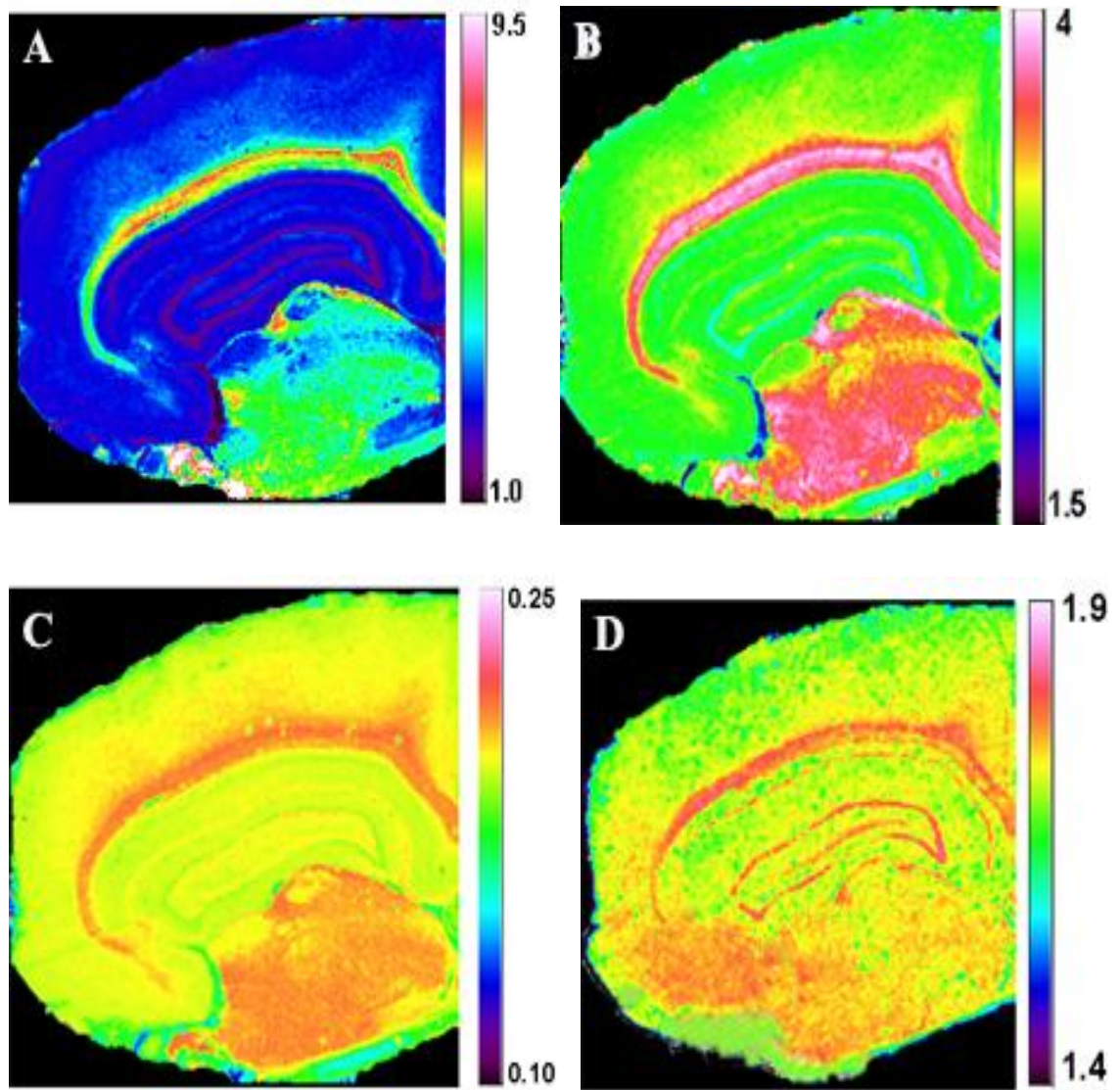


Figure 3.6 (continued)

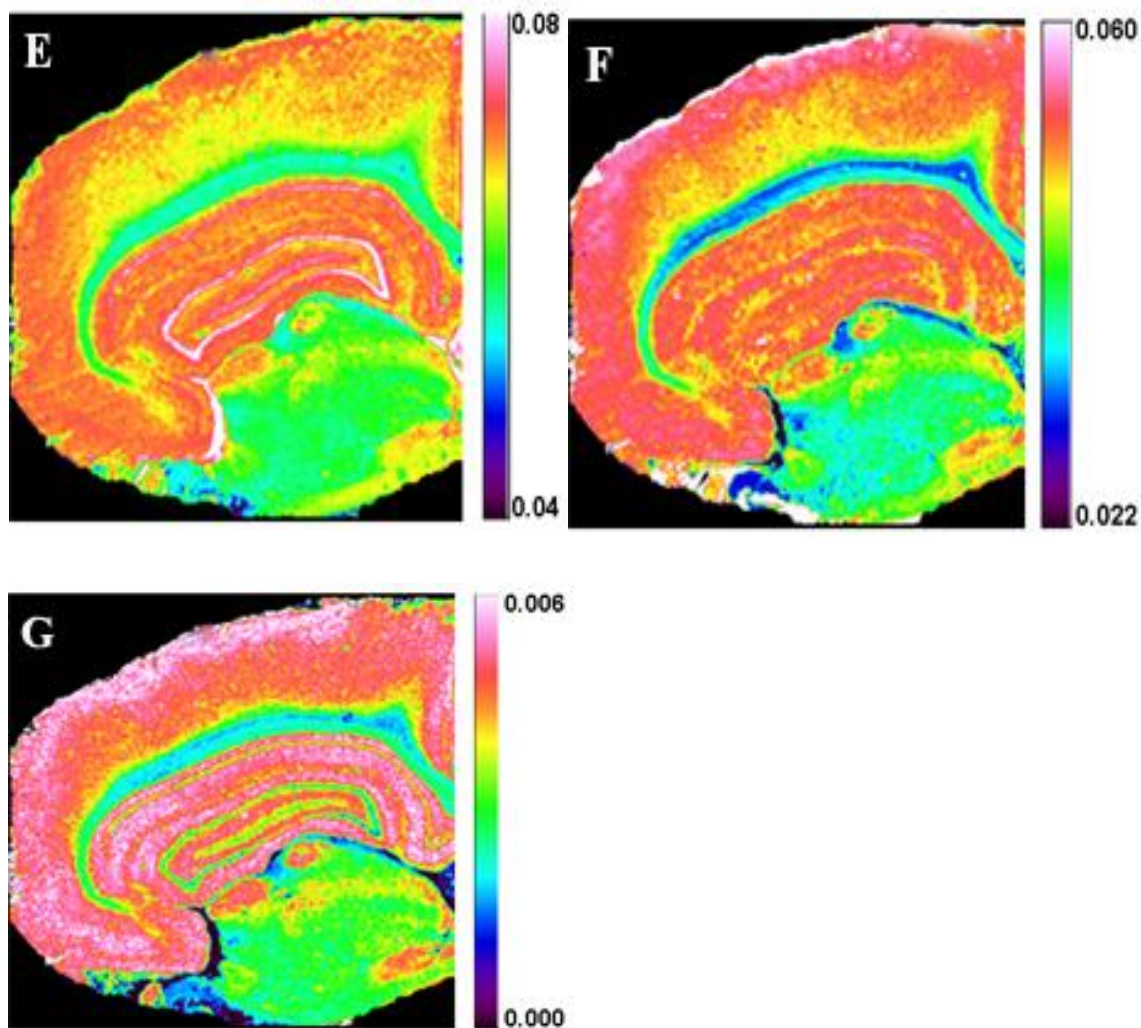


Figure 3.6 Functional group maps for one control sample obtained from the ratios of A) lipid to protein B) CH_2 to CH_3 C) CH_2 to lipid D) Amide I/Amide II E) CH_3 to lipid F) carbonyl ester to lipid G) olefinic= CH to lipid

To investigate the effects of ionizing radiation and amifostine on the composition and structure of rat brain WM and GM regions, some specific functional group ratios were evaluated. The band ratios used in this study and their assignments were reported in Table 3.2.

Table 3.2 FTIR band ratios and their assignments

IR Band Ratio	Assignment
Lipid/protein	Lipid and protein content
CH ₂ asym. str./CH ₃ asym. str.	Chain length of lipid
CH ₂ asym. str./ total lipid	Chain length of lipid
CH ₃ asym. str./total lipid	Methyl concentration in the system
Carbonyl ester/total lipid	Carbonyl status of the system
Olefinic=CH/total lipid	Unsaturation level of the system
Amide I/amide II	Protein content and structure

The numerical comparisons between control and treated samples were listed in Table 3.3. As seen from this table, there are significant differences between control and irradiated group and the values of the amifostine treated and amifostine treated + irradiated groups are very close to the control group. This result shows that amifostine didn't cause any significant alterations on the brain tissue when it was given to the rats without subsequent exposure to radiation and when amifostine was injected before radiation it had a protective effect on irradiated WM and GM regions of brain.

Table 3.3 Changes in the band area ratios of various functional groups of control, irradiated, amifostine treated and amifostine treated + irradiated groups in white matter and grey matter. The values are shown as ‘mean \pm standard deviation’ for each group. The degree of significance was denoted as: * $p < 0.05$, ** $p < 0.01$ and obtained by comparing each treated group with the control group

Parameter	White Matter				Grey Matter			
	Control (n=7)	Radiation (n=7)	Amifostine (n=6)	Amifostine + Radiation (n=7)	Control (n=7)	Radiation (n=7)	Amifostine (n=6)	Amifostine + Radiation(n=7)
Lipid/ Protein	6.789 \pm 0.224	6.220 \pm 0.313**	6.749 \pm 0.181	6.828 \pm 0.239	2.911 \pm 0.261	2.635 \pm 0.112*	2.739 \pm 0.161	2.937 \pm 0.203
CH ₂ asym/ CH ₃ asym.	3.832 \pm 0.09	3.702 \pm 0.06**	3.803 \pm 0.062	3.792 \pm 0.05	3.041 \pm 0.066	2.988 \pm 0.097	2.983 \pm 0.071	3.046 \pm 0.061
CH ₂ asym/ Lipid	0.2159 \pm 0.0021	0.2133 \pm 0.001*	0.2151 \pm 0.0005	0.2149 \pm 0.0028	0.2035 \pm 0.0009	0.2014 \pm 0.0016*	0.2028 \pm 0.001	0.2034 \pm 0.0056
CH ₃ asym/ Lipid	0.0563 \pm 0.0009	0.0575 \pm 0.0008*	0.0565 \pm 0.0008	0.0566 \pm 0.0008	0.0668 \pm 0.0009	0.0675 \pm 0.0018*	0.067 \pm 0.001	0.0666 \pm 0.0011
Carbonyl/ Lipid	0.0310 \pm 0.001	0.0330 \pm 0.001*	0.0321 \pm 0.001	0.0317 \pm 0.001	0.0379 \pm 0.004	0.0455 \pm 0.003*	0.05 \pm 0.004	0.0422 \pm 0.005
Olefinic= CH/Lipid	0.0025 \pm 0.0001	0.0027 \pm 0.0001*	0.0021 \pm 0.00007	0.0026 \pm 0.0001	0.0041 \pm 0.0005	0.0051 \pm 0.0005	0.049 \pm 0.0002	0.0046 \pm 0.0005
amide I/ amide II	1.779 \pm 0.008	1.753 \pm 0.022*	1.769 \pm 0.024	1.794 \pm 0.035	1.712 \pm 0.031	1.672 \pm 0.03*	1.689 \pm 0.028	1.724 \pm 0.041

The C-H region could be used to evaluate the total lipid content of the tissue although it contains some minor bands which have also contribution from proteins. In the present study, since the other protein side chain bands were not observed in the absorbance, deconvolved and second derivative spectra of WM and GM (Figures 3.2 and 3.3), the contribution from proteins to this region can be neglected and this region can be considered to be only due to lipids. The C-H region was also used to evaluate the total lipid content in various tissues in some previous studies (Kneipp *et al.*, 2002; Wang *et al.*, 2005a; Toyran *et al.*, 2006). FTIR images for the lipid to protein ratio were created by taking the integrated area ratios of the C-H region to the Amide II band. Figure 3.7 shows the lipid/protein ratio images of control, irradiated, amifostine treated and amifostine treated + irradiated groups. The average maps were colored according to the lipid/protein ratio, where red color corresponds to the highest ratio and blue color corresponds to the lowest ratio as shown on the color bar in the figure. As seen from this figure, the lipid/protein ratio decreased for irradiated groups. As also seen from the same figure the colors for amifostine and amifostine treated + irradiated groups are very similar to the control group implying the protective effect of amifostine. The numerical comparisons for the lipid/protein ratio of WM and GM were displayed as bar graphs for better comparison in Figure 3.8A and B, respectively. A significant decrease in the lipid/protein ratio content was observed in the irradiated brain WM ($p < 0.001$) and GM ($p < 0.005$) compared to controls. This decrease was most dramatic in the WM. No significant variations were observed in the amifostine treated and amifostine treated + irradiated groups compared to control. As seen from these figures the values of the amifostine treated + irradiated group are very close to the control group. This result indicates the protective effect of amifostine on brain tissue.

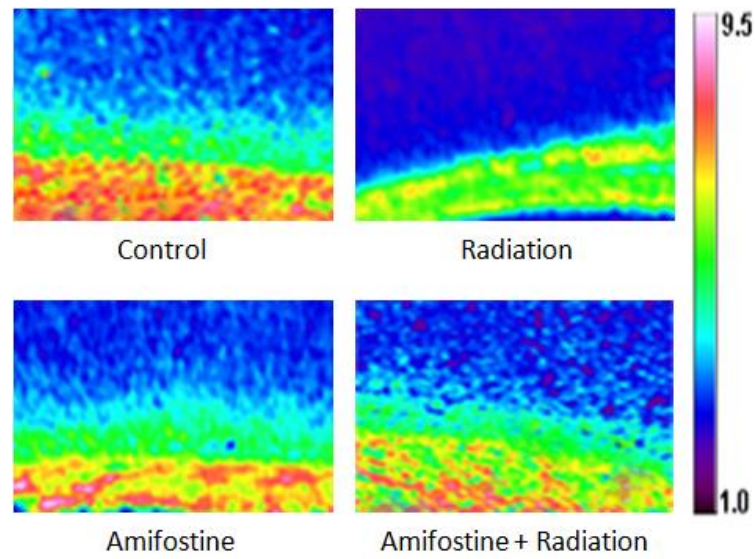


Figure 3.7 Lipid/protein ratio images of control, irradiated, amifostine treated and amifostine treated + irradiated groups

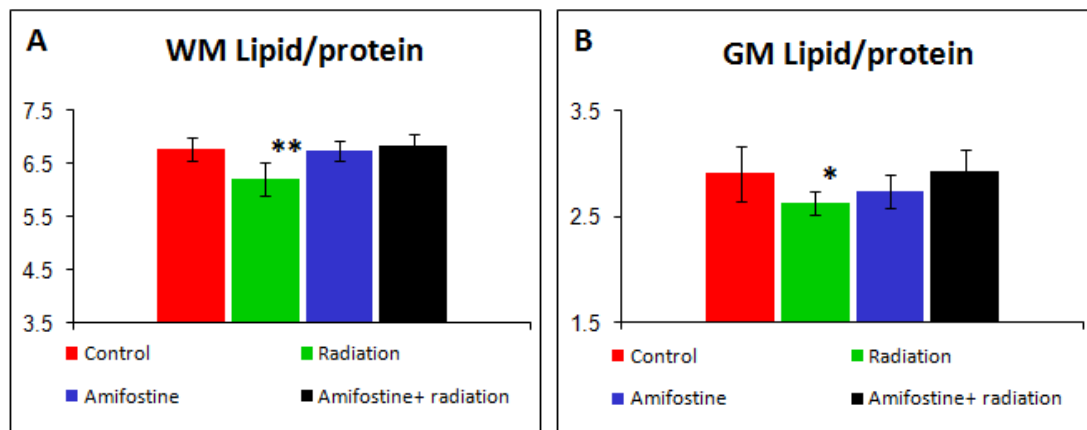


Figure 3.8 The numerical comparisons of the lipid/protein ratios of control, irradiated, amifostine treated and amifostine treated + irradiated groups in white matter (A) and grey matter (B)

The CH_2 asym. stretc./ CH_3 asym. stretc. and CH_2 asym. stretc./lipid ratios were applied to indicate the chain length of lipids, where a higher ratios indicate longer chained lipids (Wang *et al.*, 2005a). The CH_2/CH_3 ratio images were displayed in Figure 3.9 and the numerical comparisons of the CH_2/CH_3 ratios of control, irradiated, amifostine treated and amifostine treated + irradiated groups in WM and GM were shown in Figure 3.10A and B. As seen from these figures, the ratio of the CH_2/CH_3 decreased significantly for irradiated WM ($p < 0.001$) and GM of the brain. However, the CH_2/CH_3 ratios of amifostine treated and amifostine treated + irradiated groups were not changed significantly. Amifostine injection before radiation maintained this ratio as in the control group in both WM and GM regions of the brain.

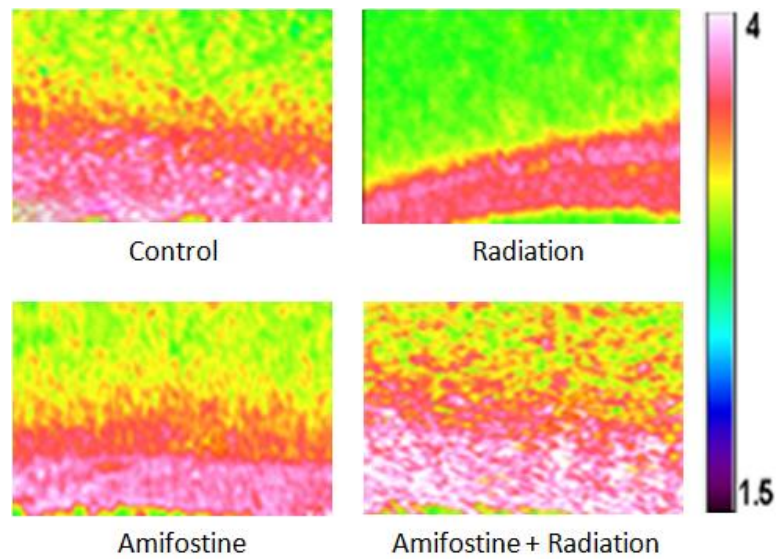


Figure 3.9 CH_2/CH_3 ratio images of control, irradiated, amifostine treated and amifostine treated + irradiated groups

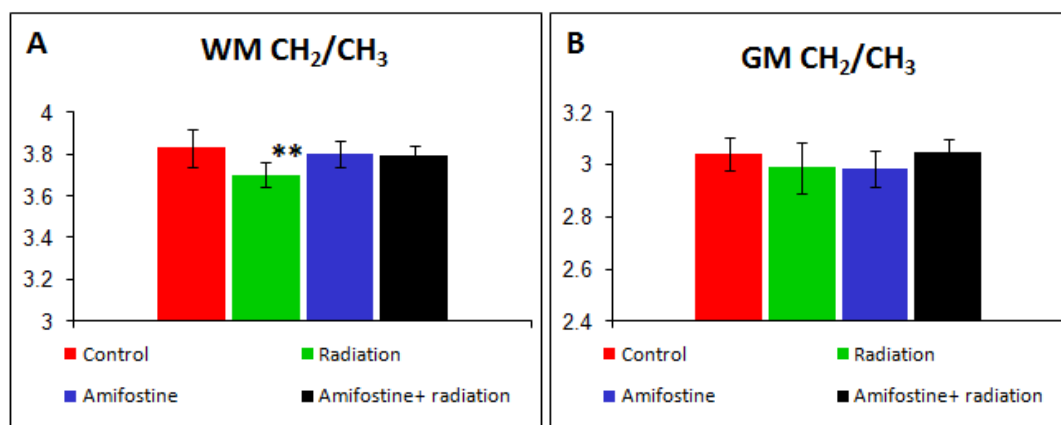


Figure 3.10 The numerical comparisons of the CH_2/CH_3 ratios of control, irradiated, amifostine treated and amifostine treated + irradiated groups in white matter (A) and grey matter (B)

Figure 3.11 shows the CH_2 /lipid ratio images of control, irradiated, amifostine treated and amifostine treated + irradiated groups. The numerical comparisons of the CH_2 /lipid ratios were displayed for control and treated groups in Figure 3.12A and B for WM and GM regions, respectively. A significant decrease in the CH_2 groups was observed in the irradiated WM ($p < 0.05$) and GM ($p < 0.05$) compared to the control group. CH_2 /lipid ratio was not affected significantly in the amifostine treated group. Pretreatment of amifostine caused an increase in the CH_2 groups of the irradiated WM and GM of brain compared to the irradiated group, which proves that amifostine has a protective effect on these regions of the brain.

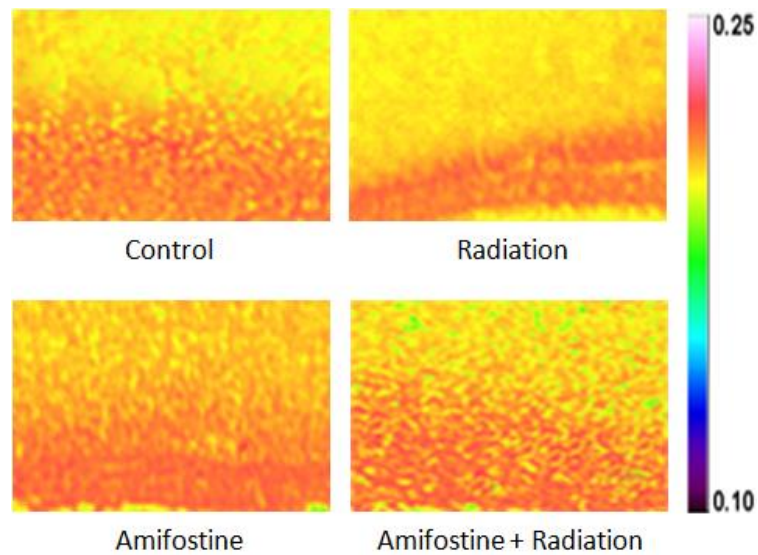


Figure 3.11 CH_2/lipid ratio images of control, irradiated, amifostine treated and amifostine treated + irradiated groups

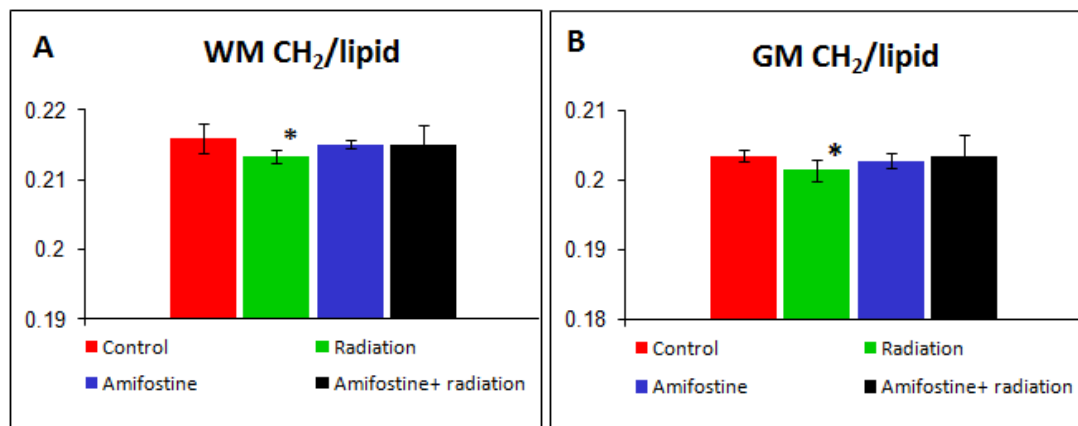


Figure 3.12 The numerical comparisons of the CH_2/lipid ratios of control, irradiated, amifostine treated and amifostine treated + irradiated groups in white matter (A) and grey matter (B)

To reveal the spectroscopic changes in the molecular structure of lipids of the treated tissues, the ratios of some specific lipid functional groups (CH_3 asym. stretc., carbonyl ester, olefinic $\text{HC}=\text{CH}$ bands) to the total lipid (C-H stretching region) were calculated. The CH_3 asym. stretc./total lipid ratio was calculated to examine the methyl concentration in the brain. Figure 3.13 displays the CH_3 /lipid ratio images and Figure 3.14A and B shows the numerical comparisons of the CH_3 /lipid ratios of control, irradiated, amifostine treated and amifostine treated + irradiated groups in WM and GM, respectively. The radiation treatment caused an increase in the CH_3 /lipid ratios in WM ($p < 0.005$) and GM ($p < 0.005$) of brain tissues compared to the control group. Amifostine didn't cause any significant changes on this ratio when it was given to the animals without subsequent exposure to radiation. Treatment of rats with amifostine before radiation exposure provided also protection against the increment of CH_3 groups induced by ionizing radiation.

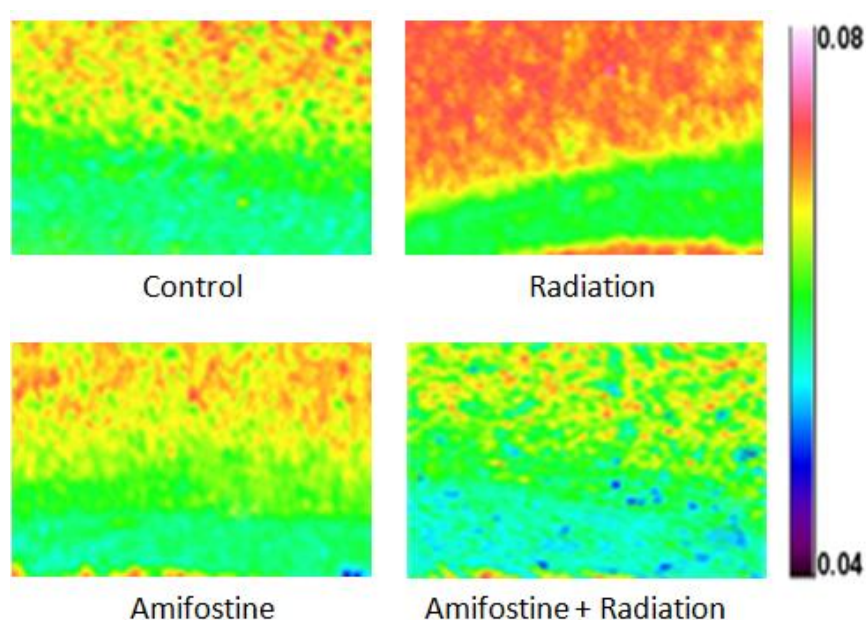


Figure 3.13 CH_3 /lipid ratio images of control, irradiated, amifostine treated and amifostine treated + irradiated groups

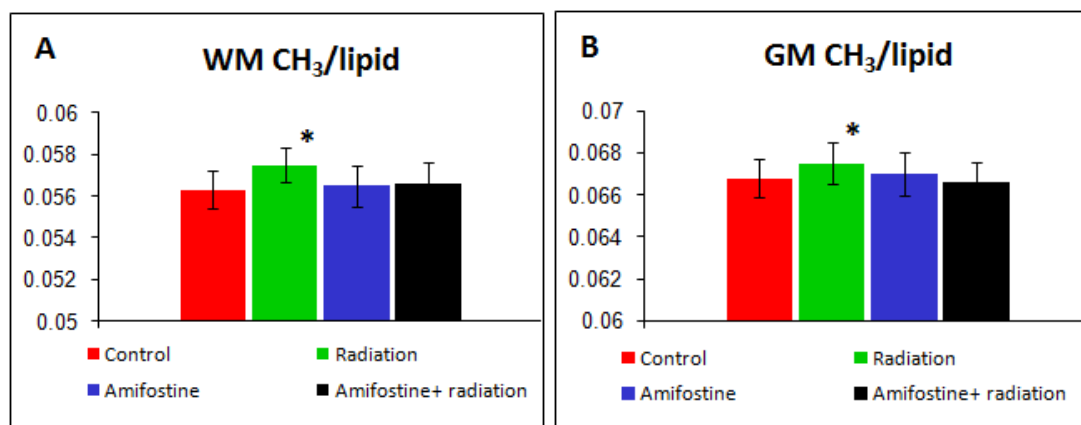


Figure 3.14 The numerical comparisons of the CH₃/lipid ratios of control, irradiated, amifostine treated and amifostine treated + irradiated groups in white matter (A) and grey matter (B)

The synchrotron source has high light brightness and high signal to noise ratio, it is more sensitive to analyze the small peaks (Miller *et al.*, 2000). In the current study, synchrotron data were used to analyze two weak bands, namely carbonyl ester and olefinic =CH bands and secondary structure of proteins. To see the carbonyl status of the system, the carbonyl ester/lipid ratios were calculated. As seen from the Figures 3.15 and 3.16A and B, the carbonyl ester to lipid ratio was increased significantly in the WM ($p < 0.05$) and GM ($p < 0.05$) regions of the irradiated group. There was no significant change in the amifostine treated group and the values of the amifostine treated + irradiated group were very close to the control group, which clearly shows the recovery effect of amifostine.

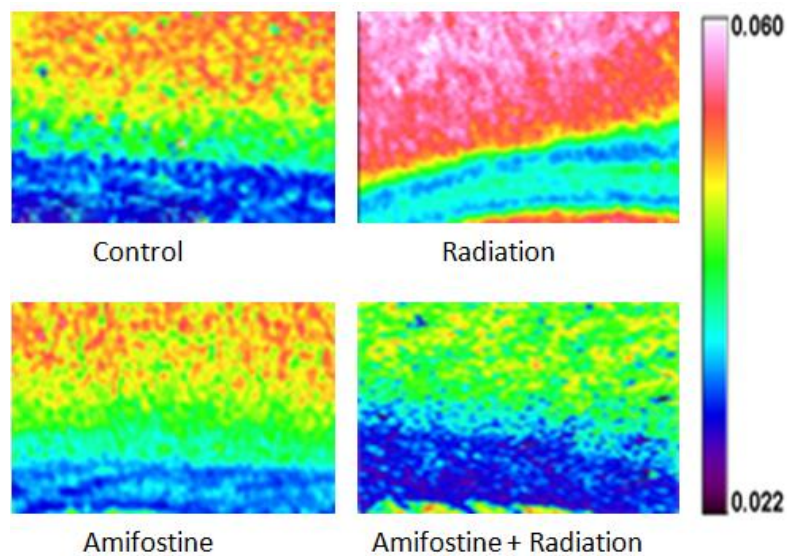


Figure 3.15 Carbonyl ester/lipid ratio images of control, irradiated, amifostine treated and amifostine treated + irradiated groups

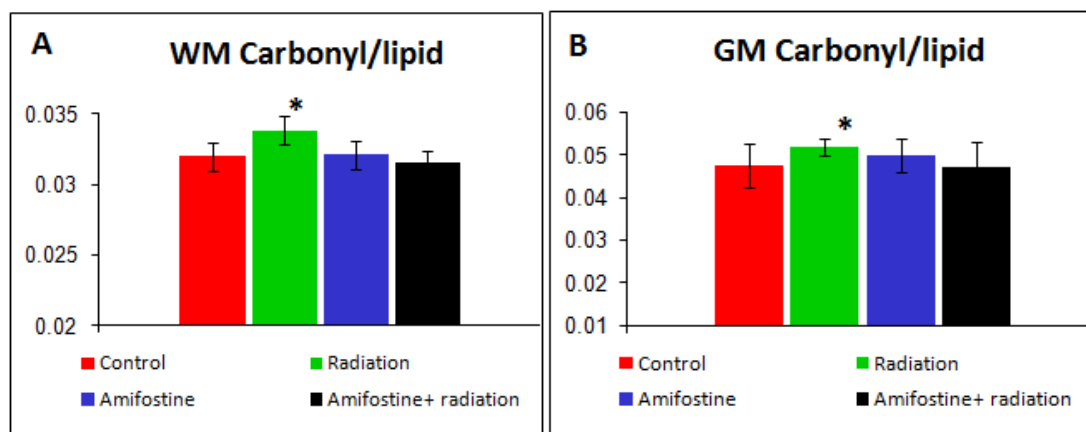


Figure 3.16 The numerical comparisons of the carbonyl ester/lipid ratios of control, irradiated, amifostine treated and amifostine treated + irradiated groups in white matter (A) and grey matter (B)

The intensity/area of olefinic=CH band can be used as an index of relative concentration of double bonds in the lipid structure of unsaturated lipids (Liu *et al.*, 2002; Severcan *et al.*, 2005). To examine the unsaturation level of the system, olefinic=CH/lipid ratio was calculated. Figure 3.17 demonstrates the olefinic=CH to lipid ratio images of the control and treated groups. Figure 3.18A and B displays the numerical comparisons of olefinic=CH ratios of control and treated groups in WM and GM. While ionizing radiation increased significantly the olefinic=CH groups in WM ($p<0.05$), amifostine didn't cause any significant changes in both WM and GM regions of the brain. Pretreatment of rats with amifostine prior to radiation provided protection against the increment of the olefinic=CH groups induced by ionizing radiation especially in WM.

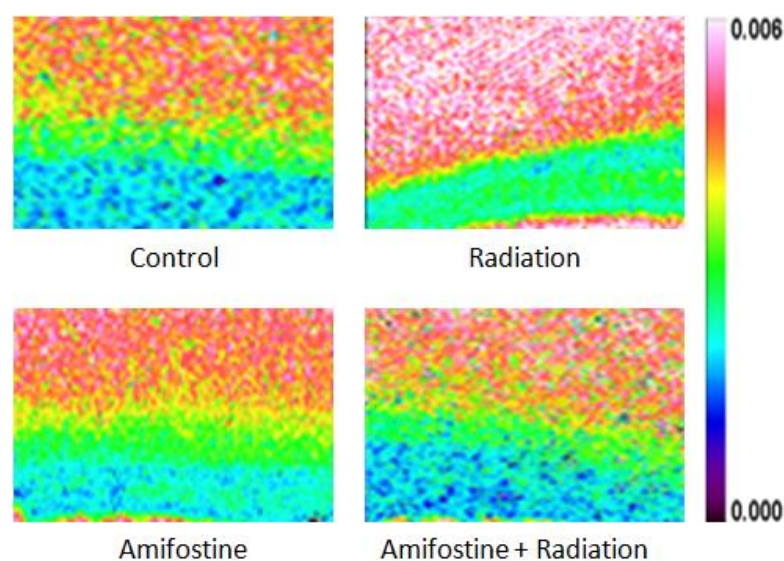


Figure 3.17 Olefinic=CH/lipid ratio images of control, irradiated, amifostine treated and amifostine treated + irradiated groups

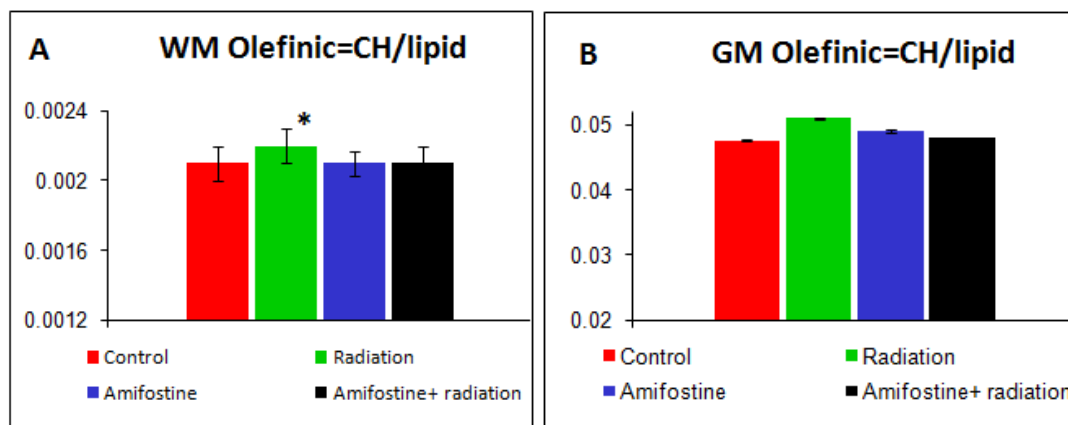


Figure 3.18 The numerical comparisons of the olefinic=CH/lipid ratios of control, irradiated, amifostine treated and amifostine treated + irradiated groups in white matter (A) and grey matter (B)

To examine the protein content and structure, Amide I/Amide II ratio was calculated. Figure 3.19 shows the Amide I/Amide II ratio images and Figure 3.20A and B shows the numerical comparisons for the Amide I/Amide II ratios of control, irradiated, amifostine treated and amifostine treated + irradiated groups in WM and GM. As seen from these figures, the ratio of the Amide I/Amide II decreased significantly both in the WM ($p < 0.05$) and GM ($p < 0.05$) regions of the brain. As also seen from these figures, there are no significant differences between the values of control and amifostine treated group and those of control and amifostine treated + irradiated group.

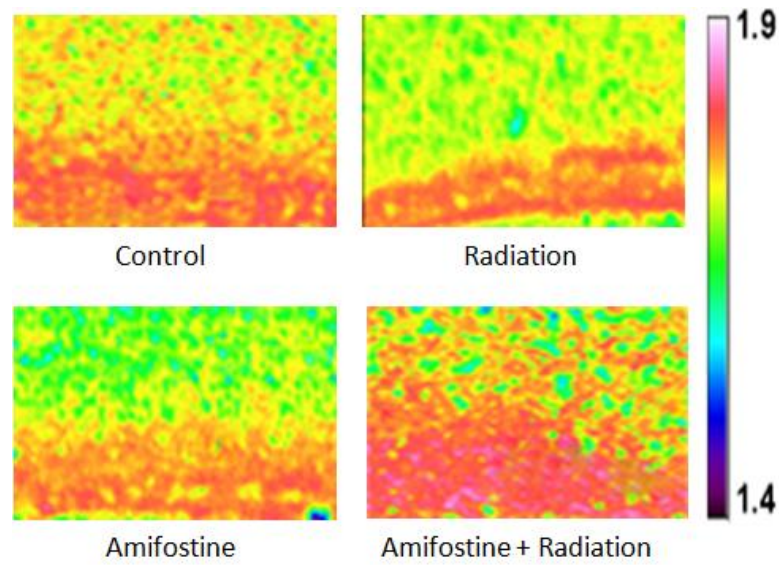


Figure 3.19 Amide I/amide II ratio images of control, irradiated, amifostine treated and amifostine treated + irradiated groups

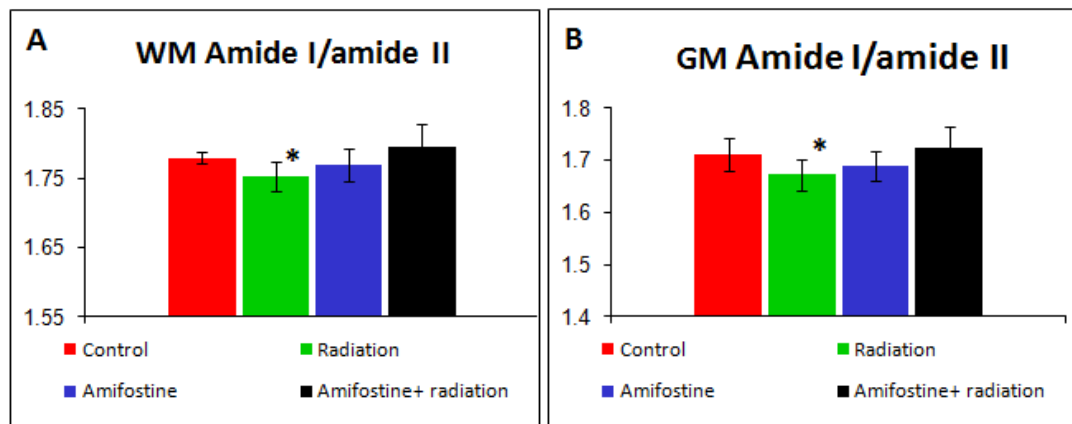


Figure 3.20 The numerical comparisons of the amide I/amide II ratios of control, irradiated, amifostine treated and amifostine treated + irradiated groups in white matter (A) and grey matter (B)

The secondary structures of proteins can be determined from the amide I band which is between 1700-1600 cm^{-1} . For this purpose, the intensities of sub-bands in the second derivatives of amide I absorption were analyzed. Figure 3.21 shows the second derivative spectra of control, irradiated, amifostine treated and amifostine treated + irradiated rat brain WM and GM, respectively. In these figures, the peak around 1682 cm^{-1} arises from β -turn structure, the peak around 1657 cm^{-1} is due to α -helix structure, the peak located at 1643 cm^{-1} arises from unordered random coil and the peak around 1630 cm^{-1} is due to β -sheet structure (Toyran *et al.*, 2004; Wang *et al.*, 2005b; Ozek *et al.*, 2009). The numerical comparisons of the changes in the protein secondary structures in WM and GM were displayed as bar graphs for better comparison in Figure 3.22 and 3.23, respectively. As seen from these figures, the peak intensities of α -helix and β -sheet structures decreased slightly and the intensities of turns and random coil structures increased significantly in the irradiated group ($p < 0.05$) compared to the control group. As also seen from these figures, there were no significant differences between control and amifostine treated groups. These results show the ameliorating effect of amifostine on the brain protein secondary structure.

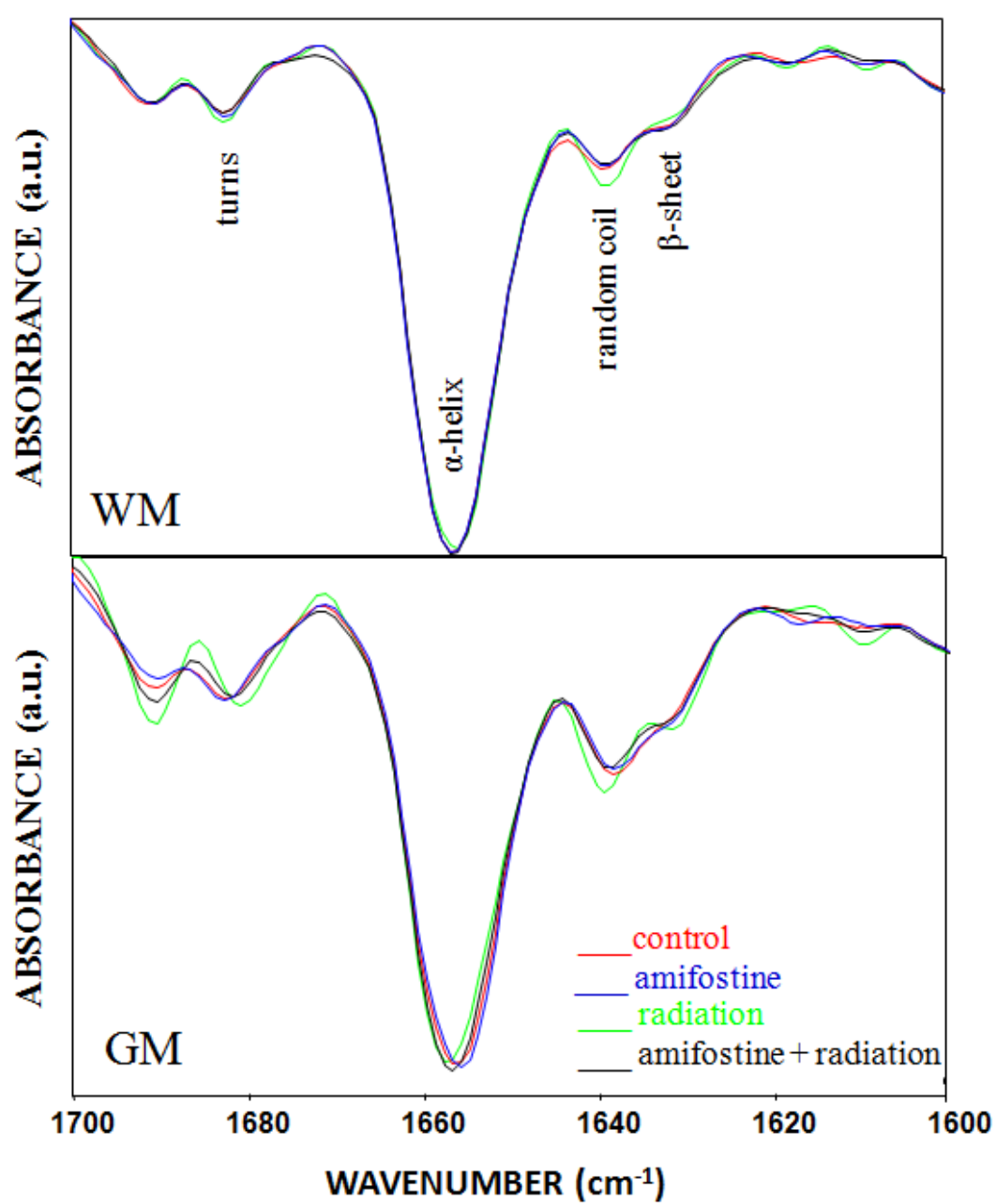


Figure 3.21 The second derivative spectra of control, irradiated, amifostine treated and amifostine treated + irradiated rat brain WM and GM in the 1700-1600 cm^{-1} region

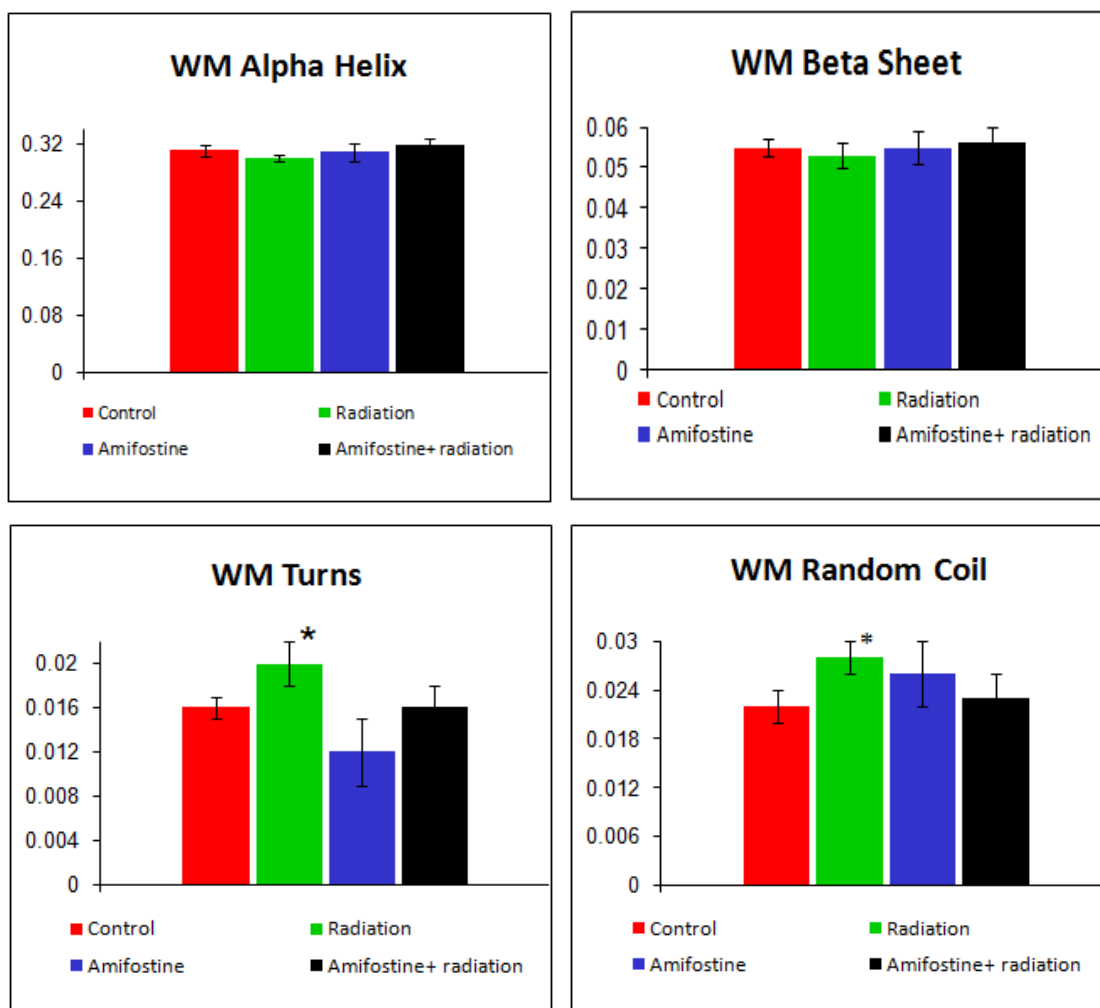


Figure 3.22 The numerical comparisons of the intensities of the main protein secondary structures for control, irradiated, amifostine treated and amifostine treated + irradiated rat brain WM

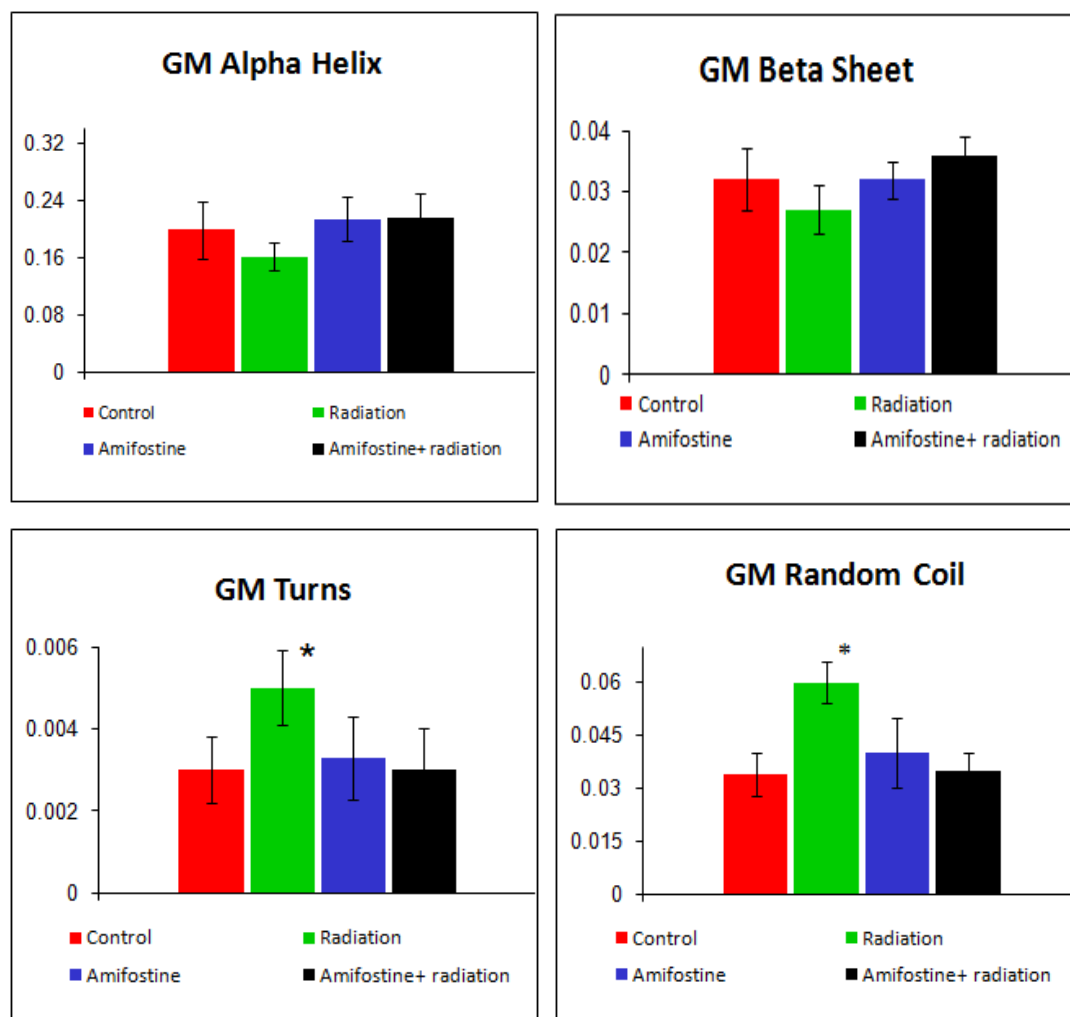


Figure 3.23 The numerical comparisons of the intensities of the main protein secondary structures for control, irradiated, amifostine treated and amifostine treated + irradiated rat brain GM

3.2 The Effects of Ionizing Radiation and Amifostine on Rat Liver Microsomal Membranes

In this part of the study, we aimed to investigate the effects of ionizing radiation on the structure, composition and dynamics of rat liver microsomal membranes and to test the protective effects of amifostine on these systems by monitoring the changes in the peak frequency, bandwidth, intensity, band area and band area ratios of main FTIR absorptions arising from lipids and proteins.

3.2.1 Band Assignment of the Liver Microsomal Membrane

Figure 3.24 shows a representative FTIR spectrum of a control rat liver microsomal membrane, in the region of 3050-1000 cm^{-1} . Main absorptions observed in the spectra were labelled in Figure 3.24 and detailed band assignments were given in Table 3.4.

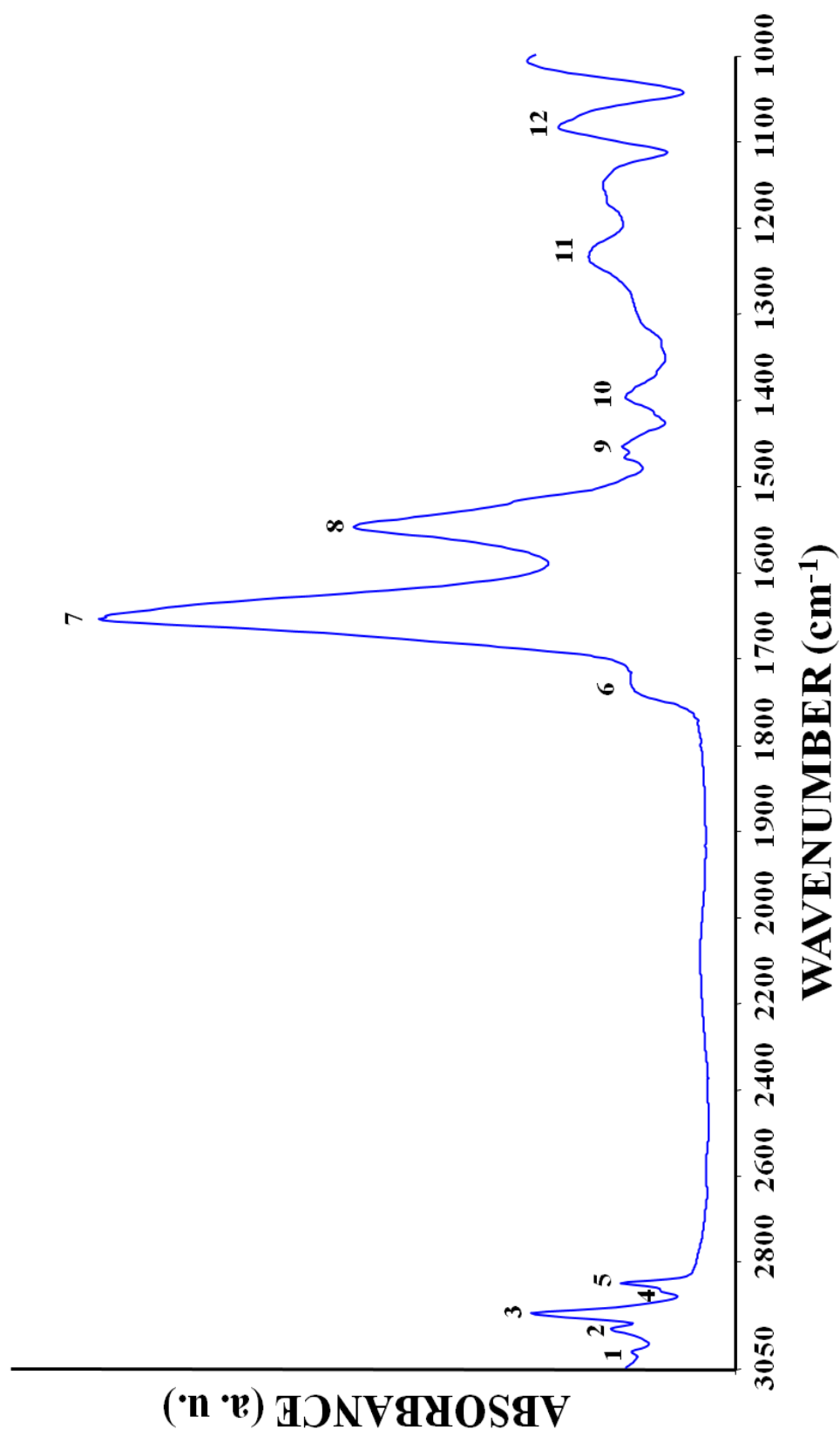


Figure 3.24 An FTIR spectrum of control rat liver microsomal membrane in 3050-1000 cm⁻¹ region

Table 3.4 FTIR spectral band assignments of rat liver microsomal membrane in the region of 3050-1000 cm⁻¹

Band #	Wavenumber (cm⁻¹)	Definition of the assignment
1	3014	Olefinic =CH : Unsaturated lipids (Severcan <i>et al.</i> , 2005)
2	2962	CH₃ asymmetric stretching : Lipids and protein side chains (Szalontai, 2009; Severcan <i>et al.</i> , 2010)
3	2925	CH₂ asymmetric stretching : Mainly Lipids (Cakmak <i>et al.</i> , 2006; Severcan <i>et al.</i> , 2010)
4	2873	CH₃ symmetric stretching : Mainly proteins (Cakmak <i>et al.</i> , 2006; Severcan <i>et al.</i> 2010)
5	2854	CH₂ symmetric stretching : Mainly lipids (Cakmak <i>et al.</i> , 2006)
6	1745	Ester C=O stretching : Lipids (Akkas <i>et al.</i> , 2007)
7	1650	Amide I : 80% protein C=O stretching, 10% protein N-H bending, 10% C-N stretching (Haris and Severcan, 1999)
8	1545	Amide II : 60% protein N-H bending, 40 % C-N stretching (Haris and Severcan, 1999)
9	1455	CH₂ bending : Mainly lipids (Cakmak <i>et al.</i> , 2006; Ozek <i>et al.</i> , 2010)
10	1401	COO⁻ symmetric stretching : Fatty acids and protein side chains (Cakmak <i>et al.</i> , 2006)
11	1234	PO₂⁻ asymmetric stretching : Phospholipids (Akkas <i>et al.</i> , 2007)
12	1084	PO₂⁻ symmetric stretching : Phospholipids (Akkas <i>et al.</i> , 2007)

3.2.2 General Comparison of the Control and Treated Spectra in 3025-2820 cm^{-1} and 1800-1000 cm^{-1} Regions

In order to display the details of spectral analysis clearly, the spectra were investigated in two regions. Figure 3.25A and B shows the average spectra of control, irradiated, amifostine treated and amifostine treated + irradiated rat liver microsomal membranes in the 3025-2820 cm^{-1} and 1800-1000 cm^{-1} , respectively. Although an average normalized spectrum from each group was presented in these figures, for the accurate determination of the mean values for the band areas, peak positions, and the bandwidth values, the raw spectrum belonging to each individual of the groups was considered. The numerical comparisons of the band area ratios, the wavenumbers and bandwidths of infrared bands were listed in Table 3.5 and 3.6, respectively. As seen from these tables and Figures 3.25A and B, there are significant ($p < 0.05$) differences between the control and irradiated group suggesting that ionizing radiation induces remarkable changes in the liver microsomal membranes. These figures and tables also indicate that the amifostine treated and amifostine treated + irradiated group's spectra are between the control and irradiated groups' spectra and in general the values of amifostine treated + irradiated group are very close to that of control group. Indeed, with respect to the control no significant variations were observed in the amifostine treated and amifostine treated + irradiated groups. This result shows that amifostine doesn't induce any significant alterations when it was given to the rats without subsequent exposure to radiation. In addition, this result implies that when amifostine was given to the animals before radiation, it has protective effect against the ionizing radiation-induced alterations in rat liver microsomal membranes.

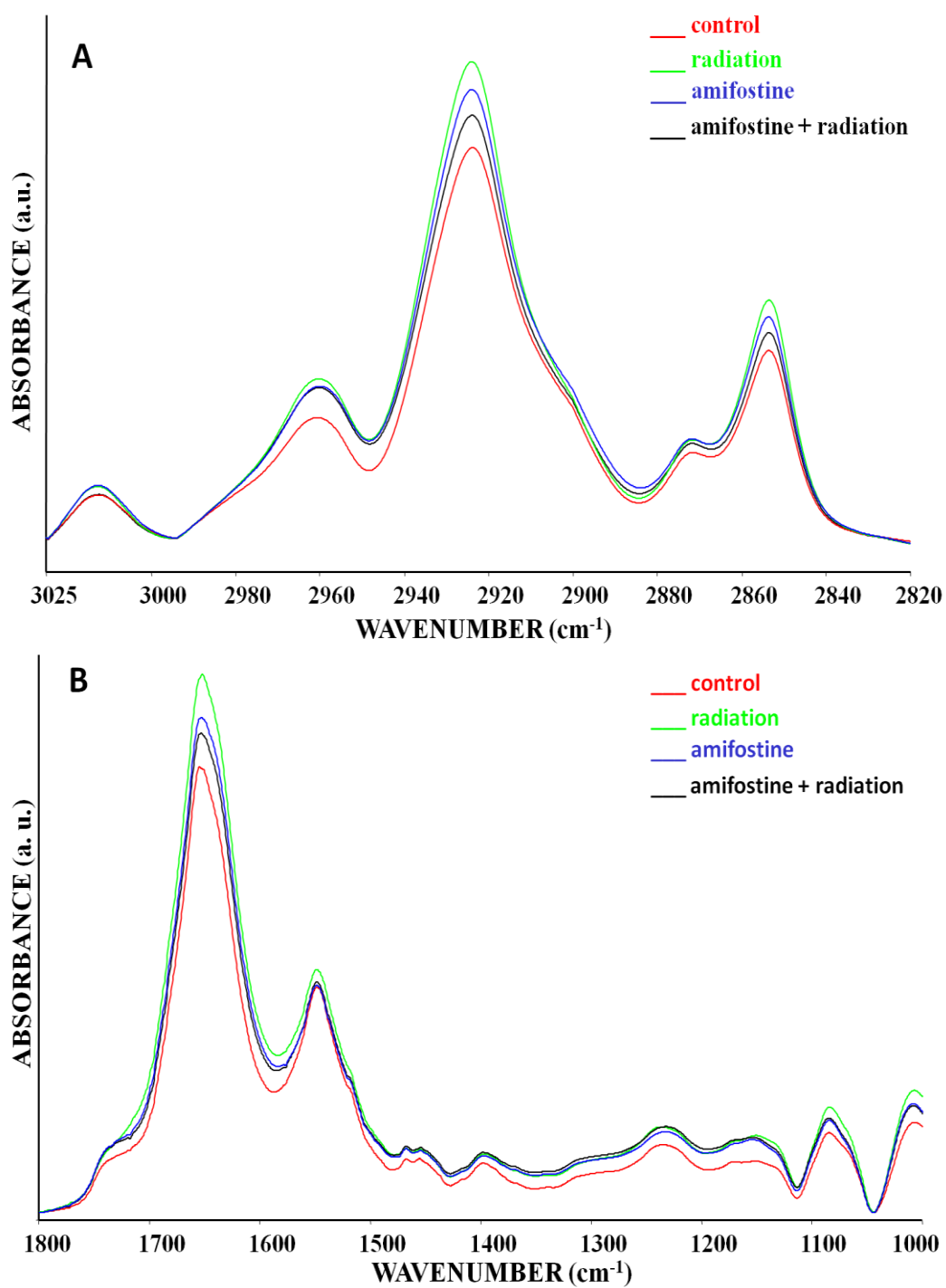


Figure 3.25 The average baseline corrected infrared spectra of control, irradiated, amifostine treated and amifostine treated + irradiated rat liver microsomal membranes **A)** in the 3025-2820 cm⁻¹ region **B)** in the 1800-1000 cm⁻¹ region. The spectra were normalized with respect to the amide I band (A) and to the CH₂ asymmetric stretching band (B)

Table 3.5 Changes in the band area ratios of various functional groups in control, irradiated, amifostine treated and amifostine treated + irradiated liver microsomal membranes. The values are shown as “mean \pm standard deviation” for each group. The degree of significance was denoted as: * $p < 0.05$

Functional Group	Control (n=6)	Radiation (n=6)	Amifostine (n=6)	Radiation + Amifostine (n=6)
Lipid/Protein	0.064 \pm 0.004	0.054 \pm 0.007*	0.06 \pm 0.006	0.062 \pm 0.004
CH ₂ asym./ CH ₃ asym.	13.052 \pm 1.709	11.543 \pm 1.349*	12.067 \pm 1.553	12.938 \pm 0.921
CH ₂ asym./ Lipid	0.874 \pm 0.01	0.816 \pm 0.007*	0.820 \pm 0.008	0.831 \pm 0.009
Carbonyl ester/ Lipid	0.102 \pm 0.005	0.115 \pm 0.006*	0.110 \pm 0.0009	0.108 \pm 0.008
CH ₃ /Lipid	0.129 \pm 0.015	0.156 \pm 0.015*	0.127 \pm 0.018	0.124 \pm 0.011
Unsaturation/ Saturation	0.042 \pm 0.005	0.049 \pm 0.003*	0.0454 \pm 0.003	0.046 \pm 0.006
Amide I/ Amide II	1.847 \pm 0.289	1.522 \pm 0.144*	1.755 \pm 0.123	1.615 \pm 0.139

Table 3.6 Changes in the **A)** wavenumber and **B)** bandwidth values of various functional groups in control, irradiated, amifostine treated and amifostine treated + irradiated liver microsomal membranes. The values are shown as 'mean \pm standard deviation' for each group. The degree of significance was denoted as: * $p < 0.05$

A)

Functional Group	Control (n=6)	Radiation (n=6)	Amifostine (n=6)	Radiation + Amifostine (n=6)
CH ₂ asym. str.	2924.857 \pm 0,164	2923.943 \pm 0,222*	2924.61 \pm 0.123	2924.538 \pm 0.099
Amid I	1649.9 \pm 0,923	1651.117 \pm 0,707*	1650.65 \pm 0.583	1650.647 \pm 0.559
CH ₃ asym. str.	2963.876 \pm 0.559	2962.057 \pm 1.45*	2963.624 \pm 0.522	2963.703 \pm 0.572
PO ₂ ⁻ asym. str.	1234.353 \pm 0.860	1232.765 \pm 1.014*	1234.162 \pm 0.319	1233.75 \pm 0.436

B)

Functional group	Control (n=6)	Radiation (n=6)	Amifostine (n=6)	Radiation + Amifostine (n=6)
CH ₂ asym. str.	12.338 \pm 0.237	12.038 \pm 0.124*	12.19 \pm 0.18	12.203 \pm 0.114
Amid I	27.972 \pm 1.166	29.514 \pm 1.250*	29.135 \pm 0.23	28.568 \pm 0.852

3.2.3 Detailed Spectral Analysis

3.2.3.1 The Effects of Ionizing Radiation and Amifostine on the Composition and Structure of Rat Liver Microsomal Membranes

The intensity and the area of infrared bands originating from special functional groups in a biological molecule are directly proportional to the concentration of that molecule (Toyran *et al.*, 2004; Cakmak *et al.*, 2006). Using the FTIR data, the lipid to protein ratio can be obtained by taking the ratio of the areas of the bands arising from lipids and proteins. The ratio of the sum of the CH₂ asymmetric and symmetric stretching bands to the sum of the amide I and II bands were used to evaluate the lipid to protein ratio of the microsomal system. A significant decrease in the lipid to protein ratio of the microsomal system. A significant decrease in the lipid/protein ratio was observed in the irradiated liver microsomal membranes ($p < 0.05$) compared to controls (Figure 3.26). There was a slight but not significant increase in the ratio of the lipid/protein in the animals given amifostine without subsequent exposure to radiation. When amifostine was given to the rats before radiation, it didn't cause any significant alterations in the lipid/protein ratio of the liver microsomal membranes which indicates the protective effect of amifostine on the lipid/protein ratio.

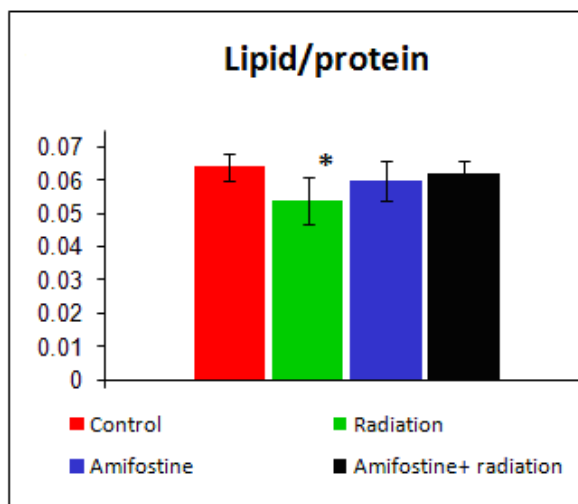


Figure 3.26 The numerical comparisons of the lipid/protein ratios of control, irradiated, amifostine treated and amifostine treated + irradiated rat liver microsomal membranes

The CH₂ asym. stretch./total lipid ratio was applied to indicate the alterations in the chain length of the phospholipids. The numerical comparison of the CH₂/lipid ratios of control, irradiated, amifostine treated and amifostine treated + irradiated rat liver microsomal membranes were displayed in Figure 3.27. Significant decrease in the ratio of the CH₂/lipid was observed in the irradiated liver microsomal membranes ($p < 0.05$) compared to the control group. As also it is seen from Figure 3.27, the ratio of the CH₂/lipid decreased slightly but not significantly in the amifostine treated group. Pretreatment of amifostine restored the significant changes observed in the irradiated liver microsomes compared to control group.

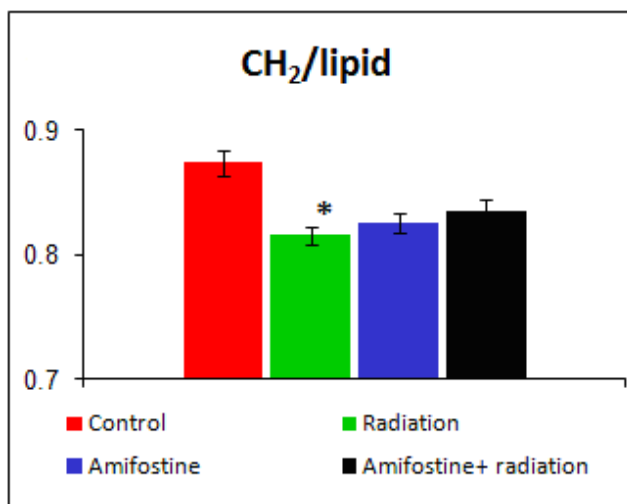


Figure 3.27 The numerical comparisons of the CH₂/lipid ratios of control, irradiated, amifostine treated and amifostine treated + irradiated rat liver microsomal membranes

In addition, to reveal the spectroscopic changes in the molecular structure of lipids, the ratios of some specific lipid functional groups (carbonyl ester stretch., CH₃ asym. stretch., olefinic=CH) to the total lipid (the sum of the CH₂ asymmetric and symmetric stretching bands) were calculated.

Figure 3.28A, B and C show the numerical comparisons of the carbonyl ester/total lipid, the CH₃ asym. stretc./total lipid, unsaturation/saturation ratios of control, irradiated, amifostine treated and amifostine treated + irradiated rat liver microsomal membranes, respectively. As seen from Figure 3.28A, the carbonyl ester/total lipid ratio increased significantly ($p < 0.05$) in the irradiated group compared to control. The values of the amifostine treated + irradiated group were very close to the control group, which clearly shows the recovery effect of amifostine. Moreover, the radiation treatment caused an increase in the CH₃/total lipid ratios in the irradiated group compared to the control group as seen from Figure 3.28B. Pretreatment of rats

with amifostine provided also protection against the increment of CH_3 groups induced by ionizing radiation. To examine the unsaturation level of the system, the ratio of the area of the band arising from unsaturated lipids (olefinic=CH band) to saturated lipids (CH_2 asymmetric + CH_2 symmetric) was calculated. As seen from Figure 3.28C, this ratio increased significantly in the radiation treated group ($p < 0.05$), while any significant changes were observed for amifostine treated + irradiated group compared to control group implying that amifostine has a ameliorating effect on the system. These figures demonstrate that there were no significant changes in the group of animals given only amifostine compared to control.

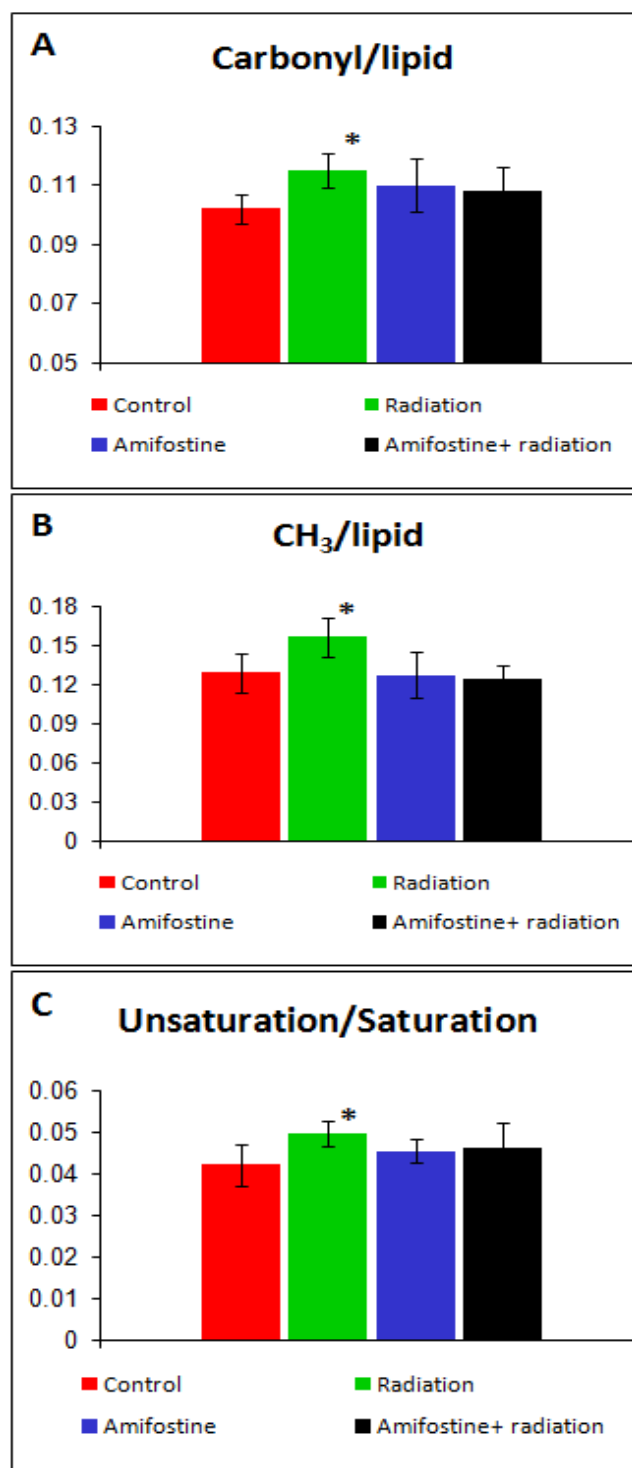


Figure 3.28 The numerical comparisons of the carbonyl ester/total lipid (A), the CH₃ asym. stretc./total lipid (B), unsaturation/saturation (C) ratios of control, irradiated, amifostine treated and amifostine treated + irradiated rat liver microsomal membranes

To examine the changes in protein composition and structure, Amide I/Amide II ratio was calculated. Figure 3.29 shows the numerical comparisons of the Amide I/Amide II ratios of control, irradiated, amifostine treated and amifostine treated + irradiated rat liver microsomal membranes. As seen from this figure, there is a significant decrease in the Amide I/Amide II ratio of the irradiated group ($p < 0.05$) and no significant change in the amifostine treated and amifostine treated + irradiated group in comparison to the control group.

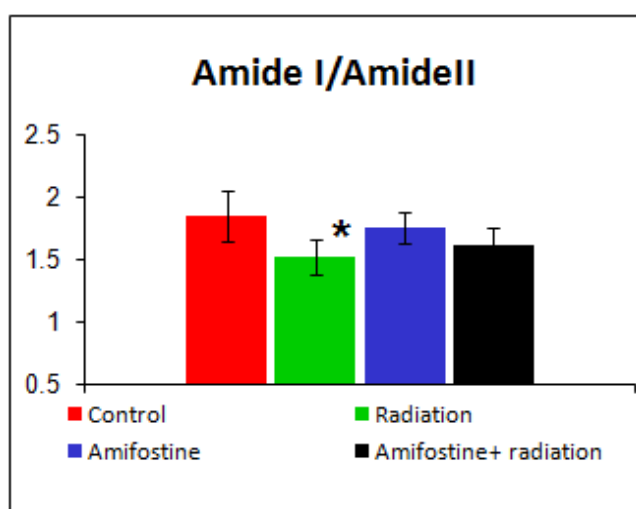


Figure 3.29 The numerical comparisons of the Amide I/Amide I ratios of control, irradiated, amifostine treated and amifostine treated + irradiated rat liver microsomal membranes

As the position of amide I absorption was sensitive to protein conformation, the bandwidth and frequency values of this band were evaluated to examine the changes

in protein conformations (Cakmak *et al.*, 2006). Figure 3.30A and B shows the numerical comparisons of the Amide I average bandwidth and band frequency values of control, irradiated, amifostine treated and amifostine treated + irradiated rat liver microsomal membranes, respectively. A significant broadening was observed in the bandwidth of the amide I band in the irradiated group ($p < 0.05$) in comparison to control group (Figure 30A). As seen from Figure 3.30A, there is no significant change in the bandwidth of amifostine treated and amifostine treated + irradiated groups. The frequency of amide I band shifted to higher values dramatically ($p < 0.05$) in the irradiated group and any significant changes were observed in amifostine treated and amifostine treated + irradiated groups compared to the control group (Figure 3.30B).

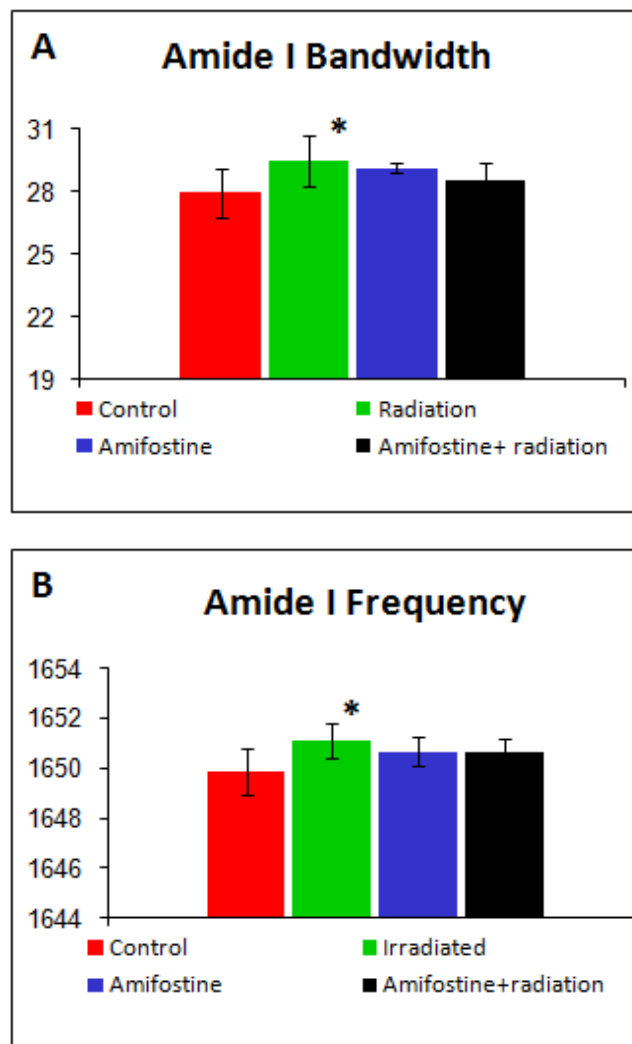


Figure 3.30 The numerical comparisons of the Amide I average bandwidth (A) and band frequency (B) values of control, irradiated, amifostine treated and amifostine treated + irradiated rat liver microsomal membranes

The changes in the protein secondary structures were determined from the intensities of sub-bands in the second derivative of the amide I absorption band in detail. The peak located at around 1680 cm^{-1} is due to turns and bends, the peak around at 1659 cm^{-1} arises from α -helix structure, the peak located at 1648 cm^{-1} is assigned to random coil and the peak around 1637 cm^{-1} is attributed to β -sheet structure (Ozek *et al.*, 2009). As seen from Figure 3.31 and 3.32, between control and irradiated group, large spectral differences appear in the shapes and intensity values of these bands. The peak intensity values of α -helical structures and β -sheet structures decreased significantly in irradiated group ($p < 0.005$) compared to control group. Moreover, the intensity values of turns and random coil structures increased in the irradiated group ($p < 0.05$) compared to the control group. As seen from Figure 3.32, there were no significant differences in the peak intensity values of the amifostine treated and amifostine treated + irradiated group compared to control group. These results imply the protective effect of amifostine on the protein secondary structure.

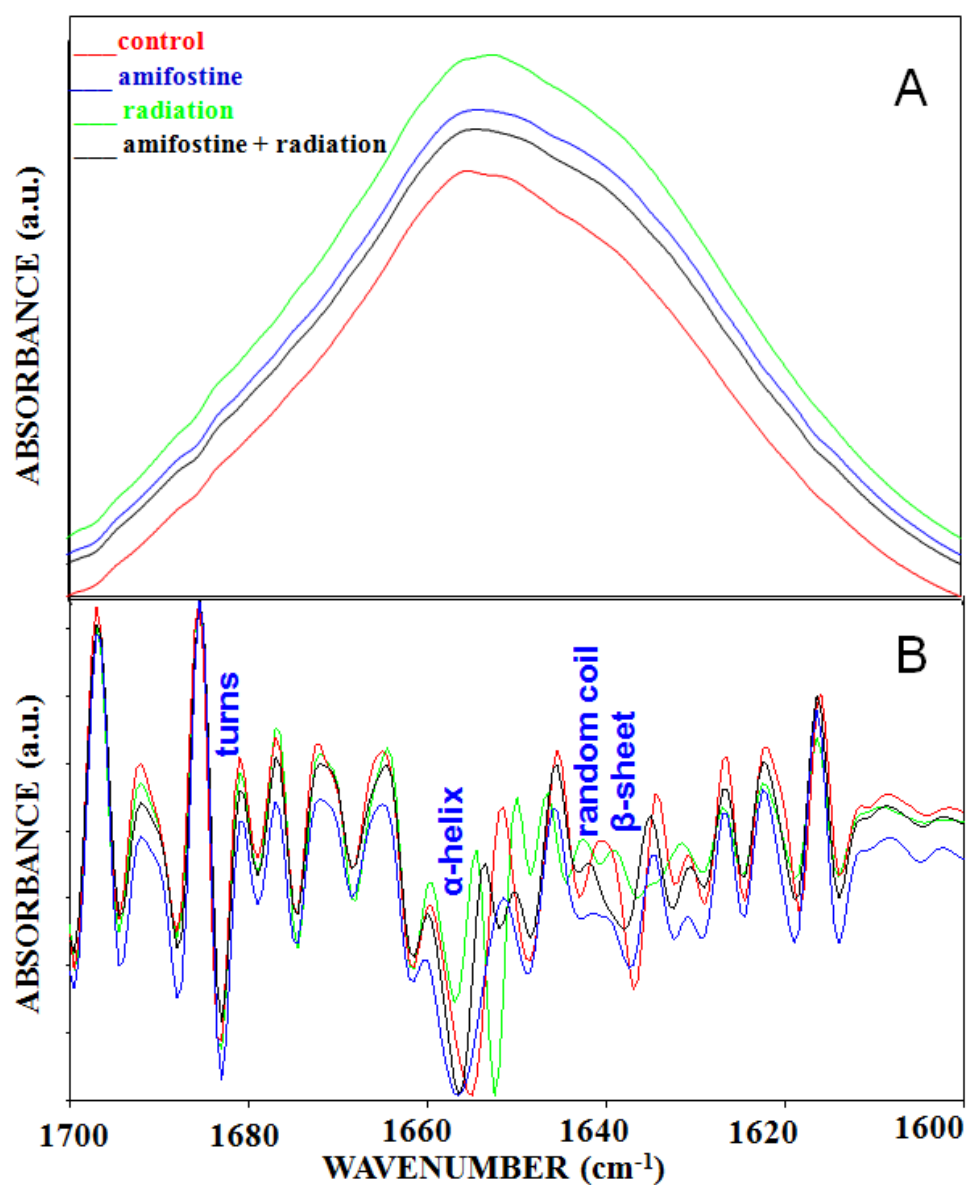


Figure 3.31 The average A) absorbance infrared spectra, B) second derivative spectra of control, irradiated, amifostine treated and amifostine treated + irradiated rat liver microsomal membranes in the $1700\text{-}1600\text{ cm}^{-1}$ region

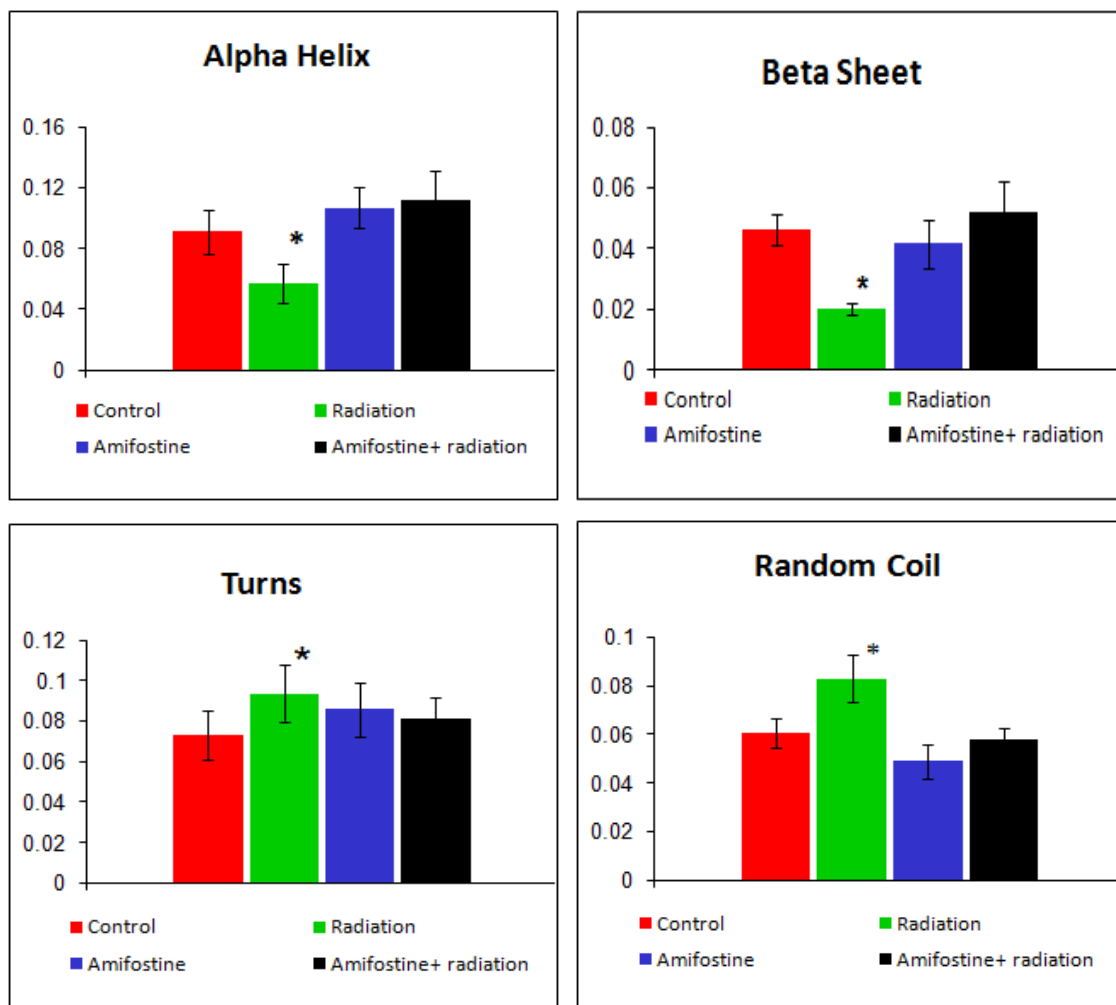


Figure 3.32 The numerical comparisons of the intensities of the main protein secondary structures for control, irradiated, amifostine treated and amifostine treated + irradiated rat liver microsomal membranes

3.2.3.2 The Effects of Ionizing Radiation and Amifostine on Rat Liver Microsomal Membrane Dynamics

The position of the asymmetric and symmetric CH₂ stretching bands gives information about the order/disorder state of lipids, i.e., lipid acyl chain flexibility. For example, the higher the frequency, the higher the acyl chain flexibility (disordering) (Lewis *et al.*, 1989; Liu *et al.*, 2002; Toyran *et al.*, 2004). Figure 3.33A shows the numerical comparisons of the CH₂ asymmetric average band frequency values of control, irradiated, amifostine treated and amifostine treated + irradiated rat liver microsomal membranes. As seen from this figure, while the frequency of the CH₂ asymmetric stretching band shifted significantly to lower values after radiation treatment ($p < 0.05$), no significant changes were observed in the amifostine treated and amifostine treated + irradiated groups in comparison to the control. This shifting to lower values indicates that lipid order increases and acyl chain flexibility decreases in the irradiated liver microsomal membranes (Cakmak *et al.*, 2006; Toyran *et al.*, 2004). Bandwidth of the same band also provides information about the dynamics of the system (Lopez-Garcia *et al.*, 1993; Cakmak *et al.*, 2003). As seen from Figure 3.33B, there is a dramatic reduction in the bandwidth of the CH₂ asymmetric stretching band of the irradiated group and there are no significant changes in the amifostine treated and amifostine treated + irradiated group in comparison to the control group. The dramatic decrease in the bandwidth shows that there is a decrease in the lipid dynamics of the radiation-treated liver microsomal membranes. Thus, ionizing radiation caused an increase in the lipid order and a decrease in the membrane fluidity in the irradiated microsomal membranes and amifostine suppressed these changes.

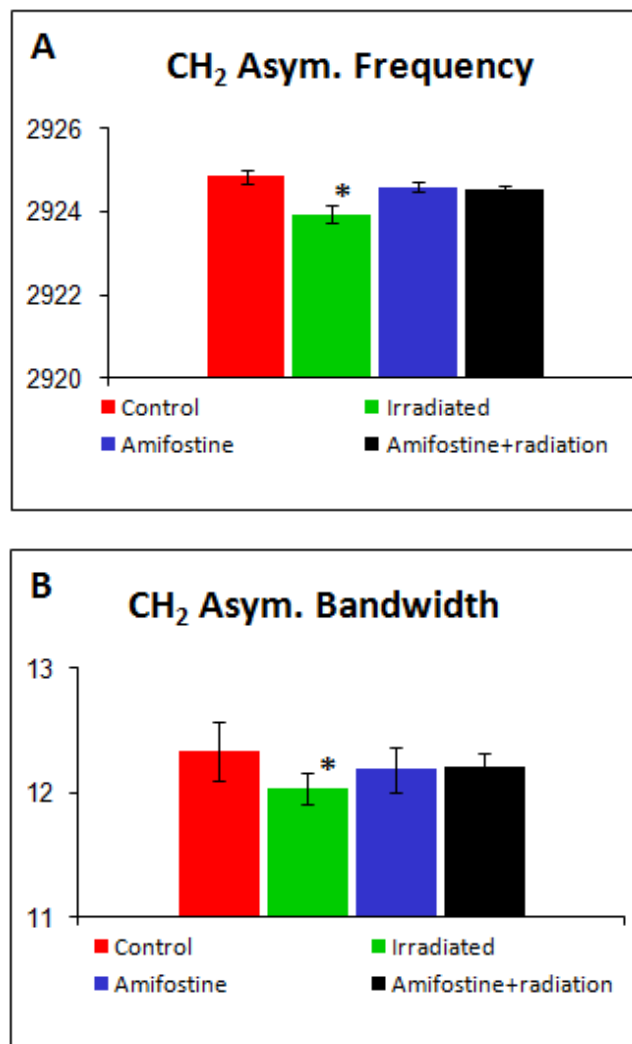


Figure 3.33 The numerical comparisons of the CH₂ asymmetric average band frequency (A) and bandwidth (B) values of control, irradiated, amifostine treated and amifostine treated + irradiated rat liver microsomal membranes

The alterations in the frequency values of CH₃ asymmetric stretching band provides information about the deep interior of the lipid bilayer. A decrease in the frequency of this band shows the stiffness of the lipid bilayer and an increase in the frequency corresponds the increase in the freedom of the acyl chains in the central area of the lipid bilayer (Umemura *et al.*, 1980). As seen from Figure 3.34A, there is a significant decrease in the frequency of the CH₃ asymmetric stretching mode in the irradiated group ($p < 0.05$) in comparison to the control group while there are no significant changes in the amfostine treated and amifostine treated + irradiated groups. The PO₂⁻ asymmetric stretching band gives information about the head-group regions of membrane lipids (Akkas *et al.*, 2007). It can be seen from Figure 3.34B that the frequency of PO₂⁻ asymmetric stretching band shifted to lower values significantly ($p < 0.05$) in the irradiated group and any significant changes were observed in the amfostine treated and amifostine treated + irradiated groups in comparison to the control group.

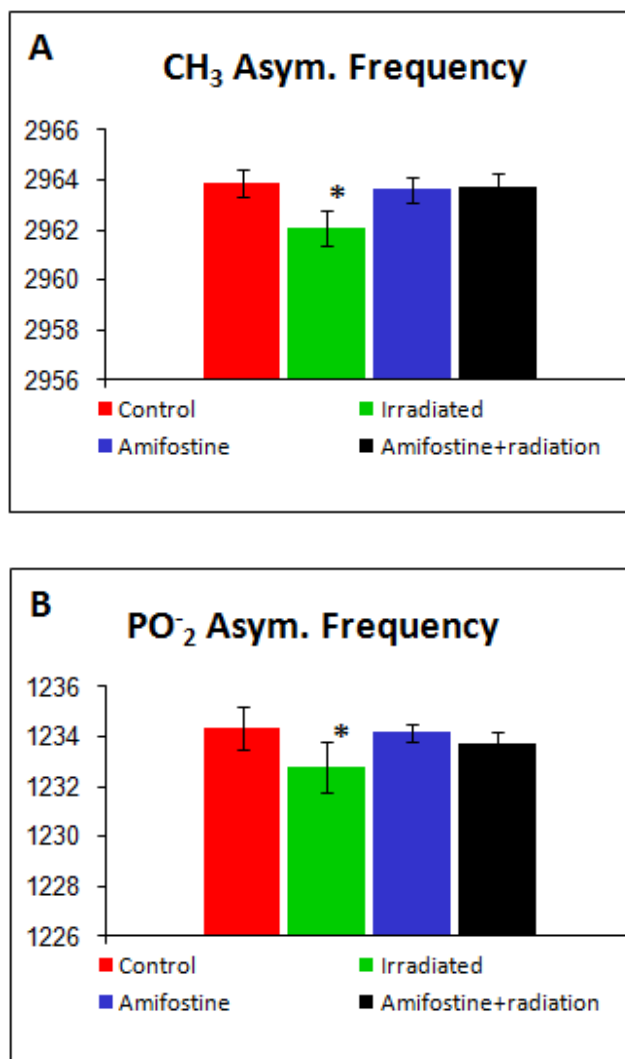


Figure 3.34 The numerical comparisons of the CH₃ asymmetric (A) and PO₂ asym. (B) average band frequency values of control, irradiated, amifostine treated and amifostine treated + irradiated rat liver microsomal membranes

CHAPTER 4

DISCUSSION

4.1 The Effects of Ionizing Radiation and Amifostine on Rat Brain Tissue

In the first part of this study, the effects of ionizing radiation on different regions of the rat brain -- namely WM and GM -- and the protective effects of amifostine has been investigated by using FTIR microspectroscopy and SR-FTIR microspectroscopy. FTIR microspectroscopy together with SR-FTIR microspectroscopy yielded spatially resolved information on unstained tissue sections of brain samples from Sprague Dawley rats that allowed the generation of infrared maps with high image contrast. Results of this part of the thesis revealed that whole body irradiation induces significant oxidative tissue damage in the WM and GM regions of the rat brain and the administration of amifostine before ionizing radiation caused protective effect against the radiation-induced damages in these regions of the brain. This study also demonstrated that the alterations induced by ionizing radiation on the content and structure of different regions of the brain can be investigated in situ using FTIR microspectroscopy and SR-FTIR microspectroscopy without altering the biochemical constituents of those regions.

FTIR microspectroscopy brings together infrared spectroscopy and light microscope for investigating the biochemical structure and composition in small sample regions on microscopic scales (Szczerbowska-Boruchowska *et al.*, 2007). Infrared spectra of biological tissues are composed of some characteristic absorption bands that represent the super position of infrared-active vibrational modes of the different

molecules present. The absorption bands originate from all different kinds of molecules in the tissue such as carbohydrates, lipids, proteins and nucleic acids. Thus, an infrared spectrum of a biological tissue may provide information about the chemical components of the probed material and its biochemical structure (Kneipp *et al.*, 2000; Kretlow *et al.*, 2006). Because the combination of the molecular parameters about the composition, structure and their interactions in a tissue is unique, an infrared spectrum of a tissue has typical wavenumbers, bandwidths and intensities. So, infrared spectrum provides fingerprint-like information and allows the determination of functional groups in biomolecules and consequently it enables us the identification of conformationally different tissue composition and structures (Kneipp *et al.*, 2000; Kretlow *et al.*, 2006). The area of infrared absorptions originating from a particular functional group is directly proportional to the concentration of that species (Ozek *et al.*, 2009). In this study, using FTIR imaging, WM and GM regions of the brain were easily discriminated (Figure 3.4).

Because the brain is a complex organ with both structural and chemical heterogeneity, many structural differences between WM and GM in the brain are expected. Indeed, the WM spectrum is quite different from GM especially for the lipid vibrational bands located at 2922, 1740, 1467, 1239 and 1075 cm^{-1} (Figure 3.5). While an axon, a part of neuron, is located in WM, the neuronal cell body is typically located in grey matter. The myelin sheath which is a phospholipid layer surrounding only the axons of neurons has very high lipid content due to its multilamellar structure and a higher lipid/protein ratio than other biological membranes (Szczerbowska-Boruchowska *et al.*, 2007). Although the lipids existing in myelin sheath are also found in other biological membranes, some lipids such as galactolipids, cerebroside and sulfatide are more plentiful in myelin sheath than in other biological membranes (Levine and Wetzell, 1993). Thus, the observed elevated lipid bands may originate from myelin sheaths in WM.

Since the attack by free radicals is the special subject of this investigation and the lipids are the most susceptible molecules to free radical damage, special emphasis

was put on the analysis of lipid composition and structure of WM in comparison to GM in this study. The lipid to protein ratio was decreased significantly in both WM ($p<0.01$) and GM ($p<0.05$) of the brain (Figure 3.8A and B). The decrease is more dramatic in the WM (Figure 3.8A). Because the data reported here are presented as ratios in order to prevent artifacts that will arise from any sample thickness variations, these results could indicate that the irradiated state possess either a lower lipid content and/or higher protein level (Wang *et al.*, 2005a; Toyran *et al.*, 2006). In addition, the CH_2/CH_3 ratio was applied to examine lipid content, where a lower ratio suggests shorter chained lipids and lower lipid content (Wang *et al.*, 2005a). In our study, ionizing radiation treated WM ($p<0.001$) and GM had a lower CH_2/CH_3 (Figure 3.10A and B). Moreover, it was found that the CH_2/lipid ratio was significantly decreased in irradiated WM ($p<0.05$) and GM ($p<0.05$) regions of the brain (Figure 3.12A and B) which shows shorter-chained lipids in the irradiated tissues. These results implied that the lower lipid/protein ratio in the irradiated tissue arises from decreased lipid content. The decrease in lipid content could be attributed to the disruption of lipid metabolism in the ionizing radiation treated brain tissue (Toyran *et al.*, 2006; Toyran *et al.*, 2007). Brain tissue has been reported to be highly susceptible to ROS damage due to its high level of oxidative metabolic activity, high level of PUFAs and metals (eg. iron) and low concentration of antioxidant enzymes such as GSH peroxidase, catalase (Floyd and Carney 1993; Zwart *et al.*, 1999). The data that have accumulated within the last decade clearly demonstrated that even very low-doses of radiation could result in cellular damage to the central nervous system (CNS) in contrast to the previous belief that only high doses of radiotherapy produce side effects in the CNS. Previous studies have shown that free radicals caused lipid peroxidation in the irradiated tissue (Samuni *et al.*, 1997; Zwart *et al.*, 1999; Hallivell and Chrigo, 1999; Dogan *et al.*, 2007a). Manda *et al.*, examined a wide variety of tissues such as brain, liver, spleen, kidney and testis after exposing the rats to the whole body radiation of 4 and 6 Gy and they found that among all the tissues, brain is the most susceptible to radiation-induced changes in lipid peroxidation (Manda *et al.*, 2007). When lipids are attacked by free radicals, a lipid

peroxidation chain reaction occurs. It is initiated by free radicals such as super oxide anion, hydrogen peroxide, singlet oxygen or hydroxyl radical abstracting a hydrogen atom from a methylene group in a lipid chain (Halliwell and Gutteridge, 1999; Krasowska *et al.*, 2001). The end results of this attack are broken chemical bonds, crosslinkages and conformational changes. As a consequence of the chain reactions, one free radical can cause the formation of many equivalents of lipid peroxides (secondary radicals). These degenerative reactions lead to degradation of lipids (Zwart *et al.*, 1999; Karbownik and Reiter, 2000). Consistent with these earlier studies, the lower lipid/protein, CH₂/CH₃ and CH₂/lipid ratios observed here suggests that ionizing radiation caused a decrease in the total content of lipid in the WM and GM regions of the brain, which would be predicted as a result of the long chain fatty acids become damaged by free radicals.

We also observed a significant increase in the carbonyl/lipid ratio in the irradiated WM ($p < 0.05$) and GM ($p < 0.05$) of the brain (Figure 3.16A and B). It has been demonstrated that peroxidation of lipids, which causes degradation of acyl chains into shorter pieces, is typically accompanied by the production of various degradation products such as carbonyl compounds and alkanes (Zwart *et al.*, 1999). Thus the higher carbonyl/lipid ratio that was detected in the irradiated group supports the results that lipids were being oxidized and as a result of this oxidation some degradation products which contains more carbonyl esters were being produced (Lamba *et al.*, 1991; Lamba *et al.*, 1994; Manda *et al.*, 2007). This was also confirmed by an increase in the methyl concentration in the irradiated WM and GM regions (Figure 3.14A and B). This result shows that the degradation products of lipids contain more methyl groups than normal lipids. Observations made in the present study in relation to the methyl contents are supported by other studies which are about the production of alkyl radicals during lipid peroxidation induced by different agents. For example, Sonia *et al.*, (2000) identified a methyl radical produced by tert-butyl hydroperoxide, which is a commonly used oxidative agent in the research of free radicals in biology, during lipid peroxidation process using EPR signal. In another study, lipid alkyl radicals generated from PUFAs via chemical or

enzymatic H-abstracting was quantified (Koshiishi *et al.*, 2005). As argued above, the mechanism of radiation-induced lipid peroxidation involves free radicals that are able to abstract a double allylic hydrogen from the acyl chain of PUFAs (Khouw *et al.*, 1993). The abstraction reaction results in an alkyl radical that rearranges to form the conjugated diene, and reacts with molecular oxygen to produce the peroxy radical. The peroxy radical, in turn, is able to propagate reaction by abstracting a hydrogen from another acyl chain to produce the lipid hydroperoxide and another alkyl radical (Khouw *et al.*, 1993).

The intensity/area of olefinic=CH band gives information about the unsaturation level of the system (Kneipp *et al.*, 2000; Severcan *et al.*, 2005; Ozek *et al.*, 2009). An increase in the olefinic=CH to lipid ratio in the WM ($p < 0.05$) and GM of irradiated group (Figure 3.18A and B) with respect to the control group suggests that ionizing radiation may induce an increase in the concentration of unsaturated fatty acids of the brain. As described above, lipid peroxidation occurs primarily at double bond sites of polyunsaturated acyl chains (Khouw *et al.*, 1993; Zwart *et al.*, 1999) and it results in the loss of olefinic bonds (Sills *et al.*, 1994; Moore *et al.*, 1995). However, in this study, instead of observing a decrease in the olefinic content, we observed an increase in both WM and GM of the irradiated brain. This result may indicate that loss of unsaturation during lipid peroxidation reactions was compensated by the presence of double bonds in the lipid peroxidation end-products such as MDA, lipid aldehydes, and alkyl radicals. Therefore, the increase in the amount of olefinic group in the irradiated brain might be the results of the accumulation of end products of lipid peroxidation as suggested by other studies (Liu *et al.*, 2002; Severcan *et al.*, 2005). For example, the content of double bonds in diabetic patients' platelets were observed to be increased suggesting a higher lipid peroxidation in these platelets (Liu *et al.*, 2002). In the other study, an increase in the area of the olefinic=CH band of diabetic rat liver microsomal membranes was reported (Severcan *et al.*, 2005) and these double bonds were attributed to lipid peroxidation end-products, such as MDA (Liu *et al.*, 2002; Severcan *et al.*, 2005). Consequently, the significant decreases in the total lipid amount, CH₂ groups of lipids, and the significant increases in the

carbonyl ester, olefinic=CH, and CH₃ groups are mainly the results of lipid peroxidation in the ionizing radiation treated brain tissues. Ionizing radiation caused degradation of lipids into smaller fragments which contain less CH₂ and more carbonyl, olefinic=CH, CH₃ groups, e.g. lipid peroxidation end products (Zwart *et al.*, 1999; Lamba *et al.*, 1991; Lamba *et al.*, 1994; Manda *et al.*, 2007). Because WM has higher lipid content than GM, the damaging effect of radiation appeared more dramatically in this part of the brain. Amifostine was found to inhibit the lipid peroxidation in the WM and GM implying its protective effect on these regions of the brain.

In recent years, there is an increasing experimental and theoretical evidence for the opinion that lipids are not the major objective of free radicals in biological tissues. Protein molecules in the tissue can also be affected by free radicals. To evaluate the alterations in protein composition and structure, the amide I/amide II ratio was calculated. A decrease in the ratio of the amide I/amide II for irradiated samples in comparison to the control was noticed in WM and GM (Figure 3.20). As the amide I and amide II profile depends on the protein structural composition, this reduction suggests that there are some alterations in the structure of proteins (Yu and Dasen, 2008; Ishida and Griffiths, 1993; Schmidt *et al.*, 2007). Consistent with our result, Dogan *et al.*, (2007a) observed a reduction in the amide I/amide II ratio after γ -irradiation in hazelnut tissue and they suggest that this reduction was associated with the changes in the protein structure. This explanation can be reliable since amide I arises predominantly from the C=O stretching vibration of the amide groups while the amide II band arises predominantly the N-H bending vibration (Haris and Severcan, 1999). Moreover, in a recent study it has been shown that compared with normal tissue, diseased tissue show a change in protein secondary structure and a reduced ratio of amide I to amide II (Szczerbowska-Boruchowska *et al.*, 2007). Thus, the decrease in the amide I/amide II ratio could be interpreted as the results of the altering the protein structure by ionizing radiation in both WM and GM regions of the brain. The changes in the protein structure might be associated with the effects of free radicals and may result in tissue damage. In addition, the results obtained from

the analysis of second derivative spectra supported this finding. The numerical comparison of the control and treated tissue revealed that ionizing radiation caused a dramatic increase in the turns and random coil structures (Figures 3.22 and 3.23). The increment in the random coil structures shows that ionizing radiation caused protein denaturation in the WM and GM regions of the brain. Our results are in consistent with Abu *et al.* (2006) who reported protein denaturation after γ -irradiation. Detectable alterations in the function and structure of proteins because of the action of free radicals have also been reported after ionizing radiation treatment (Jhun *et al.*, 1991, Samuni *et al.*, 1997). The results of the present study clearly showed that amifostine was effective in preventing the radiation-induced damage on the brain tissue proteins.

As seen from Table 3.3 and Figures 3.7-3.23 that the administration of amifostine without subsequent exposure to radiation didn't cause any significant changes on the WM and GM regions of the brain. It has been known that amifostine has limited entry to the CNS due to blood brain barrier (BBB) (Washburn *et al.*, 1974; Utley *et al.*, 1976). Consistent with these previous studies, our results suggest that amifostine could not penetrate into the brain due to BBB and, as a result, it didn't cause any significant effect on the molecules in the brain. However, the findings of the experiments demonstrated that the administration of amifostine before ionizing radiation prevented all the radiation induced variations by approaching the values near control levels in the WM and GM of the rat brain. With the administration of amifostine, significant decreases in the level of total lipid, CH₂ groups of lipids, Amide I/Amide II ratios, significant increases in the level of carbonyl esters, olefinic=CH and CH₃ groups and significant changes in the protein secondary structures caused by radiation could be suppressed. Although amifostine has limited access to the CNS, the drug appears promising for the brain tissue. Recently, it has been shown that radiation injury is not limited to the neurons of the CNS, glial cells and the cells of the vascular bed are also affected (Nieder *et al.*, 2004; Yildirim *et al.*, 2007). Vascular damage is one of the most important components in the development of CNS toxicity after radiotherapy. As a result of the damage of astrocytes and

vascular endothelial cells, the integrity of the blood-brain barrier is lost, thereby increasing microvascular permeability. Winkler (1957) showed that the exposure of forty-five rabbit heads to 4, 6 or 8 Gy X radiation produced a disturbance of the permeability of the BBB that returned to normal after 6 days. In addition, the disappearance of the BBB after radiation exposure has been reported by some previous studies (Schultheiss *et al.*, 1995; Belka *et al.*, 2001). The increased permeability of the BBB during ionizing radiation treatment might allow penetration of amifostine into the brain. In addition, several recent publications provide increasing evidence that amifostine might be able to protect blood vessels (Andreopoulos *et al.*, 1999; Grdina *et al.*, 2002b). Thus, despite the blood brain barrier amifostine seems to protect brain tissue because it protects blood vessels against radiation-induced damage and the increased permeability of BBB during radiation treatment might allow penetration of amifostine into the brain. Our results are in agreement with previous animal studies which used different approaches (McDonough *et al.*, 1992; Tabachnik, 1987). Guelman *et al.*, (2003) demonstrated cerebellar morphological damage and motor gait impairment induced by neonatal radiation treatment with a single dose of 5 Gy in rats and they have found that subcutaneously 100 mg/kg amifostine treatment 30 minutes prior to exposure partially prevented the development of this type neurotoxicity.

The protective action of amifostine may be associated with its antioxidant properties, as it possibly acts as a free radical scavenger that protects subcellular components (Denekamp *et al.*, 1982; Hall 2000). WR-1065, the dephosphorylated active form of amifostine, must be present at the time of radiation exposure (Grdina *et al.*, 2002a). Once inside the cell, WR-1065 can provide protection by several mechanisms. In some in vitro studies it has been demonstrated that WR-1065 was able to scavenge hydroxyl radicals and superoxide anions (Ohnishi *et al.*, 1992; Marzatico *et al.*, 2000). Using a pure chemical system, Ohnishi *et al.*, (1992) demonstrated that WR-1065 was able to scavenge hydroxyl radicals and superoxide anions. In 2000, Marzatico *et al.*, (2000) confirmed that scavenging activity of amifostine against hydroxyl radicals. In addition to the scavenging free radicals, several additional

mechanisms have been proposed for the radioprotective effects of amifostine. These include induction of hypoxia by reacting directly with oxygen (Durand and Olive, 1989), hydrogen donation to repair ROS in target molecules (Durand, 1983), target stabilization by binding to DNA (Savoye *et al.*, 1997) and the protection of key sulfhydryl enzymes through formation of protein-amino thiol mixed disulphides (Hospers *et al.*, 1999).

4.2 The Effects of Ionizing Radiation and Amifostine on Rat Liver Microsomal Membranes

FTIR spectroscopy monitors the changes in the structure, conformation and function of proteins and lipids, simultaneously, in cellular membranes without introducing foreign perturbing probes into the system (Lewis *et al.*, 1989; Moore *et al.*, 1995; Toyran *et al.*, 2004; Toyran *et al.*, 2005; Severcan *et al.*, 2005; Akkas *et al.*, 2007). Taking advantages of this property of the technique, this part of the thesis was conducted to determine the effects of ionizing radiation on the structure, composition and dynamics of rat liver microsomal membranes and to investigate the protective effects of amifostine against radiation-induced damages by monitoring the changes in the band area ratios, peak frequency, bandwidth, intensity of main FTIR absorptions arising from lipids and proteins.

A significant decrease in the lipid to protein ratio was observed in irradiated group (Figure 3.26). This decrease could be attributed to a lower lipid content or higher protein level (Wang *et al.*, 2005a; Toyran *et al.*, 2006) and shows that there is an alteration in the protein and lipid metabolism caused by ionizing radiation. It has been reported that the decrease observed in the lipid to protein ratio initiates changes in membrane fluidity altering the membrane potential via ion channel kinetics (Awayda *et al.*, 2004; Akkas *et al.*, 2007)

The examination of the ratios of some specific lipid functional groups (CH₂, carbonyl ester, CH₃, olefinic=CH) to the total lipid demonstrated that ionizing radiation induced important changes in the composition and structure of membrane lipids

(Figures 3.27 and 3.28). With the special sensitivity of polyunsaturated fatty acids, biological membranes are highly susceptible to ROS attack (Reiter, 1995, Zwart *et al.*, 1999). Previous reports on model membranes have shown that radiation yields oxidation fragments of unsaturated acyl chains (Tait and Bors, 1985; Yukawa *et al.*, 1985). Consistent with these earlier studies, the lower CH₂/total lipid ratio and the higher carbonyl ester/total lipid ratios observed in the irradiated group suggest that lipids were degraded by free radicals into smaller degradation products which contain less CH₂ and more carbonyl esters. These results were supported by some previous studies where an increase in carbonyl groups and a breakdown of lipid acyl chains were detected in vitro using FTIR spectroscopy after lipid peroxidation (Lamba *et al.*, 1991; Lamba *et al.*, 1994). Since free radicals can also oxidize to the membrane proteins and the oxidation of proteins causes the production of some additional carbonyls that may contribute to the increase in the carbonyl ester/total lipid ratio (Stadman, 1990; Manda *et al.*, 2007). Moreover, the breakdown of lipid acyl chains after irradiation was confirmed by an increase in CH₃/total lipid ratio which shows that the degradation products of lipids contain more methyl groups than regular membrane lipids. In addition, we found that the unsaturated lipid/saturated lipid ratio was significantly increased in the irradiated microsomes. This increase could indicate a higher lipid peroxidation in the irradiated microsomal membranes since the increase in the olefinic content mainly originate from the lipid peroxidation end-products such as MDA, alkyl radicals and lipid aldehydes (Liu *et al.*, 2002; Severcan *et al.*, 2005). Consequently, the lower CH₂/total lipid ratio and the higher carbonyl ester/total lipid, CH₃/total lipid and unsaturated lipid/saturated lipid ratios suggest that membrane lipids were oxidized by ionizing radiation and as a result of this oxidation some degradation products which contain less CH₂ group and more carbonyl esters, CH₃ and unsaturated fatty acids were produced. Thus, it is possible to deduce that there is a significant increase in peroxidative process in the liver due to radiation treatment. The pattern of chemical changes obtained from the analysis of the lipid bands suggest that lipid peroxidation is a mechanism by which radiation damage has occurred in liver microsomal membranes. It was clearly observed that

amifostine was very successful to protect the microsomal membrane lipids from peroxidation damage induced by ionizing radiation.

Exposure of biological membranes to ionizing radiation also seriously damages intrinsic proteins (Gebicki *et al.*, 2000). It was found that the protein conformation was also affected from ionizing radiation since a broadening in the bandwidth of amide I band and a shifting in the frequency of this band to higher values were observed (Figure 3.30) (Cakmak *et al.*, 2006). In a previous study, protein oxidation was found to broaden the amide I band (Signorini *et al.*, 1995). As noted above, protein oxidation results in the production of some additional carbonyls on some aminoacid residues (Stadtman, 1990). It has been suggested that some of these carbonyls reside adjacent to amines and lead to a spectroscopic absorption and a broadening in the amide I band (Signorini *et al.*, 1995; Stadtman, 1990). In addition, a decrease observed in the ratio of amide I/amide II for irradiated samples suggesting some alterations in the structure of membrane proteins (Figure 3.29) (Yu and Dasen, 2008; Ishida and Griffiths 1993; Schmidt *et al.*, 2007; Dogan *et al.*, 2007a). Thus, the decrease in the amide I/amide II ratio, the broadening and shifting of the amide I band to higher values could be interpreted as the results of the altering the protein composition, structure and conformation of the irradiated liver microsomal membranes. The results obtained from the analysis of second derivative spectra supported this finding. Ionizing radiation caused a dramatic decrease in α -helix and β -sheet structures and a dramatic increase in the turns and random coil structures (Figure 3.32). The increase in the random coil structure indicates that ionizing radiation caused protein denaturation in the system (Dogan *et al.*, 2007a). Our results are in agreement with earlier studies that reported a decrease in α -helix structure after radiation exposure (Lee and Song 2003; Ciesla *et al.*, 2004, Torreggiani *et al.*, 2005, Dogan *et al.*, 2007a). Moreover, Abu *et al.* (2006), reported protein denaturation due to γ -irradiation which also supports our findings. A metabolic disruption of some aminoacids could occur after radiation treatment in liver microsomes and could be responsible for the observed variations in the proteins

(Jhun *et al.*, 1991, Samuni *et al.*, 1997). It is known that free radicals lead to protein degradation by increasing accessibility of protein bonds and/or aggregation (Davies, 1987). In a previous study, it has been reported that radiation causes an alteration in the conformation of membrane integral proteins and radiation induced hydroxyl radicals that lead to denaturation of membrane proteins (Perromat *et al.*, 2003). On the other hand, relationships between lipid peroxidation and damage to protein synthesis have been previously reported in liver slices from rats (Fraga *et al.*, 1989). The results of the current study again indicated that amifostine was effective in preventing the radiation-induced damage on the liver microsomal membrane proteins.

Lipids play a key role in the membrane fluidity and they govern exposure and diffusion of membrane components by affecting the conformation of membrane proteins (Liu *et al.*, 2002). Liver microsomes contain cholesterol and great variety of phospholipids in a high concentration. The fatty acid composition of the bulk lipids of rat liver microsomes is so highly unsaturated and therefore they are very fluid at physiological temperatures (Catala, 1993). Our data obtained from the frequency and bandwidth analysis of the CH₂ asymmetric stretching band clearly revealed that ionizing radiation caused an increase in the lipid order and a decrease in the membrane fluidity in the microsomal membranes (Figure 3.33). Studies in a wide variety of membranes have demonstrated that free radicals produced by ionizing radiation disturb the order and lipid dynamics of the membrane (Curtis *et al.*, 1984; Watanabe *et al.*, 1990; Dinis *et al.*, 1993). Loss of freedom of motion in membranes after oxidative stress was reported using biological and liposomal membranes (Dobretsov *et al.*, 1977; Curtis *et al.*, 1984; Chen and Yu, 1994) and lipid peroxidative stress is known to decrease membrane fluidity in microsomes and other cellular membranes (Garcia *et al.*, 2001; Karbownik *et al.*, 2000; Berroud *et al.*, 1996). An important factor affecting the membrane structure and dynamics is the amount of proteins and lipids in the membranes (Szalontai *et al.*, 2000). Two important reasons could be proposed as causal relationships of the loss of membrane fluidity during ionizing radiation treatment. First, as mentioned before, radiation may

cause the cholesterologenesis and due to increased amount of cholesterol, a decrease in membrane fluidity may be observed; second, the formation of cross linking among the lipid-lipid and protein-lipid moieties as a result of oxidative stress may limit motion (Curtis *et al.*, 1984, Chen and Yu, 1994; Garcia *et al.*, 1999). The shifting in the frequency of CH₃ asymmetric stretching band to lower values revealed that the librational freedom of the acyl chains of the phospholipids decreased in the central area of the bilayer of irradiated liver microsomal membranes (Figure 3.34A). The examination of the change in the frequency of PO₂⁻ asymmetric stretching band showed that ionizing radiation caused an increase in the hydrogen bonding in the head group of the phospholipids (Figure 3.34B) (Akkas *et al.*, 2007; Severcan *et al.*, 2005). The hydrogen bonding might be between water molecules and the oxygen molecules of phosphate groups of phospholipids (Akkas *et al.*, 2007). This may create a difference in packing of phospholipid molecules (Cakmak *et al.*, 2006). The alterations in the packing of phospholipids have been reported to originate from the reaction between free radicals and membrane proteins or lipids, which may increase a cross-linking between these membrane components (Phillis *et al.*, 2006). Thus, the results obtained the frequency analysis of CH₃ asymmetric and PO₂⁻ asymmetric stretching bands support the frequency decrease of the CH₂ asymmetric stretching band which suggests ionizing radiation ordered the liver microsomal membranes. Amifostine protected microsomal membranes against the rigidity induced by ionizing radiation.

In this study, amifostine was given alone in the absence of ionizing radiation, in order to gain insight on the molecular mode of interaction of amifostine with microsomal membranes. It is clearly seen from the Table 3.5, 3.6 and Figures 3.25-3.34 that amifostine administration without following exposure to radiation didn't induce any significant changes on the structure, composition and dynamics of rat liver microsomal membranes. Such a finding highlights that amifostine does not interact with membrane molecules and is non-toxic for liver microsomal membranes. Thus this result supports the usage of amifostine as a radioprotectant agent in radiotherapy.

On the other hand, it is also clearly seen from the Tables 3.5, 3.6 and Figures 3.25-3.34 that ionizing radiation induced alterations in the parameters of structure, composition and dynamics of the microsomal membranes tend to be approached near to the control values in the amifostine treated + irradiated group so that the differences in these parameters between these two experimental groups (control and amifostine treated + irradiated groups) are no longer statistically significant. These findings suggest that when amifostine was given to the rats before ionizing radiation, all the damages induced by radiation on membrane lipids and proteins were prevented by amifostine. It has been known that amifostine uptake is greatest in the liver, kidney, salivary glands, intestinal mucosa and lung in the body (Grdina *et al.*, 2002a). In addition, Levi *et al.*, (2002) revealed that approximately 90% of the drug was extracted by the liver (ie. converted to WR-1065) in dogs, suggesting that the liver may preferentially take up the active free thiol. So it can be hypothesized that organs with high amifostine uptake and extraction would have a high activation rate of amifostine to WR-1065 and, thus would be protected by amifostine. Our findings are supported by previous animal studies which used different methodology and modality. Uguzalp-Kaldir *et al.*, (2007) has demonstrated a decrease of histopathologic changes with amifostine administration against radiation induced late damage (6 month later) in liver. Jirtle *et al.* (1985), demonstrated that systemic administration of amifostine protects irradiated hepatocytes from cell death and that the liver is protected from radiation fibrosis by amifostine (Jirtle *et al.*, 1990). Symon *et al.*, (2001) have evaluated whether systemic or portal venous administration of amifostine could protect liver from the effects of radiation using micronucleus assay. They found that either systemic or portal venous administration of amifostine effectively protected hepatocytes from ionizing radiation without compromising tumor cell kill in a rat liver tumor model (Symon *et al.*, 2001).

CHAPTER 5

CONCLUSION

The first part of the study has investigated the effects of ionizing radiation and the radioprotectant amifostine on the different regions of rat brain -- namely WM and GM -- using FTIRM and SR-FTIRM without disruption of cell and tissue morphology. Specifically, the results of this part revealed that the total lipid content and CH_2 groups of lipids decreased significantly and the carbonyl esters, olefinic=CH and CH_3 groups of lipids increased significantly in the WM and GM after exposure to ionizing radiation. These results demonstrated that ionizing radiation caused degradation of lipids into smaller fragments which contain less CH_2 and more carbonyl, olefinic=CH, CH_3 groups, e.g. lipid peroxidation end products. The changes were more prominent in the WM of the brain because WM has higher lipid content than GM. In addition, it was found that the protein composition and structure were also altered by ionizing radiation. Amifostine administration to the rats prior to whole body irradiation caused significant protective effect against all the radiation-induced damages observed in the WM and GM regions of the brain.

In the second part of the study, the effects of ionizing radiation and amifostine on the structure, composition and dynamics of rat liver microsomal membranes have been investigated using FTIR spectroscopy. The results revealed that radiation induced significant alterations in the composition and structure of microsomal lipids. In detail, CH_2 groups of lipids decreased significantly and the carbonyl esters, olefinic=CH, and CH_3 groups of lipids increased significantly after exposure to ionizing radiation.

All these results could be interpreted as a result of lipid peroxidation in the microsomal system. In addition, ionizing radiation caused dramatic increases in lipid order and in the hydrogen bonding of the head group of phospholipids and significant decreases in the membrane dynamics and in the librational freedom of acyl chains. Moreover, the composition and secondary structure of proteins were altered by ionizing radiation. Radiation caused a decrease in the α -helical and β -sheet structures and an increase in the turns and random coil structures implying protein denaturation after irradiation. Amifostine caused significant protective effect against the radiation-induced damages on microsomal membrane lipids and proteins.

The comparison of the results of the brain tissue and those of the liver microsomal membrane in terms of the damage induced by ionizing radiation suggests that there are similar results with slightly higher significance values in the WM region of the brain. Hence, this result might indicate that the higher lipid content of the WM region of the brain make it vulnerable to free radical damage induced by ionizing radiation.

The administration of amifostine without subsequent exposure to radiation didn't induce any significant changes on the WM and GM regions of the brain and on the structure, composition and dynamics of rat liver microsomal membranes. The insignificant results might be related to the fact that there was no severe complication of amifostine treatment in the tissue and membrane samples. This finding highlights that amifostine is non-toxic for the body and supports the usage of amifostine as a radioprotectant agent in radiotherapy.

In conclusion, the overall results suggest that whole body irradiation of rat leads to some important changes on the brain tissues and liver microsomal membranes and amifostine has protective effects on these systems. The protective effect of amifostine may be related to its free radical scavenger activity. We suggest that maintaining membrane fluidity against the rigidity effect of ionizing radiation may be another cytoprotective mechanism of amifostine.

Since humans can be exposed to different sources of radiation such as therapeutic, diagnostic, and accidental, the radiation model created in this study has high clinical importance. This study has produced new data that amifostine effectively protects brain tissue and liver microsomal membranes by preventing lipid and protein molecules from the damage induced by ionizing radiation.

In addition, the current study indicated that FTIR spectroscopy together with FTIR microspectroscopy and SR-FTIR microspectroscopy provides a rapid and sensitive monitoring of ionizing radiation-induced damage in biological tissues and membranes and FTIR parameters employed in this study can be used as a biological indicator of radiation-induced damage in biological systems.

REFERENCES

- Abou-Seif, M. A. M., El-Naggar, M. M., El-Far, M., Ramadan, M., Salah, N. (2003). Amelioration of radiation-induced oxidative stress and biochemical alteration by sod model compounds in pre-treated g-irradiated rats. *Clin. Chim. Acta*, **337**: 23–33.
- Abu, J. O., Muller, K., Duodu, K. G., Minnaar, A. (2006). Gamma irradiation of cowpea (*Vigna unguiculata* L. Walp) flours and pastes: Effects on functional, thermal and molecular properties of isolated proteins. *Food Chem.*, **95**: 138–147.
- Akkas, S. B., Inci, S., Zorlu, F., Severcan F. (2007). Melatonin affects the order, dynamics and hydration of brain membrane lipids. *J Mol Struct*, **834–836**: 207–215.
- Alberts, B., Johnson, A., Lewis, J., Raff, M., Roberts, K., Walter, P. (2002). *Molecular Biology of the Cell*. 4 edn. New York: Garland Science.
- Anand, A. J., Bashey, B. (1993). Newer insights into cisplatin nephrotoxicity. *Ann Pharmacother*, **27**: 1519.
- Andreassen, C. N., Grau, C., Lindegaard, J.C. (2003). Chemical radioprotection: A critical review of amifostine as a cytoprotector in radiotherapy. *Semin. Radiat. Oncol.*, **13**: 62–72.
- Andreopoulos, D., Schleicher, U.M., Cotarelo, C.L., Hand, S., Ammon, J. (1999). Radioprotection of human endothelial cells with amifostine. *Strahlenther Onkol*, **175**: 34–36.
- Arora, R. (2008). *Herbal Radiomodulators-applications in Medicine, Homeland, Defence and Space*. London, UK: CAB International.
- Arrondo, J. L. R., Muga A., Castresa, J., and Goni, F. M. (1993). Quantitative studies of the structure of proteins in solution by fourier transform infrared spectroscopy. *Progress. Biophys. Acta.*, **468**: 63–72.
- Atalay, H., Aybek, H., Koseoglu, V., Demir, S., Erbay, H., Bolaman, A. Z., Avci, A. (2006). The effects of amifostine and dexamethasone on brain tissue lipid

- peroxidation during oxygen treatment of carbon monoxide-poisoned rats. *Advances in Therapy*, **23**: 332-341.
- Awayda, M. S., Shao W., Guo F., Zeidel M., Hill, W.G. (2004). Enac-membrane interactions: Regulation of channel activity by membrane order. *J. Gen. Physiol.*, **123**: 709–27.
- Barth, A. (2000). The infrared absorption of amino acid side chains. *Progress in Biophysics & Molecular Biology*, **74**: 141–173.
- Bartosz, G., Schon, W., Kraft, G., Gartner, H. (1992). Irradiation increases proteolysis in erythrocyte ghosts: A spin label study. *Radiat. Environ. Biophys.*, **31**: 117–121.
- Beaten, V., Hourant, P., Morales, M. T. And Aparicio, R. (1998). Oil and fat classification by ft-raman spectroscopy. *J Agric Food Chem* **46**: 2638-2646.
- Becker, W. M., Kleinsmith, L. J., Hardin, J. (2002). *World of cell*. Benjamin Cummings Edition.
- Belka, C., Budach, W., Kortmann, R. D., Bamberg, M. (2001). Radiation induced cns toxicity-molecular and cellular mechanisms. *Br. J. Cancer*, **85**: 1233-1239.
- Berroud, A., Le Roy, A., Voisin, P. (1996). Membrane oxidative damage induced by ionizing radiation detected by fluorescence polarization. *Radiat. Environ. Biophys*, **35**: 289–295.
- Bonnefont-Rousselot, D., Motta, C., Khalil, A. O., Sola, R., La Ville, A. E., Delattre, J., Gardea S-Albert, M. (1995). Physicochemical changes in human high-density lipoproteins (hdl) oxidized by gamma radiolysis-generated oxyradicals. Effect on their cholesterol effluxing capacity. *Biochim. Biophys. Acta*, **1255**: 23–30.
- Bonner, H. S., Shaw L.M. (2002). New dosing regimens for amifostine: A pilot study to compare the relative bioavailability of oral and subcutaneous administration with intravenous infusion. *J Clin Pharmacol*, **42**: 166-174.
- Bozkurt, O., Bilgin, M.D., Severcan, F. (2007). The effect of diabetes mellitus on rat skeletal extensor digitorum longus muscle tissue: An FTIR study. *Spectroscopy-An Int J*, **21**: 151–160.
- Brizel, D. M., Wasserman, T.H., Henke, M. (2000). Phase III randomized trial of amifostine as a radioprotector in head and neck cancer. *J Clin Oncol*, **18**: 3339-3345.

- Budd, G. T. (1996). Amifostine and chemotherapy-related thrombocytopenia. *Semin Oncol.*, **23**: 49.
- Cadet, J., Delatour, T., Douki, T., Gasparutto, D., Pouget, J. P., Ravanat, J. L., Sauvaigo, S. (1999). Hydroxyl radicals and DNA base damage. *Mutation Research*, **424**: 9–21.
- Cakmak, G., Togan, I., Severcan, F. (2006). 17 β -estradiol induced compositional, structural and functional changes in rainbow trout liver, revealed by FTIR spectroscopy: A comparative study with nonylphenol. *Aquat. Toxicol.*, **77**: 53–63.
- Cakmak, G., Uğuz, C., Togan, I., Severcan, F. (2003). FT-IR spectroscopic analysis of rainbow trout liver exposed to nonylphenol. *Appl. Spectrosc.*, **57**: 835–841.
- Campbell, I. D., Dwek, R. A. (1984). *Biological spectroscopy*. USA: Benjamin/Cummings Publishing Company.
- Capizzi, R. L. (1999). The preclinical basis for broad-spectrum selective cytoprotection of normal tissues from cytotoxic therapies by amifostine. *Seminars in Oncology*, **26**: 3–21.
- Casarett, A. P. (1968). *Radiation biology*. NY: American Institute of Biological Sciences and US Atomic Energy Commission.
- Cassatt, D. R., Fazenbaker, C.A., Bachy, C.M., Hanson, M.S. (2002). Preclinical modeling of improved amifostine (ethiol) use in radiation therapy. *Semin. Radiat. Oncol.*, **12**: 97–102.
- Castiglione, F., Porcile, G., Gridelli, C. (2000). The potential role of amifostine in the treatment of non small cell lung cancer. *Lung Cancer*, **29**: 57–66.
- Catala, A. (1993). Interaction of fatty acids, acyl-coa derivatives and retinoids with microsomal membranes: Effect of cytosolic proteins. *Mol. Cell. Biochem.*, **120**: 89–94.
- Chan, K. L., Kazarian, S.G., Mavraki, A. (2005). Williams, fourier transform infrared imaging of human hair with a high spatial resolution without the use of a synchrotron. *Appl. Spectrosc.*, **59**: 149–155.
- Chen, J. J., Yu, B. P. (1994). Alterations in mitochondrial membrane fluidity by lipid peroxidation products. *Free Radical Biol. Med.*, **17**: 411–418.
- Chen, T., Lee, M. J., Kim, Y. S., Lee, S., Kummar, S., Gutierrez, M., Hewitt, S. M., Trepel, J. B., Levin, I. W. (2008). Pharmacodynamic assessment of histone deacetylase inhibitors: Infrared vibrational spectroscopic imaging of protein acetylation. *Anal Chem.*, **80**: 6390–6396.

- Chiriboga, L., Xie P., Yee H., Vigorita V., Zarou D., Zakim D., Diem M. (1998). Infrared spectroscopy of human tissue. I. Differentiation and maturation of epithelial cells in the human cervix. *Biospectroscopy*, **4**(1): 47-53.
- Choo, L. P., Wetzel D. L., Halliday W. C., Jackson M , Levine S. M., Mantsch H. H. (1996). In situ characterization of beta-amyloid in alzheimer's diseased tissue by synchrotron fourier transform infrared microspectroscopy. *Biophys. J.*, **71**(4): 1672-9.
- Choudhary, D., Srivastava, M., Sarma, A., Kale, R. K. (1998). Effect of high linear energy transfer radiation on biological membranes. *Radiat. Environ. Biophys.*, **37**: 177–185.
- Ci, Y. X., Gao, T.Y., Feng, J., Guo, Z.Q. (1999). FTIR spectroscopic characterization of human breast tissue: Implications for breast cancer diagnosis. *Appl. Spectrosc.*, **53**: 312–315.
- Ciesla, K., Salmieri, S., Lacroix, M., Le Tien, C. (2004). Gamma irradiation influence on physical properties of milk proteins. *Radiat. Phys. Chem.*, **71**: 93–97.
- Colthup, N. B., Daly, L. H. And Wiberley, S. E. (1975). *Introduction to Infrared and Raman Spectroscopy*. New York: Academic Press.
- Curtis, M. T., Gilfor, D., and Farber, J. L. (1984). Lipid peroxidation increases the molecular order of microsomal membranes. *Arch. Biochem. Biophys.*, **35**: 644–649.
- Davies, K. J. (1987). Protein damage and degradation by oxygen radicals. I. General aspects. *J. Biol. Chem.*, **262**: 9895 – 9901.
- Denekamp, J., Michael, B.D., Rojas, A. (1982). Radioprotection of mouse skin by WR-2721: The critical influence of oxygen tension. *Int. J. Radiat. Oncol. Biol. Phys.*, **8**: 531-534.
- Dicko, A., Morissette, M., Ameer, S.B., Pezolet, M., Paolo, T. (1999). Effect of estradiol and tamoxifen on brain membranes: Investigation by infrared and fluorescence spectroscopy. *Brain Res. Bull.*, **49**: 401–405.
- Diem, M., Chiriboga L., Lasch P., Pacifico A. (2002). IR spectra and IR spectral maps of individual normal and cancerous cells. *Biopolymers* **67**(4-5): 349-53.
- Dinis, T. C. P., Almeida, L. M., Madeira, V. M. C. (1993). Lipid peroxidation in sarcoplasmic reticulum membranes: Effect on functional and biophysical properties. *Arch. Biochem. Biophys.*, **301**: 256–264.

- Dobretsov, G. E., Borschevskaya, T. A., Petrov, V. A., Vladimirov, Y. A. (1977). *FEBS Lett.*, **84**: 125–128.
- Dogan, A., Siyakus, G., Severcan, F. (2007a). FTIR spectroscopic characterization of irradiated hazelnut (*corylus avellana*). *Food Chem.*, **100**: 1106–1114.
- Dogan, A., Ergen, K., Budak, F., & Severcan, F. (2007b). Evaluation of disseminated candidiasis on an experimental animal model: A fourier transform infrared study. *Appl. Spectrosc.*, **61**(2): 199–203.
- Dorr, R. T. (1996). Cytoprotective agents for anthracyclines. *Semin Oncol.*, **23**[Suppl 8]: 23.
- Dumas, P., Miller, L. (2003). The use of synchrotron infrared microspectroscopy in biological and biomedical investigations. *Vibr. Spectrosc.*, **32**: 3–21.
- Dumas, P., Sockalingum, G. D., Sule´-Suso, J. (2006). Adding synchrotron radiation to infrared microspectroscopy: What’s new in biomedical applications? *TRENDS in Biotechnology*, **25**(1): 40-44.
- Dunne-Daly, C. F. (1999). Principles of radiotherapy and radiobiology. *Seminars in Oncology Nursing*, **15**: 250-259.
- Durand, R. E. (1983). Radioprotection by WR-2721 in vitro at low oxygen tensions: Implications for its mechanisms of action. *Brit. J. Cancer*, **47**: 387-392.
- Durand, R. E., Olive, P.L. (1989). Radiosensitization and radioprotection by BSO and WR-2721: The role of oxygenation. *Brit. J. Cancer* **60**: 517-522.
- Elia, M. C., Deluca, J. G., Bradley, M. O. (1991). Significance and measurement of DNA double strand breaks in mammalian cells. *Pharmacol Ther.*, **51**: 291-327.
- Fabian, H., Jackson, M., Murphy, L., Watson, P. H., Fichtner, I., Mantsch, H. H. (1995). A comparative infrared spectroscopic study of human breast tumors and breast tumor cell xenografts. *Biospectroscopy*, **1**: 37–46.
- Felckenstein, L., Swynnerton N. F., Ludden T. M., Mangold D. J. (1988). Bioavailability and newer methods of delivery of phosphorothioate radioprotectors. *Pharmac Ther*, **39**: 203-212.
- Floyd, R. A., Carney, J.M. (1993). The role of metal ions in oxidative processes and aging. *Toxicol. Indust. Health*, **9**: 197-214.
- Foster-Nora, J. A., Siden R. (1997). Amifostine for protection from antineoplastic drug toxicity. *Am J Health Syst Pharm*, **54**: 787–800.

- Foucher, C., Narce, M., Nasr, L., Delachambre, M. C., Poisson, J. P. (1997). Liver microsomal membrane fluidity and microsomal desaturase activities in adult spontaneously hypertensive rats. *Journal of Hypertension*, **15**, 8: 863-869.
- Fraga, C. G., Zamora, R., Tappel, A. L. (1989). *Arch. Biochem. Biophys.*, **270**: 84–91.
- Freifelder, D. (1982). *Applications to Biochemistry and Molecular Biology*. New York: Freeman, W.H. and Company.
- Gallant, M., Rak M., Szeghalmi A., Del Bigio M. R., Westaway D., Yang, J., Julian, R., Gough, K. M. (2006). Focally elevated creatine detected in amyloid precursor protein (app) transgenic mice and alzheimer disease brain tissue. *J. Biol. Chem.*, **281**: 5–8.
- Gandhi, N. M., Gopalaswamy, U., V., Nair, C. K. K. (2004). Radiation protection by diethyldithiocarbamate: Protection of membrane and DNA *in vitro* and *in vivo* against γ -radiation. *J. Radiant. Res.*, **45**: 175-180.
- Garcia, J. J., Reiter, R. J., Karbownik, M., Calvo, J. R., Ortiz, G. G., Tan, D. X., Martinez-Ballarín, E., Acuña-Castroviejo D. (2001). N-acetylserotonin suppresses hepatic microsomal membrane rigidity associated with lipid peroxidation. *Eur. J. Pharmacol.*, **428**: 169–175.
- Garcia, J. J., Reiter, R. J., Pié J., Ortiz, G. G., Cabrera, J. J., Sáinz, R. M., Acuña-Castroviejo, D. J. (1999). *Bioenerg. Biomembr.*, **31**: 609-616.
- Garcia, J. J., Reiter, R.J., Guerrero, J.M., Escames, G., Yu, B.P., Oh, C.S., Munoz-Hoyos A. (1997). Melatonin prevents changes in microsomal membrane fluidity during induced lipid peroxidation. *FEBS Lett.*, **408**: 297-300.
- Garg, M. L., McMurchi E. J., Sabine, J. R. (1985). Membrane homeostasis: Thermotropic behaviour of microsomal membrane lipids isolated from livers of rats fed cholesterol-supplement diets. *Biochem Int.*, **11**: 677-86.
- Garip, S., Bozoglu, F., Severcan, F. (2007). Differentiation of mesophilic and thermophilic bacteria with fourier transform infrared spectroscopy. *Appl. Spectrosc.*, **61**(2): 186–192.
- Gebicki, J. M., Du, J., Collins, J., Tweeddale, H. (2000). Peroxidation of proteins and lipids in suspensions of liposomes, in blood serum, and in mouse myeloma cells. *Acta Biochim Pol.*, **47**(4): 901-11.
- Grdina, D. J., Murley, J.S. And Kataoka, Y. (2002a). Radioprotectants: Current status and new directions. *Oncology*, **63**: 2– 10.

- Grdina, D. J., Murley, J.S., Kataoka, Y. And Calvin, D.P. (2002b). Differential activation of nuclear transcription factor kappaB, gene expression, and proteins by amifostine's free thiol in human microvascular endothelial and glioma cells. *Semin. Radiat. Oncol.*, **12**: 103–111.
- Griffiths, P. R., De Haseth, J. A. (1986). *Fourier transform infrared spectrometry*. New York: Wiley.
- Grochova, D., Smardova, J. (2007). The antimutagenic and cytoprotective effects of amifostine: The role of p53. *J. Appl. Biomed.*, **5**: 171–178.
- Guelman, L. R., Zorrilla Zubilete, M.A., Rios, H. And Zieher, L.M. (2003). WR-2721 (amifostine, ethiol®) prevents motor and morphological changes induced by neonatal x-irradiation. *Neurochem. Int.*, **42**: 385–391.
- Gwozdziński, K. (1991). Ionizing radiation-induced structural modification of human red blood cells. *Radiation and Environmental Biophysics*, **30**: 45–52.
- Hall, E. J. (2000). *Radioprotectors. Radiobiology for the Radiologist*. Philadelphia, PA: Lippincott.
- Halliwell, B., Gutteridge, J. M. C. (1999). *Free Radicals in Biology and Medicine*. Oxford: University Press.
- Haris, P. I., Severcan, F. (1999). FTIR spectroscopic characterization of protein structure in aqueous and non-aqueous media. *J. Mol. Catal. B: Enzym.*, **7**: 207–221.
- Heinemann, F. S., Ozols, J. (1998). Isolation and structural analysis of microsomal membrane proteins. *Frontiers in Bioscience*, **3**: 483-493.
- Hensley, M. L., Schuchter, L. M., Lindley, C. (1999). American society of clinical oncology clinical practice guidelines for the use of chemotherapy and radiotherapy protectants. *J. Clin. Oncol.*, **17**: 3333-3355.
- Heraud, P., Caine, S., Campanale, N., Karnezis, T., McNaughton, D., Wood, B. R., Tobin, M. J. And Bernard, C.C.A. (2010). Early detection of the chemical changes occurring during the induction and prevention of autoimmune-mediated demyelination detected by FT-IR imaging. *Neuroimage*, **49**: 1180–1189.
- Herscher, L. L., Cook, J. A., Pacelli, R., Pass, H. I., Russo, A., Mitchell, J. B. (1999). Principles of chemoradiation: Theoretical and practical considerations. *Oncology*, **13**: 11-22.
- Holman, H. Y. N., Martin, M. C., Blakely, E. A., Bjornstad, K., McKinney, W. R. (2000a). IR spectroscopic characteristics of cell cycle and cell death probed

by synchrotron radiation based fourier transform IR spectromicroscopy. *Biopolymers* **57**: 329–335.

Holman, H. N., Goth-Goldstein, R., Blakely, E. A., Bjornstad, K., Martin, M. C., Mckinney, W. R. (2000b). Individual human cell responses to low doses of chemicals studied by synchrotron infrared spectromicroscopy. In *Biomedical Spectroscopy: Vibrational Spectroscopy and Other Novel Techniques*, Anita Mahadevan- 57 Jansen, Gerwin J. Puppels, Editors, *Proceedings of SPIE*.

Holman, H. Y. N., Martin, M. C., Mckinney, W. R. (2003). Synchrotron-based FTIR spectromicroscopy: Cytotoxicity and heating considerations. *J. Biol. Phys.*, **29**: 275–286.

Hospers, G. A., Eisenhauer, E. A ., De Vries, E. G. (1999). *Br. J. Cancer*, **80**: 629–638.

Hosseinimehr, S. J. (2007). Foundation review: Trends in the development of radioprotective agents. *Drug Discovery Today*, **12**.

Huang, R. Y., Miller, L. M., Carlson, C. S. And Chance, M. R. (2002). Characterization of bone mineral composition in the proximal tibia of cynomolgus monkeys: Effect of ovariectomy and nandrolone decanoate treatment. *Bone*, **30**: 492-497.

Huang, R. Y., Miller, L. M., Carlson, C. S. And Chance, M. R. (2003). In situ chemistry of osteoporosis revealed by synchrotron infrared microspectroscopy. *Bone*, **33**: 514-521.

Ishida, K. P., Griffiths, P. R. (1993). Comparison of the amide I/II intensity ratio of solution and solid-state proteins sampled by transmission, attenuated total reflectance, and diffuse reflectance spectrometry. *Appl. Spectrosc.*, **47**: 535-671.

Jackson, M., Ramjiawan, B., Hewko, M., Mantsch, H.H. (1998). Infrared microscopic functional group mapping and spectral clustering analysis of hypercholesterolemia rabbit liver. *Cell. Mol. Biol.*, **44**: 89-98.

Jagadeesan, G., Kavitha, A.V., Subashini, J. (2005). FT-IR study of the influence of tribulus terrestris on mercury intoxicated mice, mus musculus liver. *Tropical Biomedicine*, **22(1)**: 15–22.

Jagetia, G. C., Reddy, T. K. (2005). Modulation of radiation-induced alteration in the antioxidant status of mice by naringin. *Life Sciences*, **77**: 780–794.

Jamin, N., Dumas, P., Moncuit, J., Fridman, W. H., Teillaud, J. L., Carr, G. L., Williams, G. P. (1998). Highly resolved chemical imaging of living cells by

using synchrotron infrared microspectrometry. *Proc. Natl. Acad. Sci. U.S.A.*, **95**: 4837–4840.

- Jamin, N., Miller, L., Moncuit, J., Fridman, W. H., Dumas, P., Teillaud, J. L. (2003). Chemical heterogeneity in cell death: Combined synchrotron IR and fluorescence microscopy studies of single apoptotic and necrotic cells. *Biopolymers*, **72**: 366–373.
- Jhun, E., Jhun, B. E., Jones, L.R., Jung, C. Y. (1991). Direct effects of ionizing radiation on integral membrane proteins. *J Biol Chem.*, **266**: 9403-9407.
- Jirtle, R. L., Ancher, M. S., Alati, T. (1990). *Radiation sensitivity of the liver*. San Diego: Academic Press.
- Jirtle, R. L., Pierce, L. J., Crocker, I. R., Strom, S. C. (1985). Radiation protection of rat parenchymal hepatocytes with S-2-(3-aminopropylamino) ethylphosphorothioic acid. *Radiother. Oncol.*, **4**: 231-7.
- Karbownik, M., Reiter, R. J. (2000). Antioxidative effects of melatonin in protection against cellular damage caused by ionizing radiation. *Proc. Soc. Exp. Biol. Med.*, **225**: 9-22.
- Khouw, A. S., Parthasarathy, S. And Witztum, J.L. (1993). Radioiodination of low density lipoprotein initiates lipid peroxidation: Protection by use of antioxidants. *J. Lipid Res.*, **34**: 1483-1496.
- Kneipp, J., Beekes, M., Lasch P., Naumann, D. (2002). Molecular changes of preclinical scrapie can be detected by infrared spectroscopy. *J. Neurosci.*, **22**: 2989–2997.
- Kneipp, J., Lasch, P., Baldauf, E., Beekes, M., Naumann, D. (2000). Detection of pathological molecular alterations in scrapie-infected hamster brain by fourier transform infrared (FT-IR) spectroscopy. *Biochim. Biophys. Acta* **1501**: 189-199.
- Kneipp, J., Miller, L. M., Joncic, M., Kittel, M., Lasch, P., Beekes, M., Naumann, D. (2003). In situ identification of protein structural changes in prioninfected tissue. *Biochim. Biophys. Acta*, **1639**: 152–158.
- Kneipp, J., Miller, L. M., Spassov, S., Sokolowski, F., Lasch, P., Beekes, M., Naumann, D. (2004). Scrapie-infected cells, isolated prions, and recombinant prion protein: A comparative study. *Biopolymers*, **74**: 163–167.
- Kolling, A., Maldonado, C., Ojeda, F., Diehl, H. A. (1994). Membrane fluidity of microsomal and thymocytemembranes after x-ray and uv radiation. *Radiat. Environ. Biophys.*, **33**: 303–313.

- Koshiishi, I., Tsuchida, K., Takajo, T., Komatsu, M. (2005). Quantification of lipid alkyl radicals trapped with nitroxyl radical via hplc with postcolumn thermal decomposition. *J. Lipid Res.*, **46**: 2506–2513.
- Krafft, C., Sobottka, S. B., Geiger, K. D., Schackert, G., Salzer R. (2007). Classification of malignant gliomas by infrared spectroscopic imaging and linear discriminant analysis. *Anal. Bioanal. Chem.*, **387**: 1669–1677.
- Krafft, C., Sobottka, S. B., Schackert, G., Salzer R. (2004). Analysis of human brain tissue, brain tumors and tumor cells by infrared spectroscopic mapping. *Analyst* **129**: 921-925.
- Krasowska, A., Stasiuk, M., Oswiecimska, M., Kozubek, A., Bien, M., Witek, S. And Sigler, K. (2001). Supression of radical-induced lipid peroxidation in a model system by alkyl esters of cinnamate quaternary ammonium salts. *Z. Naturforsch.*, **56**: 878-885.
- Kretlow, A., Wang, Q., Kneipp, J., Beekes, M., Naumann, D., Miller, L. (2008). Changes in protein structure and distribution observed at pre-clinical stages of scrapie pathogenesis. *Biochimica et Biophysica Acta* **1782**: 559–565.
- Kretlow, A., Wang, Q., Kneipp, J., Lasch, P., Beekes, M., Miller, L. and Naumann, D. (2006). FTIR-microspectroscopy of prion-infected nervous tissue. *Biochimica et Biophysica Acta*, **1758**: 948–959.
- Labieniec, M. and Gabryelak, T. (2004) Response of DNA, proteins and membrane bilayer in the digestive gland cells of freshwater mussel *Unio tumidus* to tannins exposure. *Toxicol In Vitro*. **18**:773-81.
- Lamba, O. P., Borchman, D., Garner, W. H. (1994). Spectral characterization of lipid peroxidation in rabbit lens membranes induced by hydrogen peroxide in the presence of $\text{Fe}^{2+}/\text{Fe}^{3+}$ cations: A sitespecific catalyzed oxidation. *Free Radical Biol Med.*, **10**: 591–601.
- Lamba, O. P., Lal, S., Yappert, M. C., Lou, M. F., Borchman, D. (1991). Spectroscopic detection of lipid peroxidation products and structural changes in a sphingomyelin model system. *Biochim. Biophys. Acta*, **1081**: 181–187.
- Lasch, P., Haensch, W., Naumann, D., Diem, M. (2004). Imaging of colorectal adenocarcinoma using FT-IR microspectroscopy and cluster analysis. *Biochim. Biophys. Acta*, **1688**(2): 176-86.
- Lasch, P. and Naumann, D. (1998). FT-IR microspectroscopic imaging of human carcinoma thin sections based on pattern recognition techniques. *Cell Mol Biol (Noisy-le-grand)*, **44**(1): 189-202.

- Lee, S. and Song, K. B. (2003). Effect of gamma irradiation on the physicochemical properties of porcine and bovine blood plasma proteins. *Food Chem.*, **82**: 521–526.
- Lehninger, A. L. (1984). *Principles of biochemistry*. New York: Worth Publishers, Inc.
- Leskovjan, A. C., Lanzirotti, A., Miller, L.M. (2009). Amyloid plaques in psapp mice bind less metal than plaques in human alzheimer's disease. *Neuroimage*, **47**: 1215-20.
- Lester, D. S., Kidder, L.H., Levin, I.W., Lewis, E.N. (1998). Infrared microspectroscopic imaging of the cerebellum of normal and cytarabine treated rats. *Cell Mol. Biol.*, **44**: 29-38.
- Levi, M., Knol, J. A., Ensminger, W. D., Deremer, S. J., Dou, C., Lunte, S., M., Bonner, H. S., Shaw, L., M., Sidth, D., M. (2002). Regional pharmacokinetics of amifostine in anesthetized dogs: Role of the liver, gastrointestinal tract, lungs, and kidneys. *Drug Metabolism and Disposition*, **30**: 1425-1430.
- Levin, I. W. and Bhargava, R. (2005). Fourier transform infrared vibrational spectroscopic imaging: Integrating microscopy and molecular recognition. *Annu. Rev. Phys. Chem.*, **56**: 429–74.
- Levine, S. M., Wetzel D. L. B. (1993). Analysis of brain tissue by FT-IR microspectroscopy. *Appl. Spectrosc.*, **28**: 385-412.
- Levine, S. M., Wetzel, D. L. (1998). Chemical analysis of multiple sclerosis lesions by FT-IR microspectroscopy. *Free Radical Biology & Medicine*, **25(1)**: 33-41.
- Lewanski, C. R., Gullick, W., J. (2001). Radiotherapy and cellular signalling. *The Lancet Oncology*, **2**: 366-370.
- Lewis, E. N. L., I. W. Steer, C. J. (1989). Infrared spectroscopic study of ethanol-induced changes in rat liver plasma membrane. *Biochim. Biophys. Acta*, **1989**: 161–166.
- Little, M. P. (2001). Cancer after exposure to radiation in the course of treatment for benign and malignant disease. *Lancet Oncol*, **2**: 212–20.
- Liu, K., Jackson, M., Sowa, M.G., Ju, H., Dixon, I.M.C., Mantsch, H.H. (1996). Modification of the extracellular matrix following myocardial infarction monitored by FTIR spectroscopy. *Biochim. Biophys. Acta* **1315**: 73–77.
- Liu, K. Z., Bose, R., Mantsch, H. H. (2002). Infrared spectroscopic study of diabetic platelets. *Vibr. Spectrosc.*, **28**: 131–136.

- Liu, K. Z., Man, A., Shaw, R.A., Liang, B., Xu, Z., Gong, Y. (2006). Molecular determination of liver fibrosis by synchrotron infrared microspectroscopy. *Biochim. Biophys. Acta*, **1758**: 960–967.
- Lopez-Garcia, F., Villian, J., Gomez-Fernandez, J.C. (1993). Infrared spectroscopic. *Biochim. Biophys. Acta*, **1169**: 264-272.
- Manda, K., Ueno, M., Moritake, T., Anzai, K. (2007). α -lipoic acid attenuates X-irradiation-induced oxidative stress in mice. *Cell Biol. Toxicol.*, **23**: 129–137.
- Manoharan, R., Baraga, J.J., Rava, P.R., Dasari, R.R., Fitzmaurice, M., Feld, M.S. (1993). Biochemical analysis and mapping of atherosclerotic human artery using FT-IR microspectroscopy. *Atherosclerosis*, **103**: 181–193.
- Mantsch, H. H. (1984). Biological applications of fourier transform infrared spectroscopy. A study of phase transitions in biomembranes. *J. of Molecular Structure*, **113**: 201-212.
- Marnett, L. J. (1999). Lipid peroxidation—DNA damage by malondialdehyde. *Mutation Research*, **424**: 83–95.
- Marzatico, F., Porta, C., Moroni, M., Bertorelli, L., Borasio, E., Finotti, N., Pansarasa, O., Castagna, L. (2000). In vitro antioxidant properties of amifostine (wr-2721, ethylol). *Cancer Chemother. Pharmacol*, **45**: 172-176.
- Mccumber, L. M. (2004). The potential influence of cell protectors for dose escalation in cancer therapy: An analysis of amifostine. *Med. Dosim.*, **29**: 139-43.
- Mcdonough, J. H., Mele, P.C. And Franz, C.G. (1992). Comparison of behavioral and radioprotective effects of wr-2721 and wr-3689. *Pharmacol. Biochem. Be.*, **42**: 233–243.
- Meade, A. D., Byrne, H. J., Lyng, F.M. (2010). Spectroscopic and chemometric approaches to radiobiological analyses. *Mutation Research*, **704**: 108–114.
- Mendelsohn, R., Chen, H. C., Rerek, M. E., Moore D. J. (2003). Infrared microspectroscopic imaging maps the spatial distribution of exogenous molecules in skin. *J. Biomed. Opt.*, **8**: 185-190.
- Mendelsohn, R., Mantsch, H. H. (1986). *Fourier transform infrared studies of lipid-protein interaction*. Netherlands: Elsevier Science Publishers.
- Miller, L. M., Carr, G. L., Jackson, M., Williams, G. P., Dumas, P. (2000). The impact of infrared synchrotron radiation on biology: Past, present, and future. *Synchrotron Radiation News*, **13**: 31-37.

- Miller, L. M. and Dumas, P. (2006a). Chemical imaging of biological tissue with synchrotron infrared light. *Biochimica et Biophysica Acta* **1758**: 846–857.
- Miller, L. M., Novatt, J. T., Hamerman, D., Carlson, C. S. (2004). Alterations in mineral composition observed in osteoarthritic joints of cynomolgus monkeys. *Bone*, **35**: 498–506.
- Miller, L. M., Vairavamurthy, V., Chance, M.R., Mendelsohn, R., Paschalis, E.P., Betts, F., Boskey, A.L. (2001). In situ analysis of mineral content and crystallinity in bone using infrared micro-spectroscopy of the $\text{Nu}(4) \text{Po}(4) (3-)$ vibration. *Biochim. Biophys. Acta* **1527**: 11–19.
- Miller, L. M., Wang, Q., Telivala, P. T., Smith R.J., Lanzirotti, A. And Miklossy, J. (2006b). Synchrotron-based infrared and X-ray imaging shows focalized accumulation of Cu and Zn co-localized with β -amyloid deposits in alzheimer's disease. *J. Struct. Biol.*, **155**: 30-37.
- Moore, D. J., Sills, R.H., Mendelsohn, R. (1995). Peroxidation of erythrocytes: FTIR spectroscopy studies of extracted lipids, isolated membranes, and intact cells. *Biospectroscopy*, **1**: 133-140.
- Mozumder, A. (1999). *Fundamentals of radiation chemistry*. San Diego: Academic Press.
- Murley, J. S., Kataoka, Y., Weydert, C. J., Oberley, L. W., Gridina, D. J. (2006). Delayed radioaprotection by nuclear transcription factor kb-mediated induction of manganese superoxide dismutase in human microvascular endothelial cells after exposure to the free radical scanger WR-1065. *Free Radical Biology and Medicine*, **40**: 1004-1016.
- Nair, C. K. K., Parida, D. K., Nomura, T. (2001). Radioprotectors in radiotherapy. *J. Radiat. Res.*, **42**: 21-37.
- Nair, M. (2007). Diabetes mellitus, part 1: Physiology and complications. *Br. J. Nurs.*, **16**: 184–188.
- Nakajima, Y., Nakashima, T., Inaba, K., Sumida, Y., Yoh, T., Ishikawa, H., Mitsuyoshi, H., Shima, T., Senmaru, H. (2002). Effects of nitric oxide on the redox status of liver microsomes—electron spin resonance monitoring using nitroxide probes. *Hepatology Research*, **24**: 72–79.
- Nieder, C., Andratschke, N.H., Wiedenmann, N., Molls, M. (2004). Prevention of radiation induced central nervous system toxicity: A role of amifostine. *Anticancer Research*, **24**: 3803-3810.

- Ohnishi, S. T., Ohnishi, T., Glick, J. H., Schein, P. S. (1992). In vitro study on the antioxidant activities of amifostine (WR-2721). *Proc. Am. Assoc. Cancer Res.*, **33**: 419.
- Ozek, S. N., Sara, Y., Onur, R., Severcan, F. (2009). Low dose simvastatin induces compositional, structural and dynamical changes on rat skeletal extensor digitorum longus muscle tissue. *Biosci Rep.*, **30**: 41-50.
- Perromat, A., Melin, A.M., Lorin, C., Deleris, G. (2003). Fourier transform IR spectroscopic appraisal of radiation damage in micrococcus luteus. *Biopolymers (Biospectroscopy)*, **72**: 207–216.
- Petibois, C., Deleris, G. (2006). Chemical mapping of tumor progression by FT-IR imaging: Towards molecular histopathology. *Trends in Biotechnology*, **24**: 455-462.
- Phillis, J. W., Horrocks, L.A., Farooqui, A.A. (2006). Cyclooxygenases, lipoxygenases and epoxygenases in CNS: Their role and involvement in neurological disorders. *Brain Res.*, **52**: 201-243.
- Pribrush, A., Agam, G., Yermiahu, T., Dvilansky, A., Meyerstein, D., Meyerstein, N. (1994). Radiation damage to the erythrocyte membrane: The effects of medium and cell concentrations. *Free Radical Research*, **21**: 135-146.
- Prise, K. M., Schettino, G., Folkard, M., Held, K. D. (2005). New insights on cell death from radiation exposure. <http://oncology.thelancet.com>, **6**.
- Reiter, R. J. (1995). Oxidative processes and antioxidative defense mechanisms in the aging brain. *FASEB J.*, **9**: 526-33.
- Rigas, B., Morgello, S., Goldman, I.S., Wong, P.T.T. (1990). Human colorectal cancers display abnormal fourier-transform infrared spectroscopy. *Proc. Natl. Acad. Sci. U.S.A.*, **87**: 8140–8144.
- Riley, P. A. (1994). Free radicals in biology: Oxidative stress and the effects of ionizing radiation. *Int. J. Radiat. Biol.*, **65**: 27-33.
- Romeo, M. J., Quinn, M. A., Burden, F. R., Mcnaughton, D. (2002). Influence of benign cellular changes in diagnosis of cervical cancer using IR microspectroscopy. *Biopolymers*, **67(4-5)**: 362-6.
- Rubin, P., Casarett, G. W. (1968). *Clinical radiation pathology*. Philadelphia: W. B. Saunders.
- Samuni, A. M., Barenholz, Y., Cromellin, D.J.A., Zuidam, N.J. (1997). Gamma irradiation damage to liposomes differing in composition and their protection by nitroxides. *Free Radical. Biol. Med.*, **23**: 972-979.

- Santini, V., Giles, F. J. (1999). The potential of amifostine: From cytoprotectant to therapeutic agent. *Haematologica*, **84**(11): 1035-1042.
- Savoie, C., Swenberg, C. And Hugot, S. (1997). Thiol WR-1065 and disulphide WR-33278, two metabolites of the drug ethiol (WR-2721), protect DNA against fast neutron-induced strand breakage. *Int. J. Radiat. Biol.*, **71**: 193-202.
- Schmidt, M., Wolfram, T., Rumpler, M., Tripp, C. P., Grunze M. (2007). Live cell adhesion assay with attenuated total reflection infrared spectroscopy. *Biointerphases*, **2**: 1-5.
- Schultheiss, T. E., Kun, L.E., Ang, K. K., Stephens, L. C. (1995). Radiation response of the central nervous system. *Int. J. Radiat. Oncol., Biol., Phys.*, **31**: 1093-1112.
- Schultz, C. P., Liu, K. Z., Kerr, P. D., Mantsch, H. H. (1998). In situ infrared histopathology of keratinization in human oral/oropharyngeal squamous cell carcinoma. *Oncol. Res.*, **10**: 277-286.
- Severcan, F., Bozkurt O., Gurbanov R., Gorgulu G. (2010). FT-IR spectroscopy in diagnosis of diabetes in rat animal model. *J. Biophotonics*, **3**: 621–631.
- Severcan, F., Gorgulu, G., Gorgulu, S. T., Guray, T. (2005). Rapid monitoring of diabetes-induced lipid peroxidation by fourier transform infrared spectroscopy: Evidence from rat liver microsomal membranes. *Anal. Biochem.*, **339**: 36–40.
- Severcan, F., Toyran, N., Kaptan, N. And Turan, B. (2000). Fourier transform infrared study of the effect of diabetes on rat liver and heart tissues in the c–h region. *Talanta*, **53**: 55–59.
- Shikazona, N., Yokota, Y., Kitamura, S., Suzuki, C., Watanabe, H., Tano, S., Tanaka, A. (2003). Mutation rate and novel *tt* mutants of *arabidopsis thaliana* induced by carbon ions. *Genetics*, **163**: 1449–1455.
- Signorini, C., Ferrali, M., Ciccoli, L., Sugherini, L., Magnani, A., Comporti, M. (1995). Comporti, m. Iron release, membrane protein oxidation and erythrocyte ageing. *FEBS Lett.*, **362**: 165–170.
- Sills, R. H., Moore, D. J., Mendelsohn, R. (1994). Erythrocyte peroxidation: Quantitation by fourier transform infrared spectroscopy. *Anal. Biochem.*, **218**: 118-123.
- Smith, B. C. (1999). *Infrared spectral interpretation*. Printed in USA: CRC Press LLC.

- Snyder, R. D., Grdina, D. J. (2000). Further evidence that the radioprotective aminothiols, WR-1065, catalytically inactivates mammalian topoisomerase α . *Cancer Res.*, **60**: 1186–1188.
- Sonia, H., Maria, B. K., Ronald, P.M., Ohara, A. (2000). In vivo metabolism of tert-butyl hydroperoxide to methyl radicals. Epr spin-trapping and DNA methylation studies. *Chem. Res. Toxicol.*, **13**: 1056–1064.
- Spencer, C. M., Goa, K. L. (1995). Amifostine. *Drugs.*, **50**: 1001-1025.
- Stadtman, E. R. (1990). Metal ion-catalyzed oxidation of proteins: Biochemical mechanism and biological consequences. *Free Radical Biol. Med.*, **9**: 315–325.
- Stuart, B. (1996). *Modern infrared spectroscopy*. England: John & Sons, Ltd.
- Stuart, B. (1997). *Biological applications of infrared spectroscopy*. England: John & Sons, Ltd.
- Stuart, B. (2004). *Infrared Spectroscopy Fundamentals and Applications Analytical Techniques in the Sciences*. England: John & Sons, Ltd.
- Symon, Z., Levi, M., Ensminger, W. D., Smith, D. E., Lawrence, T. S. (2001). Selective radioprotection of hepatocytes by systemic and portal vein infusions of amifostine in a rat liver tumor model. *I. J. Radiation Oncology*, **50**: 473–478.
- Szalontai, B. (2009). Membrane protein dynamics: Limited lipid control pmc. *PMC Biophys.*, **2**: 1-17.
- Szalontai, B., Nishiyama, Y., Gombos, Z., Murata, N. (2000). Membrane dynamics as seen by fourier transform infrared spectroscopy in a cyanobacterium, *synechocystis pcc 6803*. The effects of lipid unsaturation and the protein-to-lipid ratio. *Biochim. Biophys. Acta*, **1509**: 409–419.
- Szczerbowska-Boruchowska, M., Dumas, P., Kastyak, M.Z., Chwiej, J., Lankosz, M., Adamek, D., Krygowska-Wajs, A. (2007). Biomolecular investigation of human substantia nigra parkinson's disease by synchrotron radiation fourier transform infrared microspectroscopy. *Arch. Biochem. Biophys.*, **459**: 241–248.
- Tabachnik Schor, N. F. (1987). Adjunctive use of ethiofos (WR-2721) with free-radical-generating chemotherapeutic agents in mice: New caveats for therapy. *Cancer Res.*, **47**.
- Tait, D., Bors, W. (1985). Interaction of phospholipid liposomes with a DNA compound in irradiated systems. *Int. J. Radiat. Biol.*, **47**: 497-508.

- Torreggiani M.T., I., Manco, I., Faraone-Mennella, M. R., Ferreri, C., Chatgililoglu C. (2006). Investigation of radical-based damage of rnase a in aqueous solution and lipid vesicles. *Biopolymers*, **81**: 39–50.
- Toyran, N., Lasch, P., Naumann, D., Turan, B., Severcan, F. (2006). Early alterations in myocardia and vessels of the diabetic rat heart: An FTIR microspectroscopic study. *Biochem. J.*, **397**: 427-436.
- Toyran, N., Severcan, F., Severcan, M., Turan, B. (2007). Investigation of diabetes-induced effect on apex of rat heart myocardium by using cluster analysis and neural network approach: An FTIR study. *Spectroscopy-An International Journal*, **21**: 269-278.
- Toyran, N., Zorlu F., Dönmez, G., Oğe, K., Severcan, F. (2004). Chronic hypoperfusion alters the content and structure of proteins and lipids of rat brain homogenates: A fourier transform infrared spectroscopy study. *Eur. Biophys. J.*, **33**: 549-554.
- Toyran, N., Zorlu, F., Severcan, F. (2005). Effect of stereotactic radiosurgery on lipids and proteins of normal and hypoperfused rat brain homogenates: A fourier transform infrared spectroscopy study. *Int. J. Radiat. Biol.*, **81**: 911–918.
- Uguzalp-Kaldir, M., Yurut-Caloglu, V., Cosar-Alas, R., Cermik, T. F., Altaner, S., Eskiocak, Saymak, M., Ibis, K, Caloglu, M., Tokatli, F., Kocak, Z., Uzal, C. (2007). Radyasyona bagli olusan karaciger ve böbrek toksitesini onlemede amifostinin rolü. *Türk Onkoloji Dergisi*, **22(3)**: 105-117.
- Umemura, J., Cameron, D. G., Mantsch, H. H. (1980). A fourier transform infrared spectroscopic study of the molecular interaction of cholesterol with 1,2-dipalmitoyl-sn-glycero-3- phosphocholine. *Biochim. Biophys. Acta*, **602**: 32-44.
- Utley, J. F., Marlowe, C. and Waddell, W.J. (1976). Distribution of 35s labeled WR-2721 in normal and malignant tissues of the mouse. *Radiat. Res.*, **68**: 284–291.
- Van Blitterswijk, W. J. (1985). In membrane fluidity in biology. **Vol. 3**: pp. 85–159.
- Volland, W. (1999). *Organic compound identification using infrared spectroscopy*. Washington: Bellevue Community College.
- Wang, Q., Sanad, W., Miller, L.M., Voigt, A., Klingel, K., Kandolf, R., Stangl, K. and Baumann, G. (2005a). Infrared Imaging of Compositional Changes in Inflammatory Cardiomyopathy. *Vibrational Spectroscopy* **38**: 217-22.

- Wang, Q., Kretlow, A., Beekes, M., Naumann, D. And Miller, L. (2005b). In situ characterization of prion protein structure and metal accumulation in scrapie-infected cells by synchrotron infrared and x-ray imaging. *Vibr. Spectrosc.*, **38**: 61–69.
- Washburn, L. C., Carlton, J.E., Hayes, R.L. (1974). Distribution of WR-2721 in normal and malignant tissues of mice and rats bearing solid tumors: Dependence on tumour type, drug, dose and species. *Radiat. Res.*, **59**: 475–483.
- Watanabe, H., Kobaayashi, A., Yamamoto, T., Suzuki, S., Hayashi, H., Yamazaki, N. (1990). Alterations of human erythrocyte membrane fluidity by oxygen-derived free radicals and calcium. *Free Radical Biol. Med.*, **9**: 507–514.
- Wetzel, D. L. (1995). *Microbeam molecular spectroscopy of biological materials*. Elsevier Press.
- Wetzel, D. L., Srivarin, P., Finney, J.R. (2003). Revealing protein infrared spectral detail in a heterogeneous matrix dominated by starch. *Vibr. Spectrosc.*, **31**: 109-114.
- Winkler, H. (1957). Examination of the effect of roentgen rays on hemato-encephalic barrier by means of radioactive phosphorus. *Zentralbl Allg Pathol*, **27**: 301-7.
- Yano, K., Ohoshima, S., Shimizu, Y., Moriguchi, T., Katayama, H. (1996). Evaluation of glycogen level in human lung carcinoma tissues by an infrared spectroscopic method. *Cancer Letters.*, **110**: 29-34.
- Yildirim, O., Comoglu, S., Yardimci, S., Akmansu, M., Bozkurt, G., Avunduk, M.C. (2007). Melatonin treatment for prevention of oxidative stress: Involving histopathological changes. *Gen. Physiol. Biophys.*, **26**: 126-132.
- Yoneoka, Y., Satoh, M., Akiyama, K., Sano, K., Fujii, Y., Tanaka, R. (1999). An experimental study of radiation-induced cognitive dysfunction in an adult rat model. *Brit. J. Radiol.*, **72**: 1196-1201.
- Yu, P., Kevin, D., Dasen, L. (2008). Shining light on the differences in molecular structural chemical makeup and the cause of distinct degradation behavior between malting- and feed-type barley using synchrotron FTIR microspectroscopy: A novel approach. *J. Agric. Food Chem.*, **56**: 3417–3426.
- Yuhas, J. M., Davis, M.E., Glover, D., Brown, D.Q., Ritter, M. (1982). Circumvention of the tumor membrane barrier to WR-2721 absorption by reduction of drug hydrophilicity *Int J Radiat Oncol Biol Phys*, **8**: 519-522.

- Yukawa, O., Miyahara, M., Shiraishi, N., Nakazawa, T. (1985). Radiation-induced damage to mitochondrial D-F-hydroxybutyrate dehydrogenase and lipid peroxidation. *Int. J. Radiat. Biol.*, **48**: 107-15.
- Zabbarova, I., Kanai, A. (2008). Targeted delivery of radioprotective agents to mitochondria. *Molecular Interventions*, **8**: 294-302.
- Zhang, L., Small, G. W., Haka, A. S., Kidder, L. H., Lewis, E. N. (2003). Classification of fourier transform infrared microscopic imaging data of human breast cells by cluster analysis and artificial neural networks. *Appl Spectrosc.*, **57**(1): 14-22.
- Zwart, L. L., Meerman, J. H. N., Commandeur, J. N. M., Vermeulen, N. P. E. (1999). Biomarkers of free radical damage applications in experimental animals and in humans. *Free Radical Biol. Med.*, **26**: 202–226.

CURRICULUM VITAE

PERSONEL INFORMATION

Surname, Name: Çakmak, Gülgün
Nationality: Turkish (TC)
Date and Place of Birth: 02 June 1975, Denizli
Marital Status: Single
Phone: +90 312 210 51 57
E-mail: gulguncakmak@yahoo.com
Foreign Languages: English

EDUCATION

Degree	Institution	Graduation	C.GPA
Ph.D.	METU Biology Dept.	2010	3.58
M.Sc.	METU Biology Dept.	2001	3.21
B.Sc.	Hacettepe Uni. Biology Dept.	1997	3.24

WORK EXPERIENCE

Year	Place	Enrollment
1998-2001	Polatlı, Ankara	English Teacher
2001-2007	TTKB, Ankara	Biology Teacher
2007-2008	BNL, NSLS, USA	Invited Researcher
2008-present	Keçiören, Ankara	Primary School Teacher

ACADEMIC ACTIVITIES

A) Articles in Refereed Journals

Cakmak, G., Togan I. and Severcan F. “17 β -Estradiol Induced Compositional, Structural and Functional Changes on Rainbow Trout Liver, Revealed by FT-IR Spectroscopy: A Comparative Study with Nonylphenol” **Aquatic Toxicology**, **77 53-63 (2006)**

Cakmak, G., Togan I. and Severcan F. “A Comparative FTIR Spectroscopic Analysis of Rainbow Trout Liver Exposed to Nonylphenol and Estradiol” **WSEAS Transactions on Biology and Biomedicine 2(4) 359-365 (2005)**

Cakmak, G., Uğuz, C., Togan, I. and Severcan, F. “FT-IR Spectroscopic Analysis of Rainbow Trout Liver Exposed to Nonylphenol” **Applied Spectroscopy 57(7) 835-841 (2003)**

Cakmak G., Miller L. M. Zorlu F. and Severcan F. “Amifostine, a Radioprotectant Agent, Protects Rat Brain Tissue Lipids against Ionizing Radiation Induced Damage: An FTIR Microspectroscopic Imaging Study” **Manuscript submitted to International Journal of Radiation Oncology • Biology • Physics**

Cakmak G., Zorlu F. and Severcan F. “Screening of Restoring Effect of Amifostine on Radiation Induced Structural and Functional Variations in Rat Liver Microsomal Membranes by FTIR Spectroscopy as a Novel Method” **Manuscript submitted to Analytical Chemistry**

B) Academic Research Projects

“Molecular Studies on the effects of Radioprotectant Amifostine on Irradiated Tissues”

Funded by: TUBITAK-SBAG-2939; 2005-2007, Investigator.

Principal Investigator: Prof. Dr. Faruk Zorlu

Status: Completed (2 years)

C) Abstracts in refereed journals (SCI)

Cakmak G., Severcan M., Zorlu F. and Severcan F. (2009), “Amifostine, a Radioprotectant Agent, Protects Rat Hepatic Microsomal Membranes Against Ionizing Radiation Induced Damage” **Biophysical Journal 96(3): 353A Suppl. 1**

Cakmak G., Zorlu F., Severcan F. (2008), The Investigation of Ionizing Radiation-Induced Damages on Liver Microsomal Membranes by FTIR Spectroscopy, **Biophysical Journal, Volume 94, Supplement, pp. 113**

Cakmak G., Severcan F., (2008), The Effects of Radioprotectant Amifostine on Zwitterionic Dipalmitoyl Phosphatidylcholine (DPPC) Membranes, **Biophysical Journal, Volume 94, Supplement, pp. 117**

Severcan F., Togan I. and **Cakmak, G.** (2005) "FT-IR Spectroscopic Analysis of Rainbow Trout Liver Exposed to 17- β Estradiol" **Biophysical Journal** **88(1): 159A-160A Part 2 Suppl. S**

Abstracts in Congress Proceedings

A) Oral Presentations

Cakmak G., Zorlu F., Miller L. M. and Severcan F. "Amifostine, a Radioprotectant Agent, Protects Rat Brain Tissue Lipids Against Ionizing Radiation Induced Damage: A Fourier Transform Infrared Microspectroscopic Imaging Study" 2nd International Biophysics Congress and Biotechnology at GAP & 21st National Biophysics Congress. 5-9 October **2009**, Diyarbakir, **TURKEY**.

Cakmak G., Wetzel David L. and Severcan F. "Effects of Radioprotectant Amifostine on Irradiated Rat Brain Tissues Studied by FTIR Microspectroscopy and Imaging" PITTCON **2008**, 2-7 March 2008, New Orleans, **USA**.

Cakmak G., Zorlu F., Miller L. M. and Severcan F. "The Molecular Effects of Radioprotectant Amifostine on Irradiated Rat Brain Tissues" NSLS Lunch Time Seminar, November 7th **2008**, Brookhaven National Laboratory, Upton, NY, **USA**.

Cakmak, G., Togan I. and Severcan F. "A Comparative FTIR Spectroscopic Analysis of Rainbow Trout Liver Exposed to Nonylphenol and Estradiol" 2005 WSEAS International Conference on Cellular and Molecular Biology, Biophysics and Bioengineering, 15-17 July **2005**, Vouliagmeni, Athens, **GREECE**.

Çakmak, G., Uğuz, C., Togan, İ. ve Severcan, F. "Spectroscopic Analysis of the Livers in Rainbow Trout (*Oncorhynchus mykiss*) Exposed to Nonylphenol" XIIIth National Biophysics Congress, 5-7 September **2001**, Eskişehir, **TURKEY**.

B) Poster Presentations

Cakmak G., Severcan M., Zorlu F. and Severcan F. "Investigation of Radioprotective Effects of Amifostine on Rat Liver Microsomal Membrane and Brain Tissue Proteins by FTIR Spectroscopy: An imaging and Neural Network Approach" 2nd International Conference on Vibrational Optical Activity (VOA-2) and Bio-Medical Applications of Raman Spectroscopy (BMARS), August 5-7, **2010** Albany, NY, **USA**.

- Cakmak G.**, Togan I. Ozek N. S. and Severcan F. “Nonilfenolün Alabalık Karaciğer Makromoleküllerinde Neden Olduğu Yapısal Ve Fonksiyonel Değişimlerin Fourier Dönüşüm Kızılötesi (FTIR) Spektroskopisi Belirlenmesi” 1. Ulusal Palandöken Toksikoloji Sempozyumu, 28-30 Mayıs **2010**, Erzurum, **TURKEY**.
- Severcan M., **Cakmak G.**, Gorgulu S. T., Akkas S. B., Severcan F. “Prediction of Protein Secondary Structure Using Neural Networks in Biological Systems” 4th International Symposium On Health Informatics And Bioinformatics, Turkey’09 April 16-17, **2009**, Metu Informatics Institute, Ankara, **TURKEY**.
- Cakmak G.**, Severcan M., Zorlu F. and Severcan F. “Amifostine, a Radioprotectant Agent, Protects Rat Hepatic Microsomal Membranes Against Ionizing Radiation Induced Damage” Biophysical Society 53rd Annual Meeting, February 28-March 4, **2009** Boston, MA, **USA**.
- Cakmak G.**, Zorlu F., Severcan F. and Miller L. M. “The Molecular Effects of Radioprotectant Amifostine on Irradiated Rat Brain Tissues” **2008**, NSLS & CFN Joint Users’ Meeting, May 19-21 **2008**, Upton, NY, **USA**.
- Cakmak G.**, Togan I. and Severcan F. “17 β -Estradiol induced compositional, structural and functional changes in rainbow trout liver, revealed by FT-IR spectroscopy: A comparative study with Nonylphenol” Spec 2006, Shedding Light on Disease: Optical Diagnosis for the New Millennium, May 20-24 **2006**, Heidelberg, **GERMANY**.
- Cakmak G.** and Severcan F. “The Effects of Radioprotectant Amifostine on Zwitterionic Dipalmitoyl Phosphatidylcholine (DPPC) Membranes.” Biophysical Society 52nd Annual Meeting, February 2-6, **2008**, Long Beach, CA, **USA**.
- Cakmak G.**, Zorlu F. and Severcan F. “The Investigation of Ionizing Radiation-Induced Damages on Liver Microsomal Membranes by FTIR Spectroscopy” 52nd Biophysical Society Annual Meeting, February 2-6 **2008**, Long Beach, CA, **USA**.
- Çakmak, G.**, Togan İ. and Severcan F. “A Comparative FTIR Spectroscopic Analysis of Rainbow Trout Liver Exposed to Nonylphenol and Estradiol” IX. National Spectroscopy Congress, June 9-11, **2005**, Ankara, **TURKEY**.
- Severcan F.**, Togan I. and Cakmak, G. “FT-IR Spectroscopic Analysis of Rainbow Trout Liver Exposed to 17- β Estradiol” 49th Biophysical Society Annual Meeting, February 12-16, **2005**, Long Beach, CA, **USA**.

Çakmak, G., Togan İ. and Severcan F. “FT-IR Spectroscopic Analysis of Rainbow Trout Liver Exposed to 17- β Estradiol” **Xth** National Biophysics Congress, October 8-12 **2003**, Denizli, **TURKEY**.

Çakmak, G., Uğuz, C., Togan, İ. ve Severcan, F. “Spectroscopic Analysis of the Livers in Rainbow Trout (*Oncorhynchus mykiss*) Exposed to Nonylphenol” **XIIIth** National Biophysics Congress, September 5-7 **2001**, Eskişehir, **TURKEY**.

Scholarships and Awards

Scholarship from “**TUBITAK (The Scientific & Technological Research Council of Turkey)**” for Ph.D students’ abroad studies (December, 2007-June, 2008).

Scholarship from “**U.S. Department of Energy's (DOE) Cooperative Research Program for SESAME**” for Synchrotron User’s (July-August 2008).

Scholarship from “**Brookhaven National Laboratory, National synchrotron Light Source**” for visiting scientist (September-October 2008).

Scholarship from “**TUBITAK**” for Ph. D studies (2005-2007).

The Best Student’s Paper Award, **2005 WSEAS International Conference on Cellular and Molecular Biology, Biophysics and Bioengineering**, 15-17 July 2005, Vouliagmeni, Athens, Greece.

Citations:

I- Cakmak, G., Togan I. and Severcan F. “17 β -Estradiol Induced Compositional, Structural and Functional Changes on Rainbow Trout Liver, Revealed by FT-IR Spectroscopy: A Comparative Study with Nonylphenol” *Aquatic Toxicology*, 77 53-63 (2006)

Cited by:

1. Palaniappan PR, Pramod KS “FTIR study of the effect of nTiO(2) on the biochemical constituents of gill tissues of Zebrafish (*Danio rerio*)” *Food and Chemical Toxicology*, **48 (8-9)**: 2337-2343 (2010)
2. Beklioglu M, Akkas SB, Ozcan HE, *et al.* “Effects of 4-nonylphenol, fish predation and food availability on survival and life history traits of *Daphnia magna* straus” *Ecotoxicology* **19 (5)**: 901-910 (2010)

3. Lu XN, Webb M, Talbott M, *et al.* "Distinguishing Ovarian Maturity of Farmed White Sturgeon (*Acipenser transmontanus*) by Fourier Transform Infrared Spectroscopy: A Potential Tool for Caviar Production Management" *Journal of Agricultural and Food Chemistry* **58 (7)**: 4056-4064 (2010)
4. Palaniappan PR, Nishanth T, Renju VB "Bioconcentration of zinc and its effect on the biochemical constituents of the gill tissues of *Labeo rohita*: An FT-IR study" *Infrared Physics & Technology* **53 (2)**: 103-111 (2010)
5. Ozek NS, Sara Y, Onur R, *et al.* "Low dose simvastatin induces compositional, structural and dynamic changes in rat skeletal extensor digitorum longus muscle tissue" *Bioscience Reports* **30(1)**: 41-50 (2010)
6. Palaniappan PR, Krishnakumar N, Vadivelu M, *et al.* "The Study of the Changes in the Biochemical and Mineral Contents of Bones of *Catla catla* Due to Lead Intoxication" *Environmental Toxicology* **25 (1)**: 61-67 (2010)
7. Akkas SB, Kepenek AO, Beklioglu M, *et al.* "Molecular approach to the chemical characterization of fish-exuded kairomone: a Fourier transform infrared spectroscopic study" *Aquatic Sciences* **72(1)**: 71-83 (2010)
8. Palaniappan PR, Pramod KS, Vijayasundaram V "Effect of acute concentration of zinc on the biochemical contents of brain of *Labeo rohita*: an FT-IR study" *Environmental Chemistry Letters* **7 (4)**: 313-319 (2009)
9. Palaniappan PLRM, Vijayasundaram V "Arsenic-Induced Biochemical Changes in *Labeo rohita* Kidney: An FTIR Study" *Spectroscopy Letters* **42**: 213-218 (2009)
10. Ceylan C, Severcan M, Bozoglu F, *et al.* "Evaluation of high hydrostatic pressure effects on bovine red blood cells and platelets Source:" *High Pressure Research* **29**: 358-368 (2009)
11. Ekman DR, Teng QN, Villeneuve DL, *et al.* "Profiling lipid metabolites yields unique information on sex- and time-dependent responses of fathead minnows (*Pimephales promelas*) exposed to 17 alpha-ethynylestradiol" *Metabolomics* **5 (1)**: 22-32 (2009)
12. Huang P, Tian WP, Tuo Y, *et al.* "Estimation of Postmortem Interval in Rat Liver and Spleen Using Fourier Transform Infrared Spectroscopy" *Spectroscopy Letters* **42 (2)**: 108-116 (2009)
13. Palaniappan PR, Renju VB "FT-IR study of the effect of zinc exposure on the biochemical contents of the muscle of *Labeo rohita*" *Infrared Physics & Technology* **52 (1)**: 37-41 (2009)

14. Palaniappan PLRM, Vijayasundaram V “The FT-IR study of the brain tissue of Labeo rohita due to arsenic intoxication” *Microchemical Journal* **91 (1)**: 118-124 (2009)
15. Garip S, Gozen AC, Severcan F. “Use of Fourier transform infrared spectroscopy for rapid comparative analysis of Bacillus and Micrococcus isolates” *Food Chemistry* **113 (4)**: 1301-1307 (2009)
16. Palaniappan P, Pramod K, Vijayasundaram V “FTIR study of zinc-induced biochemical changes in the liver of Indian carp Labeo rohita” *Journal Of Applied Spectroscopy* **75(5)**:752-758 (2008)
17. Palaniappan PLRM, Vijayasundaram V “Fourier transform infrared study of protein secondary structural changes in the muscle of Labeo rohita due to arsenic intoxication” *Food and Chemical Toxicology* **46 (11)**: 3534-3539 (2008)
18. Palaniappan PLRM, Krishnakumar N, Vadivelu M “FT-IR study of the effect of lead and the influence of chelating agents, DMSA and D-Penicillamine, on the biochemical contents of brain tissues of Catla catla fingerlings” *Aquatic Sciences* **70(3)**: 314-322 (2008)
19. Bhattacharya H, Xiao Q, Lun L “Toxicity studies of nonylphenol on rosy barb (Puntius conchionius): A biochemical and histopathological evaluation” *Tissue & Cell* **40(4)**: 243-249 (2008)
20. Palermo FA, Mosconi G, Angeletti M, *et al.* “Assessment of water pollution in the Tronto River (Italy) by applying useful biomarkers in the fish model Carassius auratus” *Archives of Environmental Contamination And Toxicology* **55 (2)**: 295-304 (2008)
21. Toyran N, Severcan F, Severcan M, *et al.* “Effects of selenium supplementation on rat heart apex and right ventricle myocardia by using FTIR spectroscopy: A cluster analysis and neural network approach” *Food Chemistry* **110(3)**: 590- (2008)
22. Huang P, Ke Y, Lu QY, *et al.* “Analysis of postmortem metabolic changes in rat kidney cortex using Fourier transform infrared spectroscopy” *Spectroscopy-an International Journal* **22 (1)**: 21-31 (2008)
23. Bozkurt O, Bilgin MD, Severcan F “The effect of diabetes mellitus on rat skeletal extensor digitorum longus muscle tissue: An FTIR study” *Spectroscopy-an International Journal* **21 (3)**: 151-160 (2007)

24. Biruss B, Dietl R, Valenta C “The influence of selected steroid hormones on the physicochemical behaviour of DPPC liposomes” *Chemistry and Physics of Lipids* **148** (2): 84-90 (2007)
25. Akkas SB, Severcan M, Yilmaz O, *et al.* “Effects of lipoic acid supplementation on rat brain tissue: An FTIR spectroscopic and neural network study” *Food Chemistry* **105** (3): 1281-1288 (2007)
26. Gorgulu ST, Dogan M, Severcan F “The characterization and differentiation of higher plants by Fourier transform infrared spectroscopy” *Applied Spectroscopy* **61** (3): 300-308 (2007)
27. Ozek NS, Sara Y, Onur R, *et al.* “The investigation of the possible effects of cholesterol reducing agent simvastatin on rat testis tissue” *Biophysical Journal* 336A-336A Supplement: Suppl. S (2007)
28. Toyran N, Turan B, “Severcan F Selenium alters the lipid content and protein profile of rat heart: An FTIR micro spectroscopic study” *Archives of Biochemistry and Biophysics* **458** (2): 184-193 (2007)
29. Garip S, Bozoglu F, Severcan F “Differentiation of mesophilic and thermophilic bacteria with Fourier transform infrared spectroscopy” *Applied Spectroscopy* **61** (2): 186-192 (2007)
30. Du W, Wang Y, Luo QM, *et al.* “Optical molecular imaging for systems biology: from molecule to organism” *Analytical and Bioanalytical Chemistry* **386** (3): 444-457 (2006)
31. Lee YM, Seo JS, Kim IC, *et al.* “Endocrine disrupting chemicals (bisphenol A, 4-nonylphenol, 4-tert-octylphenol) modulate expression of two distinct cytochrome P450 aromatase genes differently in gender types of the hermaphroditic fish *Rivulus marmoratus*” *Biochemical and Biophysical Research Communications* **345** (2): 894-903 (2006)

II- Cakmak, G., Uğuz, C., Togan, I. and Severcan, F. “FT-IR Spectroscopic Analysis of Rainbow Trout Liver Exposed to Nonylphenol” *Applied Spectroscopy* **57**(7): 835-841 (2003)

Cited by:

1. Beklioglu M, Akkas SB, Ozcan HE, *et al.* “Effects of 4-nonylphenol, fish predation and food availability on survival and life history traits of *Daphnia magna* straus” *Ecotoxicology* **19**(5): 901-910 (2010)

2. Tuo Y, Huang P, Ke Y, *et al.* "Attenuated Total Reflection Fourier Transform Infrared Spectroscopic Investigation of the Postmortem Metabolic Process in Rat and Human Kidney Cortex" *Applied Spectroscopy* **64 (3)**: 268-274 (2010)
3. Lu XN, Webb M, Talbott M, *et al.* "Distinguishing Ovarian Maturity of Farmed White Sturgeon (*Acipenser transmontanus*) by Fourier Transform Infrared Spectroscopy: A Potential Tool for Caviar Production Management" *Journal of Agricultural and Food Chemistry* **58 (7)**: 4056-4064 (2010)
4. Akkas SB, Kepenek AO, Beklioglu M, *et al.* "Molecular approach to the chemical characterization of fish-exuded kairomone: a Fourier transform infrared spectroscopic study" *Aquatic Sciences* **72 (1)**: 71-83 (2010)
5. Huang P, Tian WP, Tuo Y, *et al.* "Estimation of Postmortem Interval in Rat Liver and Spleen Using Fourier Transform Infrared Spectroscopy" *Spectroscopy Letters* **42 (2)**: 108-116 (2009)
6. Palaniappan PLRM, Vijayasundaram V "The FT-IR study of the brain tissue of Labeo rohita due to arsenic intoxication" *Microchemical Journal* **91(1)**: 118-124 (2009)
7. Garip S, Gozen AC, Severcan F "Use of Fourier transform infrared spectroscopy for rapid comparative analysis of *Bacillus* and *Micrococcus* isolates" *Food Chemistry* **113 (4)**: 1301-1307 (2009)
8. Palaniappan P, Pramod K, Vijayasundaram V "FTIR study of zinc-induced biochemical changes in the liver of Indian carp *Labeo rohita*" *Journal Of Applied Spectroscopy* **75 (5)**: 752-758 (2008)
9. Peuchant E, Richard-Harston S, Bourdel-Marchasson I, *et al.* "Infrared spectroscopy: a reagent-free method to distinguish Alzheimer's disease patients from normal-aging subjects" *Translational Research* **152 (3)**: 103-112 (2008)
10. Bhattacharya H, Xiao Q, Lun L "Toxicity studies of nonylphenol on rosy barb (*Puntius conchionius*): A biochemical and histopathological evaluation" *Tissue & Cell* **40 (4)**: 243-249 (2008)
11. Huang P, Ke Y, Lu QY, *et al.* "Analysis of postmortem metabolic changes in rat kidney cortex using Fourier transform infrared spectroscopy" *Spectroscopy-An International Journal* **22 (1)**: 21-31 (2008)
12. Akkas SB, Inci S, Zorlu F, *et al.* "Melatonin affects the order, dynamics and hydration of brain membrane lipids" *Journal of Molecular Structure* **834 Sp. Iss. SI** 207-215 (2007)

13. Wu ZY, Bertram HC, Bocker U, *et al.* "Myowater dynamics and protein secondary structural changes as affected by heating rate in three pork qualities: A combined FT-IR microspectroscopic and H-1 NMR relaxometry study" *Journal of Agricultural and Food Chemistry* **55 (10)**: 3990-3997 (2007)
14. Gorgulu ST, Dogan M, Severcan F "The characterization and differentiation of higher plants by Fourier transform infrared spectroscopy" *Applied Spectroscopy* **61 (3)**: Pages: 300-308 (2007)
15. Toyran N, Turan B, Severcan F "Selenium alters the lipid content and protein profile of rat heart: An FTIR micro spectroscopic study" *Archives of Biochemistry and Biophysics* **458 (2)**: 184-193 (2007)
16. Garip S, Bozoglu F, Severcan F "Differentiation of mesophilic and thermophilic bacteria with Fourier transform infrared spectroscopy" *Applied Spectroscopy* **61(2)**: 186-192 (2007)
17. Dogan A, Ergen K, Budak F, *et al.* "Evaluation of disseminated candidiasis on an experimental animal model: A Fourier transform infrared study" *Applied Spectroscopy* **61 (2)**: 199-203 (2007)
18. Dogan A, Siyakus G, Severcan F "FTIR spectroscopic characterization of irradiated hazelnut (*Corylus avellana* L.)" *Food Chemistry* **100(3)**: 1106-1114 (2007)
19. Toyran N, Lasch P, Naumann D, *et al.* "Early alterations in myocardia and vessels of the diabetic rat heart: an FTIR microspectroscopic study" *Biochemical Journal* **397**: 427-436 Part 3 (2006)
20. Cakmak G, Togan I, Severcan F "17 beta-estradiol induced compositional, structural and functional changes in rainbow trout liver, revealed by FT-IR spectroscopy: A comparative study with nonylphenol" *Aquatic Toxicology* **77 (1)**: 53-63 (2006)
21. Toyran N, Zorlu F, Severcan F "Effect of stereotactic radiosurgery on lipids and proteins of normal and hypoperfused rat brain homogenates: A Fourier transform infrared spectroscopy study" *International Journal of Radiation Biology* **81 (12)**: 911-918 (2005)
22. Severcan F, Togan I, Cakmak G "FTIR spectroscopic analysis of rainbow trout liver exposed to 17 beta-estradiol" *Biophysical Journal* **88(1)**: 159A-160A Part 2 Suppl. S (2005)

23. Hackl EV, Kornilova SV, Blagoi YP “DNA structural transitions induced by divalent metal ions in aqueous solutions” *International Journal of Biological Macromolecules* **35 (3)**: 4175-191 (2005)
24. Murphy MG, Al-Khalidi M, Crocker JFS, *et al.* “Two formulations of the industrial surfactant, Toximul, differentially reduce mouse weight gain and hepatic glycogen in vivo during early development: effects of exposure to Influenza B Virus” *Chemosphere* **59 (2)**: 235-246 (2005)
25. Severcan F, Gorgulu G, Gorgulu ST, *et al.* “Rapid monitoring of diabetes-induced lipid peroxidation by Fourier transform infrared spectroscopy: Evidence from rat liver microsomal membranes” *Analytical Biochemistry* **339 (1)**: 36-40 (2005)
26. Boyar H, Zorlu F, Mut M, *et al.* “The effects of chronic hypoperfusion on rat cranial bone mineral and organic matrix - A Fourier transform infrared spectroscopy study” *Analytical and Bioanalytical Chemistry* **379 (3)**: 433-438 (2004).